Ole Tessmer

The Use of Biocarbon in the Acheson Process for Production of Silicon Carbide

Bacheloroppgave

NTNU
Norges teknisk-naturvitenskapelige universitet
Fakultet for naturvitenskap
Institutt for materialteknologi

NTNU
Kunnskap for en bedre verden

FIVEN

Ole Tessmer

The Use of Biocarbon in the Acheson Process for Production of Silicon Carbide

NTNU
Kunnskap for en bedre verden

The Use of Biocarbon in the Acheson Process for Production of Silicon Carbide

Ole Tessmer

Bachelor's thesis in Material Science & Engineering

Employer: FIVEN Norge AS

Supervisor: Kjersti Kleveland, IMA   **Co-supervisor**: Eirik A. Nordbø, FIVEN

Project Number: IMA-B-23-2023

Norwegian University of Science and Technology
Department of Material Science and Engineering

May 2023

NTNU
Norwegian University of
Science and Technology

FIVEN

Statutory Declaration

I declare that I have developed and written the enclosed thesis entirely by myself and have not used sources or means without declaration in the text. Any thoughts or quotations, which were inferred from these sources, are clearly marked as such.

This report was not submitted in the same or in a substantially similar version, not even partially, to any other authority to achieve an academic grading and was not published elsewhere.

Ole Tessmer

Trondheim, May 2023

Abstract

The largest fraction of silicon carbide (SiC) is produced through the Acheson process which generates large amounts of climate emissions. To combat this, biocarbon may be used to replace the fossil carbon sources which are most commonly used in the industry, such as petroleum coke [1].

Biocarbon in the form of charcoal, was used in combination with petroleum coke to produce SiC in a pilot furnace. The furnace was charged with a carbon source mixture of 30% charcoal, and 70% petroleum coke. A reference furnace with 0% charcoal was also fired to function as a point of comparison. The quality and yield of the produced SiC was compared with that of the reference furnace, as well as internal standards at FIVEN. Furthermore, properties of the carbon sources, such as bulk and absolute density, as well as morphology were investigated to support the findings.

It was found that SiC production in a pilot Acheson furnace using the specified carbon source mixture was possible, but with a lower yield compared to a reference furnace with no present charcoal. The SiC produced with charcoal had higher values of metal impurities such as Ti, Fe, V and Ca, but these were still within company specifications. Through XRD analysis it was found that the primary polytype of SiC produced using charcoal was α-SiC, which corresponded to that of the reference furnace. There was however a higher fraction of α-SiC in the firesand section of the furnace when compared with the reference.

Characterisation of the carbon sources was done through measurement of bulk and absolute density. It was found that the used biocarbon had a lower bulk, but a higher absolute density compared to the petroleum coke. This could be linked to a higher amount of open porosity in the charcoal, but requires further research.

Whilst the production of SiC using a mixture of charcoal and petroleum coke is possible, it is apparent that the yield is not satisfactory. However, there are many factors that feed into this value, such as the type of biocarbon, charge density, particle size, moisture, particle distribution, porosity and surface area of particles. Therefore, further research into these factors is necessary to facilitate the large scale adoption of biocarbon in the industry.

Sammendrag

Den største andelen silisiumkarbid (SiC) produseres gjennom Acheson-prosessen, noe som forårsaker høye klimautslipp. For å motvirke dette kan biokarbon brukes som erstatning av petroleumskoks, som er den mest brukte karbonkilden i industrien [1].

Biokarbon, i form av trekull, ble brukt i blanding med petroleumskoks for produsere SiC i en pilotovn. Ovnen ble fylt med en karbonkilde-blanding av 30% trekull og 70% petroleumskoks. En referanseovn med 0% trekull ble også kjørt for å gi et sammenligningsgrunnlag. Kvaliteten og utbyttet av produsert SiC ble sammenlignet med referanseovnen og de interne standardene til FIVEN. Egenskapene til karbonkildene, som bulk og absolutt tetthet, og morfologi ble også testet for å støtte funnene.

Det ble funnet at SiC-produksjon i en Acheson ovn med den spesifiserte kabonkilde-blandingen er mulig, men med et lavere utbytte enn referanseovnen. SiC produsert med trekull hadde en høyere andel metalliske urenheter, som Ti, Fe,V, og Ca, men disse var fortsatt innenfor bedriftens spesifikasjoner. Gjennom XRD-analyse ble det funnet at den dominante polytypen av SiC produsert med trekull var α-SiC, noe som samsvarte med refereanseovnen. Det var også en høyere andel α-SiC i firesand-området av ovnen enn i referansen.

Karakterisering av karbonkildene ble gjort ved å måle bulk og absolutt tetthet. Det ble funnet at det brukte biokarbonet hadde lavere bulktetthet, men høyere absolutt tetthet enn petroleumskoks. Dette kan skyldes en større mengde åpen porøsitet i trekullet, noe som krever mer forskning. Mens produksjon av SiC med en blanding av trekull og petroleumskoks er mulig, er ikke utbyttet bra nok. Det er mange faktorer som påvirkerdette utbyttet, nemlig typen biokarbon, ovnsmassens tetthet, partikkelstørrelse, fuktighet, partikkelfordeling, porøsitet, og overflateareal av partiklene. Disse faktorene må forskes videre på for å kunne støtte storskala etablering av biokarbon i industrien.

Preface

This thesis concerns the use of biocarbon in the Acheson process for production of silicon carbide, and how this affects the quality of the resulting product. The work is the basis for evaluation in the course TMAK3001 at the Norwegian University of Science and Technology, NTNU. The work has been done in cooperation with FIVEN Norge AS.

I would like to thank my guidance councillors Kjersti Kleveland, and Eirik Andre Nordbø for their honesty and invaluable feedback. They have helped me organize my tumultuous thoughts and ideas into a coherent piece of work. Furthermore, I would like to thank FIVEN for giving me the opportunity to write about this topic, and for providing support for the research and work conducted.

I also wish to extend my deepest gratitude to Dr. Rania Hendawi and Elin Harboe Albertsen, as well as all other lab technicians and supervisors who have provided me with training in the proper use of equipment.

Ole Tessmer

Trondheim, May 2023

Contents

List of Figures

x

List of Tables

Chapter 1

Introduction

1.1 Background

In 1891, American chemist Edward Goodrich Acheson attempted to produce artificial diamonds by running electricity through a graphite electrode surrounded with a mixture of coke and sand, reaching temperatures of 2200°C and upwards. Instead of achieving his goal he created an incredibly hard abrasive ceramic he titled "carborundum". Today we know this ceramic as silicon carbide (SiC), and its hardness is close to that of diamond. An example of a SiC crystal is shown in figure 1.1. Whilst Acheson would also go on to develop a process for generating graphite on an industrial scale, it's his aptly named Acheson process for the production of silicon carbide which remains largely in use today [2].
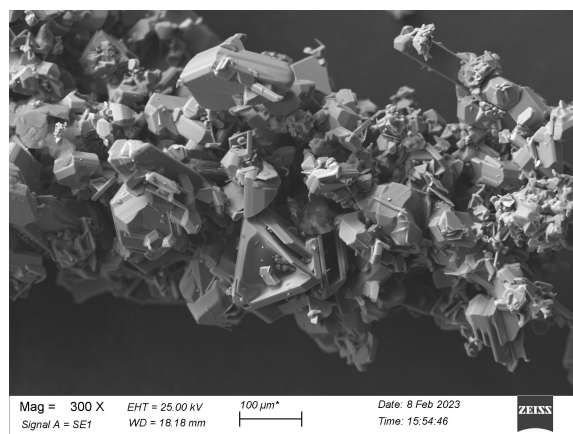
Figure 1.1: A crystal of SiC

Silicon carbide has many applications due to its excellent mechanical, electronic and chemical properties, even at high temperatures, as well as excellent thermal conductivity and shock resistance [3]. Some major applications include foundry, refractory and technical ceramics, as well as abrasives and more recently, electrical applications [4]. SiC is a semiconductor, which also makes it very attractive within the electronics industry [5].

As the world moves into a more climate-oriented era, the emissions of heavy industry needs to be analysed and reduced. The Acheson process is often scrutinized due to its production of CO_2 and hazardous particles that are spread through the off-gas [6]. Furthermore, there has been an increased industry incentive to replace fossil materials with renewable alternatives. The Acheson process needs a form of carbon source to produce silicon carbide, and this source needs certain properties in order to produce high quality SiC [7]. Therefore, any renewable candidate must achieve similar results as the currently used petroleum coke to be a viable option. An interesting way of reducing the overall emissions of this process is with the use of biocarbon as a carbon source. Biocarbon is considered renewable, because it is part of a carbon cycle which spans far less time when compared with its fossil counterparts. Currently, there is not enough research on the industrial use of biocarbon for production of SiC, and most investigations have been done on a lab-scale. This investigation utilises a pilot furnace to increase the experimental size, and therefore gains new insights into the use of biocarbon in larger scale Acheson furnaces.

Therefore the questions arises whether the use of biocarbon in the process has a substantial effect on the quality and yield of product. This information may be used to evaluate whether this new carbon source is a viable alternative on a larger industrial scale. With SiC becoming ever more relevant in electronics, ensuring purity with sustainable production practices will be key in future industry developments.

FIVEN is a relatively new company which builds on the foundations set by, amongst others, Saint-Gobain. In total, the company has over 100 years of experience in the production of silicon carbide. Currently, the products that FIVEN has specialised in, include SiC grains and powders for applications in refractory and technical ceramics as well as composite materials and ready-to-press granules for sintering. The company has production sites in Norway, Brazil and Belgium. With sustainable operation becoming ever more important, FIVEN has invested and focused heavily on sustainability in recent years, and this has opened for research into reducing carbon footprints globally. This company initiative has also contributed to making this project a possibility [8].

1.2 Objective and Experimental Work

The primary objective of this project is to compare the quality and yield of silicon carbide produced in a pilot furnace using a mixture of biocarbon and petroleum coke with the quality and yield of silicon carbide produced with only petroleum coke.

To produce SiC, a pilot furnace at the R&D department of FIVEN in Lillesand will be used. For this project, the chosen biocarbon is a form of charcoal that FIVEN has tested before, meaning availability will not be an issue. The furnace will be charged first with a mixture of charcoal and petroleum coke and fired till completion. Crude SiC will be collected and weighed before being analyzed further. This process will be repeated for a furnace with no charcoal present which will serve as a reference.

The quality of SiC will be compared in terms of metallic impurity contents, measured using ICP-analysis. The crystal structure of the produced SiC will also be analysed using XRD to determine concentration of desired polytypes (α-SiC). Finally SEM and EDS-analysis will be used to analyze sample morphology and structure as well as chemical composition.

Furthermore, the carbon sources (charcoal and petroleum coke) will be analyzed to determine bulk and absolute density. SEM will also be used to identify and compare morphological structures.

The conclusion of this work will ideally be able to comment on the viability of using charcoal as a biocarbon alternative to petroleum coke in the Acheson process. It will also comment on how the produced SiC quality was affected, and what further research could be done to further aid in the wide-scale industrial use of biocarbon in the production of SiC.

Chapter 2

Theory

This chapter covers the theory necessary to understand the production of silicon carbide, as well as the properties of the raw materials that are used in the process. The principles behind the relevant analysis methods for this investigation will also be covered.

2.1 The Acheson Process

Whilst the Acheson process has existed for over 100 years, it remains largely the same today. An electrode composed of graphite is surrounded by a mixture of silica sand and a carbon source (usually a form of petroleum coke) [2]. An example of this design is shown in figure 1 below.
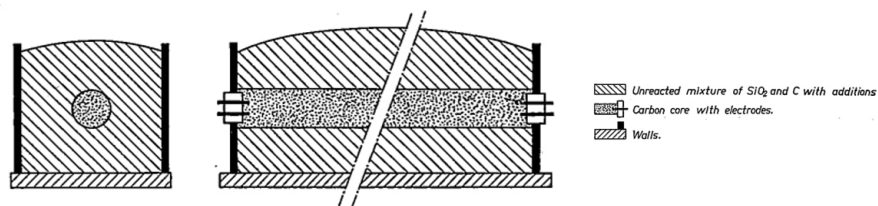
Figure 2.1: Acheson furnace before firing [9]

The standard Acheson furnace resembles the sketch in figure 1, however there are several alternate designs in the industry, such as furnaces with U-shaped electrodes [1]. These allow for a larger product yield on an industrial scale but also come with their unique set of challenges [7].

The Acheson furnace is a resistance furnace, meaning it uses heat generated by the Joule effect when current flows through the system. More specifically, this kind of furnace utilises direct resistance heating (DRH), as the heat is generated by sending current directly through the work-piece or charge. During this kind of process, a constant voltage is applied to the system, whilst the current is variable throughout the process due to the changes in material properties as the temperature increases [10].

The overall reaction that occurs during firing of the furnace is shown in equation 2.1 [1].

$$SiO_2(s) + 3\,C(s) \longrightarrow SiC(s) + 2\,CO(g) \tag{2.1}$$
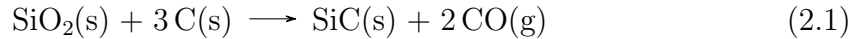
It must be noted that the solid-state reaction shown in equation 2.1 was assumed to be a direct reaction by Acheson himself, as well as Margrave and Mamatov [7]. This reaction can occur, and its rate increases when temperatures are high enough to melt the SiO_2 particles allowing Si atoms to have more direct surface contact with carbon. However, Lee and Cutler originially suggested that mass transfer of the reaction occurs primarily through gas phase [1]. This was later supported by Weimer et al., and a set of four sub-reactions was suggested for this mechanism. These can be seen in equation 2.2, 2.3, 2.4, and 2.5 [7].

$$SiO_2 + C \longrightarrow SiO(g) + CO(g) \tag{2.2}$$

$$SiO_2 + CO(g) \longrightarrow SiO(g) + CO_2(g) \tag{2.3}$$

$$C + CO_2(g) \longrightarrow 2\,CO(g) \tag{2.4}$$

$$2\,C + SiO(g) \longrightarrow SiC + CO(g) \tag{2.5}$$
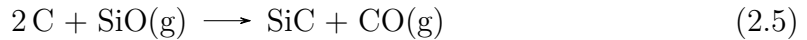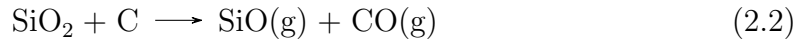
The reaction starts with SiO_2 particles reacting with adjacent carbon particles, forming SiO and CO gas. The CO gas reacts further with other SiO_2 particles or sites[1], releasing more SiO gas and generating CO_2. This CO_2 interacts with carbon particles and is reduced to CO gas, continuing the reaction. The SiO gas will react directly with carbon particles in the charge, forming SiC. A phenomena that occurs at lower temperatures in the furnace is that SiO will react with the surface of carbon particles and form SiC only at the surface level, and proceed to flake off over time [7]. If these layers do not flake off, and instead there is a build-up of carbon particles encapsulated by a layer of SiC, or the ratio is offset to: $C/SiO_2 < 3$, this will result in a reaction consuming the formed SiC as shown in equation 2.6 [1].

---

[1]Depending on the temperature SiO_2 may be present either in solid or liquid state

$$SiC(s) + SiO_2(l) \longrightarrow 3\,SiO(g) + CO(g) \tag{2.6}$$
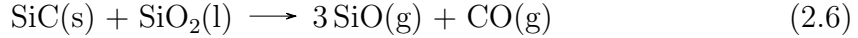
Most of the reactions in the furnace occurs through gas phase transport. This also presents challenges related to loss of process gas. Throughout the process gas may build up in the charge and form large off-gas channels. This is problematic as SiO and fines may escape the furnace through these channels.

At peak temperatures the core can reach up to 2800°C, though it will normally stabilize around 2500°C [11]. At this temperature, the SiO_2 in the charge will exist in molten liquid form close to the core.

The equilibrium phase diagram for the Si-C system is shown in figure 2.2. It shows the peritectic decomposition temperature of SiC lies around 2800°C, at which point the system will exist as a Carbon-rich Si-liquid in equilibrium with graphite.
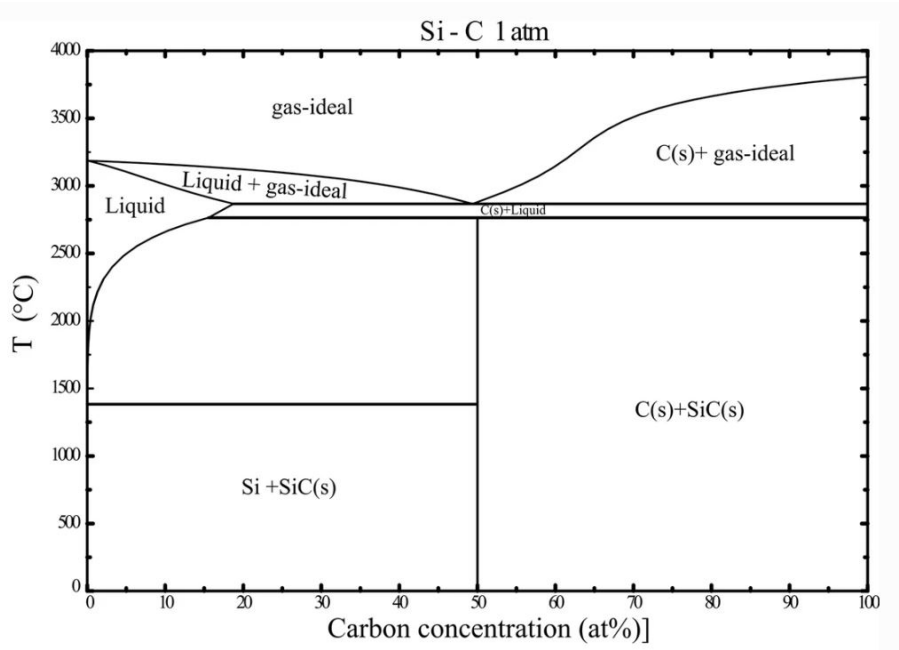
Figure 2.2: Equilibrium phase diagram for Si-C system [12]

During the process, graphite will also be generated surrounding the electrode. This happens due to several major mechanisms. Firstly, there is a mass transport caused by gaseous species like SiO, and CO moving in the direction of decreasing temperature in the charge. This is most significant in the hotter zones of the furnace, and is responsible for some of the expansion of the graphite core due to the deposition

6

of carbon. Secondly, when temperatures reach the peritectic decomposition temperature of SiC at around 2800°C, as mentioned above, graphite will form together with a carbon-rich Si-liquid which will drip down from the core and be redeposited as SiC in the crude beneath. For the liquid that forms above the core, this will evaporate once hitting the core and be pushed into the crude where it also will be deposited as SiC. The graphite left behind will form a porous structure around the furnace core [1].

An example of a furnace after firing is shown below in figure 2.3. The phases that are generated during the process are crude SiC, which has a relatively high purity (98-99.9%)[13], and firesand which is a mixture of crude SiC and raw materials from the charge [14][1]. This firesand is often referred to as a mixture of amorphous SiC and unreacted material, also shown in figure 2.3 [3][9]. Take note of the distinct layering that the SiC, firesand and graphite sections display. This layering allows for easy separation of the different products.
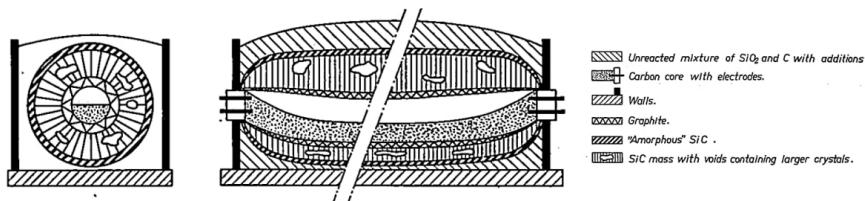
Figure 2.3: Acheson furnace after firing [9]

During the dismantling stage the layers are shaved off separately to ensure product purity. The firesand is usually reused in subsequent furnace runs. The crude SiC is processed further into finished products.

A challenge that is often encountered in the Acheson process is the potential for material-loss of the carbon source in the form of primarily the Boudouard reaction shown in equation 2.7 [15].

$$CO_2(g) + C(s) \longrightarrow 2\,CO(g) \tag{2.7}$$
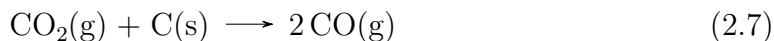
In a recent study, Wang et al. also described a water-coke reaction (eq. 2.8) at high temperatures leading to coke degradation. This was also experimentally verified by heating coke in an atmosphere of water vapour. Whilst a lot of the moisture of the charge is evaporated at the start of the process, some may remain trapped and later be released, causing loss of carbon. Due to the lack of supporting literature, this will not be considered further in this investigation, but may serve as a point of interest for future study.

7

$$H_2O(g) + C(s) \longrightarrow CO + H_2 \qquad (2.8)$$
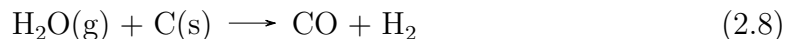
The loss of carbon through the Boudouard reaction requires the presence of CO_2. This gas is generated in the process as shown in equation 2.2 above, thereby readily feeding the reaction at higher temperatures [7]. As this reaction is a surface reaction, the reaction rate with CO_2 will be related to the available surface area. More surface area may therefore lead to faster carbon loss in the furnace [16]. Carbon loss throughout the process can lead to increased production costs [15].

2.2 Raw Materials

The production process for SiC includes a mixture of a carbon source, often in the form of coke, and a source for SiO_2, which is often a form of silica-rich sand. The scope of this investigation seeks to replace the current carbon source with biocarbon, or more specifically charcoal. This section serves as an introduction to the different raw materials and their properties. The composition and purity of the raw materials that enter the process are paramount, as the impurities that enter the process tend to end up in the product. Therefore, the purity of the raw materials has a direct impact on the purity of the product.

2.2.1 Petroleum Coke

The primary carbon source in modern silicon carbide production is most commonly a form of coke, of which petroleum coke has been found to work excellently [1]. Petroleum coke is a byproduct of the oil industry, and is best defined as "a carbonization product of high-boiling hydrocarbon fractions (heavy residues)" [17]. It is produced from the "bottom of the barrel" heavy materials which gather during the primary filtering of crude oil as shown in figure 2.4. These heavy compounds are transferred from the atmospheric tower to the vacuum tower where they are further filtered and distilled [18]. The remaining heavy residue is then filled into a delayed coker, which is often comprised of a collection large silos. Here the raw material is thermally treated, reaching temperatures of around 500°C [18]. This allows firstly for further cracking of the larger hydrocarbon chains to release valuable gas and fluid products to be removed wit a fractioner. Secondly, due to polymerization and crosslinking reactions, a solid residual layer of carbon will form in the coking silo. Once enough mass has formed and cooled down it is cut out using a pressure water jet or similar machinery [18]. The final product is what is referred to as green petroleum coke, or GPC.
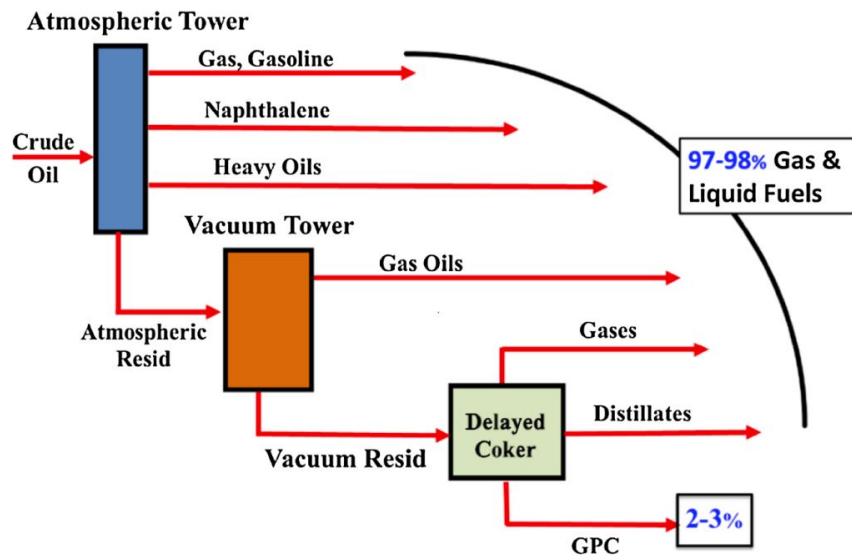
Figure 2.4: Simplified refinery flow chart showing relative product values [18]

When the GPC is cut from the coking drums, it will usually have a volatile matter (VM) content between 9-14 wt% depending on the coking severity[2] [18]. To lower the amount of impurities the GPC is usually calcined or heat-treated in large coking furnaces in absence of oxygen. Temperatures tend to reach 1200°C and above. This pyrolysis allows the coke to further shrink and densify, increasing bulk density [18]. After heat treating for the desired amount of time, the coke is removed and quenched in steam. Finally it is dried and either chemically purified further or sold [18].

Typically, the resulting petroleum coke has a carbon content between 70-85 wt%, but depending on the level of processing this content can reach as high as 97 wt% [17].

It is this grade of petroleum coke that is used in the production of silicon carbide, all be it in relatively small particles. Particle size is very important, as a relatively homogeneous mixture with silica sand is ideal for the yield of the process [7]. Furthermore, petroleum coke has a low ash content and a relatively low CO_2 reactivity. Whilst petroleum coke also has a low reactivity with SiO, the aforementioned effect of SiC forming and flaking off is more pronounced in petroleum coke, making it a great candidate for SiC production [19][7].

The petroleum coke utilised in this investigation is a mixture of different coke qualities. This is normal procedure in the industry, as suppliers mix different cokes

---

[2]This is a measure of the extent of polymerisation and crosslinking in the GPC

9

together to match impurity specifications of a client [20].

2.2.2 Biocarbon

Biocarbon is a form of amorphous carbon with biological precursor that is not of fossil origins [21]. Bio-based carbon has many industrial applications, even in its raw form, such as the use of wood-chips in Si-furnaces [22] [23]. However, the most typical application is in the form of charcoal, often referred to as biochar or biocarbon [24]. Even this charcoal can be produced in different ways, yielding a variation of product geometries, such as pellets or larger particles. What makes biocarbon so attractive is the fact that it is considered a low-emission carrier. Because of photosynthesis, plants will deposit as much carbon in their cells as will be combusted in the end, placing CO_2 balance in the atmosphere at net zero [25][26].

Charcoal is biomass (usually lignocellulose or wood) which has been heat treated through pyrolysis [27]. Pyrolysis is defined as the irreversible thermochemical decomposition of complex solid or fluid chemical substances (in this case, biomass) at elevated temperatures in the absence of oxygen [28]. Pyrolysis of wood precursors will often yield a highly porous carbon which retains the structure of the precursor, with tube-like pores going along the growth direction of the tree. Radial pores will also be present, and their concentration is highly dependent on the density of the wood precursor. Furthermore, biocarbon has an abundance of crystallites that stick to its carbon matrix walls. Compared to most other carbon sources, biocarbon is highly porous, reaching up to 75% porosity, depending on the precursor. [21]. In this thesis, biocarbon is used to refer to a form of charcoal acquired by FIVEN which is stated to have European origins.

This pyrolysis process allows the removal of volatiles and increases the fixed carbon content of the biomass [29]. This allows for a far higher heating value when compared to its precursor materials, and thereby makes it a viable alternative to other carbon-compounds in both heating and industrial applications [29]. The production route for biocarbon also has the potential to yield several useful bi-products such as bio-oil and bio-gas which his often used to partially power the process. A simplified example of a typical biocarbon production route is shown in figure 2.5. The flow chart has been heavily simplified, but shows all the major process steps. There are currently a large range of pyrolysis reactors, with some of the prominent technologies including: fluidized bed reactors, rotating cone reactors, ablative reactors, and vacuum reactors, to name a few [30].
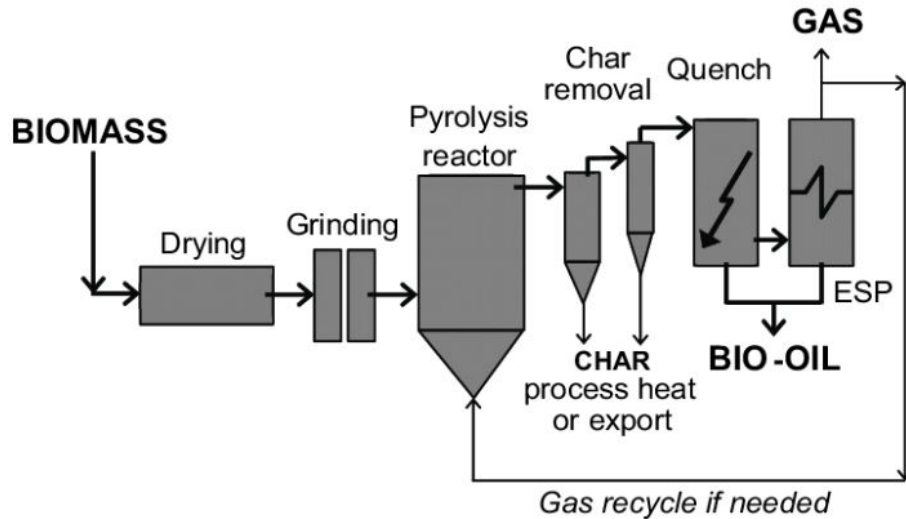
Figure 2.5: A simplified biomass pyrolysis process [31]

Kaffash compared three different kinds of biocarbon with varying degrees of densification, and found that in terms of composition, these have less sulphur content than metallurgical grade coke, but higher contents of volatiles. Not all biocarbon is the same, but this is a rather important factor to consider, as sulphur emissions remain a major industry challenge that biocarbon may help combat [16]. What Kaffash also presented is the wide variety of production methods for biocarbon. It functions as a material that can be tailored to desired applications.

According to a life cycle analysis (LCA) performed by Riva et al., the carbon footprint of biocarbon is highly dependent on area of production as well as production methods. However, replacing metallurgical grade coke with biocarbon will cause a large decrease in generated emissions [32].

A downside of using biocarbon is its properties. Whilst fixed carbon content may rival that of certain cokes, biocarbon often has low mechanical strength, higher surface area, and therefore also a higher CO_2 reactivity. This means more material will be lost to the Boudouard reaction when compared to standard metallurgical grade coke. [15]. Furthermore, biocarbon tends to have a lower bulk density than other reductants, meaning less carbon will fit into the same volume of charge [16]. This may have adverse consequences on processes that operated batch-wise such as an Acheson furnace.

Biocarbon has been used for millennia, primarily as a heat source [27]. It was first after the industrial revolution and the emergence of cheaper fossil alternatives, that biocarbon was phased out of mainstream industry. With growing climate concerns

11

however, biocarbon had a re-emergence in the 1970's and remains a major interest point for most heavy industry applications [29]. Biocarbon can be processed further from biochar in many ways and final products range from pellets and briquettes to fine powders, depending on necessary application.

The Acheson process most commonly uses high grade petroleum coke as a carbon source [1]. This material is derived from oil, and is therefore considered a fossil material which generates climate gas emissions upon use. Biocarbon is therefore desirable over petroleum coke because of its reduction in long-term climate emissions. Due to biocarbon being a relatively regenerative material, it is considered sustainable [29]. As the metallurgical and ceramic industries push to meet emission goals and develop into greener business models, the use of biocarbon offers an effective way of improving process sustainability. However, it is important to note that total emissions through the process will not decrease, but as these emissions are compensated for through the planting of new trees and cultivation of new biomass, they are considered sustainable emissions [29].

Currently, Sweden, Germany, Austria and Latvia are large producers of wood precursors in terms of pellets. These may also undergo pyrolysis and become charcoal [26]. Europe in general also produced around 250,000 tons of charcoal a year. However, due to high consumption, over 750,000 tons are imported from countries like Ukraine, Nigeria, and Cuba [33]. With the ongoing political struggles in some of these countries, supply is not guaranteed. Depending on geography, biocarbon precursors may be wood based or originate from other biomass such as agricultural waste (for example rice husks). Wood biomass is the most typical precursor for charcoal, and this may either come from forestation, process waste, or fast-growing tree plantations [25][34].

2.2.3   Silica Sand

One of the two main raw materials in the Acheson process is sand, from here on referred to as silica sand as silica is the primary component of quartz, and the desired raw material for the Acheson process. This sand supplies the reaction with silicon to bond with the present carbon to form SiC. Silica sand has a high content of SiO_2, and whilst the exact content varies depending on the desired application, a minimum content of 96% SiO_2 is normal [35]. For application in the production route for SiC, a content of 99% is usually used as impurities easily carry over to the product. This ensures enough silica is available to react in the charge and form SiC, both through solid-state, and gas-state reactions. Other common contaminants in this type of sand are aluminium-, iron-, and titanium oxide [35]. These can cause

problems for the resulting SiC, and therefore purity of the sand is highly important. For this experiment silica sand with SiO_2 content between 99-100% was utilised.

Silica sand is produced all over world, with the primary exporters being the United States of America and Australia, however, several European nations such as Belgium, Germany, and the Netherlands also export high quality silica sand [36].

2.3   The Production Process of Silicon Carbide

In the industrial sector, furnaces following the standard Acheson design are often 20 m in length, and 5 m in width. Furnaces utilising the U-shaped electrode design can range up to sizes even larger than this. Acheson furnaces are operated batch-wise, meaning the furnace must be partially dismantled and rebuilt between each run [1]. The following production steps may however be applied to all types of furnaces.

According to Lindstad, the production of silicon carbide can be divided into five main steps:

1. Mixing of raw materials: In this step, the electrode is prepared by mixing graphite and sometimes a carbon filler such as calcined coke [1]. Also, the main material mixture (charge) is prepared by combining silica-rich sand and coke. High purity silica sand[3] is necessary for the production of the highest grade SiC. At this stage, recycled charge from earlier furnace runs will also be mixed in with then new charge. Whilst exact amounts are dependent on the composition of the recycled charge and dimensions of the furnace, typical contents lie between 40-70% recycled charge [7]. It is not unusual for only 10-15% of the charge to actually be converted to SiC [3].

2. Building of the furnace: The furnace is built by first preparing a bed of material mixture, and then building the graphite electrode on top of the bed. Once the electrode is complete, more material mix is added until the heap has a desired height above the electrode heads [7]. A movable furnace that is ready to be started is shown in figure 2.6 [37].

---

[3]This may also be replaced with a form of quartzite or crystalline rock quartz [7]

13

Figure 2.6: A movable furnace from the Volga abrasive plant, ready to be fired [37].

3. Firing of the furnace: Firing the furnace starts with running electricity at high voltage through the electrode. This is necessary as the original resistance will be relatively high, and power input needs to remain high. Over time, the current is increased until it reaches a desired level. Once enough CO gas is generated, the furnace is lit on fire. An example of a furnace during firing is shown in figure 2.7. At this stage the process is continued for several hours whilst being closely monitored. The resistance will lower throughout the process as temperatures increase and the produced SiC area grows in diameter. Typically, voltage levels are slowly lowered throughout operation to minimize excessive currents [7].

Figure 2.7: A furnace during firing. The CO gas burns blur along the surface of the furnace [38].

During firing, gas may build up in the furnace, causing small outbursts of gas

and energy that can somewhat compromise the structure of the charge. These flares can also lead to gas channelling where process gas escapes the furnace at a higher rate due to large openings forming in the charge. Larger gas eruptions, also called "blows" may also occur somewhat infrequently. These usually come in the form of hot gases and sparks spewing from the top of the furnace. To work against this, more material mixture is added on top of these cracks and holes to ensure the gas flows more evenly through the mixture. With larger blows, electricity may also be shut off for short periods of time (10-15 minutes) [7][1].

Once the desired total power consumption is reached, the furnace is shut off and left to cool. The total power of an industrial furnace varies with furnace dimensions, but a good point of comparison between furnaces is the consumed power per kg SiC produced. Theoretically this value should be around 2.2 kWh/kg, but realistically the value will be between 6-12 kWh/kg for most modern Acheson furnaces [3].

4. Cooling: The furnace will have to cool for several hours, up to days depending on the size [7]. During operation maximum temperatures can reach 2800°C and above, meaning heat dissipation will take time due to large amount of material surrounding the core [11].

5. Dismantling of furnace and sorting of products: Once fully cooled the furnace is dismantled using diggers and a large crane which extracts the electrode surrounded by SiC and firesand. This part is referred to as the ingot [1]. Usually this section is broken into smaller pieces to ease handling. Metal impurities are typically convected radially away from the core at high temperatures and tend to form a "crust" which will have to be removed as it contains a high concentration of metal oxides. The firesand is then peeled off the ingot to expose the crude SiC, which is further peeled off the graphite core. Whilst the firesand and graphite are recycled for subsequent runs, the crude is sorted and processed further to be sold [7].

Whilst not all production sites follow this exact method it can be seen as a general outline for how the process is performed in the industry. Depending on the desired products, only sections of the ingot produced are used, however for metallurgical grade SiC, where purity is not vital, the ingot may be ground up in its entirety [7].

Figure 3 is an illustration of an ingot of crude SiC generated through the Acheson process. The separate sections of the ingot are marked. This will be relevant for the subsequent sections.

2.4 Types of Silicon Carbide

SiC is a compound combining Si and C atoms in a tetrahedral coordination. This compound can exist in several crystallographic variations, which are called polytypes. These polytypes typically differ in atomic layer sequencing, which has an effect on the crystallographic growth directions. For all polytypes of SiC the covalent bond remains in place, and the chemical composition of the material does not change. However, the different arrangements of atomic layers means polytypes have different properties, amongst which electronic properties is one of the most important [12].

All SiC polytypes are typically divided into two categories, β-SiC, which has a cubic symmetry, and α-SiC which has a hexagonal or rhombohedral symmetry. The specific structures are further identified by a number which represents number of tetrahedron layers, and a letter which represents the shape of the unit cell.[12] Primary lattice structures for α-SiC include: wurtzite (2H), hexagonal (6H), and rhombohedral (15R) [1]. For β-SiC, the most typical structure is cubic (3C). These crystal structures are illustrated in figure 2.8.
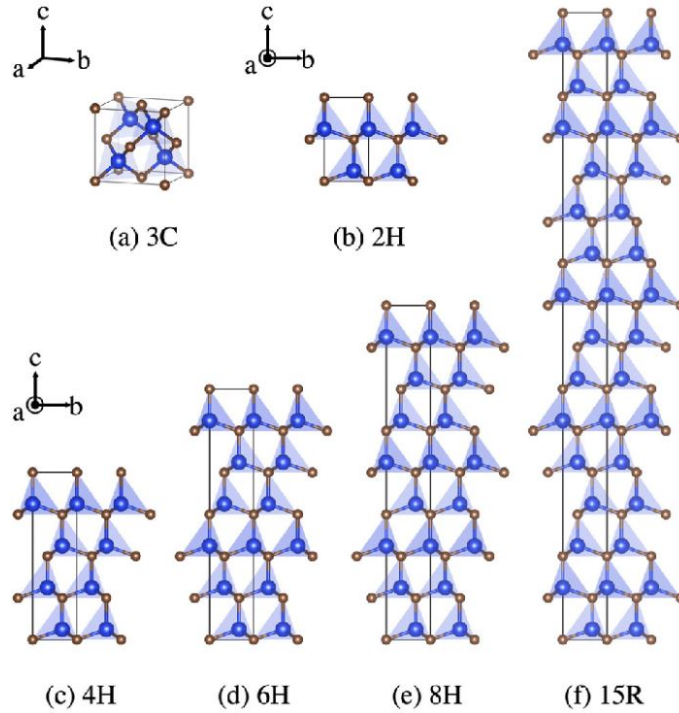
Figure 2.8: Main SiC polytype crystal structures. 3C-SiC is considered β-SiC. 2H, 4H, 6H, 8H, and 15R are considered α-SiC [39]

.

According to theory there are a huge amount of SiC polytypes. This has led to the discovery of amongst others, a 6O-SiC, where the "O" signifies orthorhombic. However this polytype is mainly an intermediate step in the formation of natural 6H-SiC. Furthermore, this polytype has very similar crystallographic properties compared to the more common 6H-polytype. In principle this means that several polytypes may exist that are both very similar in structure, and in crystallographic properties, making their detection far more difficult [40].

Whilst the primary product during SiC production is α-SiC, it is actually β-SiC which is considered the most stable configuration of SiC up to its peritectic decomposition temperature at around 2800°C [11]. Whilst both α- and β-SiC share several mechanical properties, their hardness is somewhat different as shown in table 2.1. It should be noted that both polytypes share a Mohs hardness number of 9.5 which is just below that of boron-carbide (9.75) and diamond (10) [41].

Table 2.1: Summary of Mechanical Properties of α- and β-SiC [41]

Property	Units	Type of SiC	
		α	β
Hardness:	Mohs no.	9.5	
Knoop(100g) ∥ c-axis	GPa	2130	2670
Knoop(100g) ⊥ c-axis	GPa	2755	2815
Young's Modulus (20°C)	MPa	294 000	
Young's Modulus (1300°C)	MPa	350 000	
Compressive Strength	MPa	180 000	
Density	g/cm^3	3.218	

Jayakumari and Tangstad studied the formation of SiC from various carbon sources, and found that between 1750-1900°C, β-SiC is the most abundant polytype [12]. Yoo and Matsunami further investigated the thermal stability of β-SiC (3C) betwen 1800-2400°C and found that at temperatures above 2150°C a solid-state phase transformation from 3C to 6H structures was observed [42]. This transition from α- to β-SiC occurred due to displacement of atoms via thermal diffusion [42]. Lindstad found that at a temperatures above 2570°C the amount of observed α-SiC decreased substantially, and therefore this temperature is often considered as the

decomposition temperature for α-SiC [1]. All these observations can be combined to support the proposed stability diagram for polytypes of SiC originally proposed by Knippenberg, shown in figure 2.9.
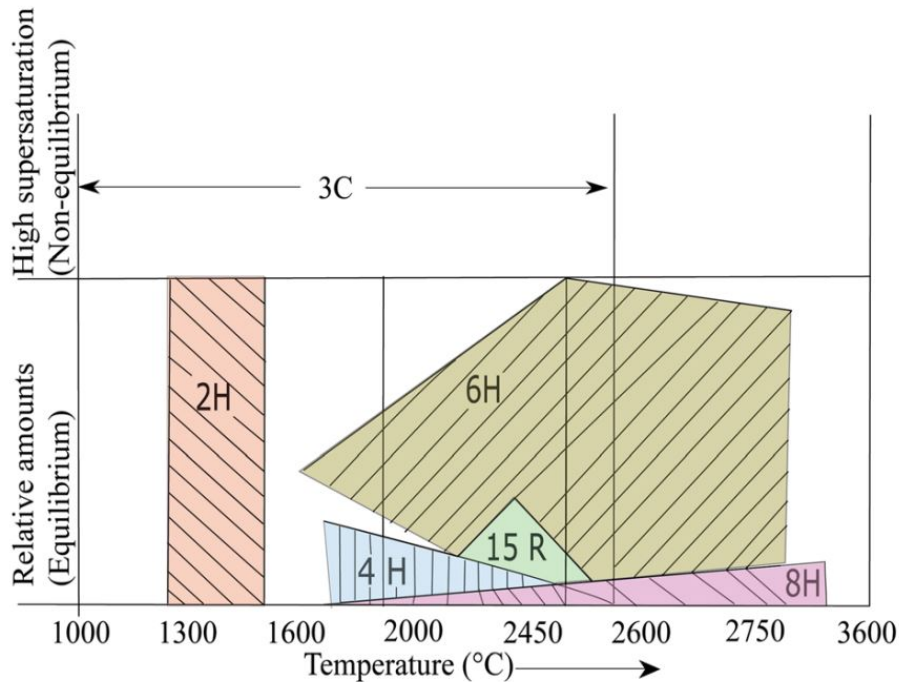
Figure 2.9: Stability diagram of SiC polytypes originally proposed by Knippenberg, taken from Jayakumari and Tangstad [12]

A common theory, supported by Lindstad states that during production, fine β-SiC will form first, and it is only due to further heating over longer periods of time that the SiC will deposit, recrystallize, and grow to form α-SiC crystals. These will then eventually decompose around 2570°C. It should be noted that impurities from the process may be present in the α-SiC that is produced, and this will change the apparent colour of the crystals. Therefore, one can identify major contaminants from simple visual inspection [1]. Table 2.2 gives a summary of dopants and their effect on crystal colour.

Table 2.2: The Effect of Dopants on SiC Colour

Type of SiC	Colour
Pure α-SiC	Colourless
Al-doped α-SiC	Blue-black
B-doped α-SiC	Brown-black
N-doped α-SiC	Green (6H), yellow orange (4H,8H), orange-yellow (15R)
Pure β-SiC	Yellow
N-doped β-SiC	Yellow-green

The formation of SiC on various forms of carbon sources was investigated by Jayakumari and Tangstad and it was found that several carbon particles were only partially converted to SiC [12]. This was also found by Nordbø, further illustrating a "shrinking core" model of SiC conversion. Therefore, it may be assumed that SiC formation occurs first at the surface of particles, and then the reaction front proceeds to move towards the core of the carbon particles [43]. This means that particle size is a major factor in the production of SiC, as larger particles would mean slower, and potentially incomplete conversion of the carbon to SiC.

2.5   The Applications of Silicon Carbide

Silicon carbide has exceptional mechanical properties, even at high temperature. It has high thermal conductivity and shock resistance, as well as excellent chemical and electrical properties [5]. Therefore, SiC has many different applications, one of the largest of which is within abrasives, as the material also has a extremely high relative hardness [3].

Other large applications for SiC are in refractory and foundry linings, machining tools, ballistic armour, and protective clothing, as well as several other applications within the metallurgical industry [44]. Recent developments have also been made within the sintering of SiC to be used within the automobile industry, industrial seals, valves and nozzles, and other applications which require high thermal resistance, and hardness properties [45]. Some further applications as well as the SiC market share are shown in figure 2.10.
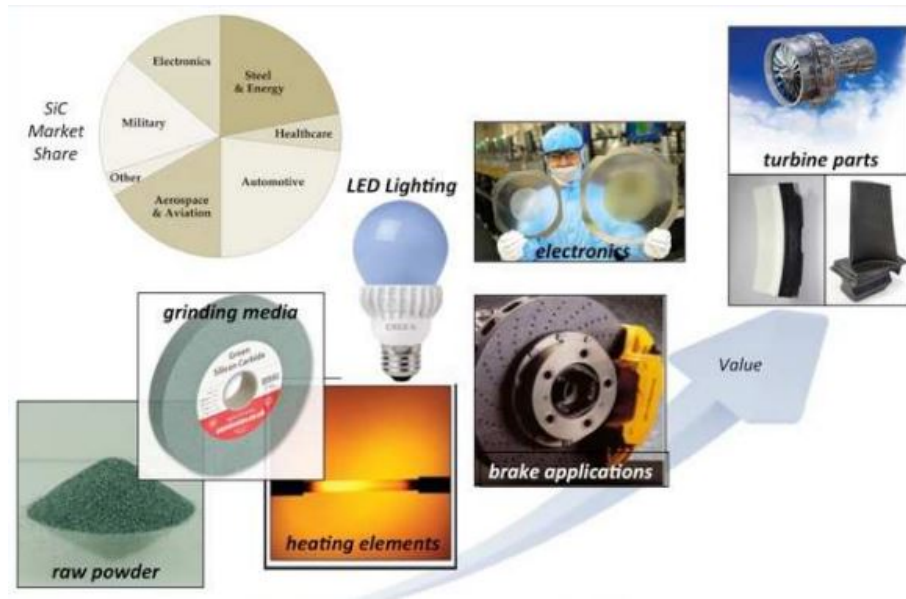
Figure 2.10: Applications and market share of silicon carbide products [46]

Current industry focus lies on the future applications of SiC in electronics, as pure SiC is a good wide band-gap semi-conductor [4]. To enable this property, the SiC must be doped with the correct elements such as group III elements (p-type semiconductor), and group V elements (n-type semiconductor) [1]. Due to the material properties of SiC, such as high electronic mobility, good thermal conductivity and radiation resistance, and excellent mechanical properties, it remains an excellent candidate for applications within high temperature electronics. Currently, challenges related to this application lie in controlled crystal growth, and the related crystal defects. Furthermore, due to the materials brittleness, shaping it is also complicated. As mentioned in section 2.4, SiC may form in an abundance of polytypes, and this further complicates the application of SiC in electronics [1].

2.6   Sustainable Production

The Acheson process is a process with high emissions. Not only does the chemical reaction generate masses of CO and CO2, but the off gases also carry a large number of fines, such as carbon dust from the raw materials, and volatiles that are freed throughout the process [47]. Depending on the purity of the raw materials, there will often be a large production rate of sulfur-based compounds which remain an industry challenge [7]. To combat this, some factories have implemented the use of fume

20

hoods or other forms of covers over cells that are being fired [37]. This preventative measure reduces the number of harmful particles that are released directly into the atmosphere, and thereby contributes to cleaner operation.

However the primary global production is still done outdoors in open pits, without any form of filtration system for the off-gases, and this can have adverse effects on the surrounding area as well as the air quality. Studies have also shown that workers in SiC plants have an increased risk of lung cancer as well as other forms of lung-diseases [48][6]. Therefore pollution remains a major challenge in the industry. The scope of this investigation does not fully analyse changes in atmospheric emissions when using biocarbon as a carbon-source, but concerns itself with the overall reduction of climate emissions as an effect of changing the carbon source.

Due to larger industry incentives to reduce emissions, finding a way to make the Acheson process more sustainable has been a major point of research [37]. One way to do this is to change the raw materials that are used. Currently, the use of petroleum coke, a fossil carbon source, contributes to releasing large amounts of CO_2 into the atmosphere. To exchange this material with biocarbon is interesting as this source of carbon is relatively regenerative. This means it as a life cycle between 50-100 years, instead of thousands, such as the petroleum coke currently in use. Whilst the total amount of CO_2 produced will not decrease, the portion of these off-gases generated by the biocarbon may be considered as clean. Whilst an immediate change from fossil carbon to biocarbon may not be possible due to the impact on the produced product, partial replacement may be possible. This means that replacing 30% of the carbon in the Acheson process with biocarbon would lead to a decrease in emissions. The idea to phase out fossil fuels is also encouraged strongly by governments around the world. A simplified carbon cycle for biocarbon is shown in figure 2.11 below.
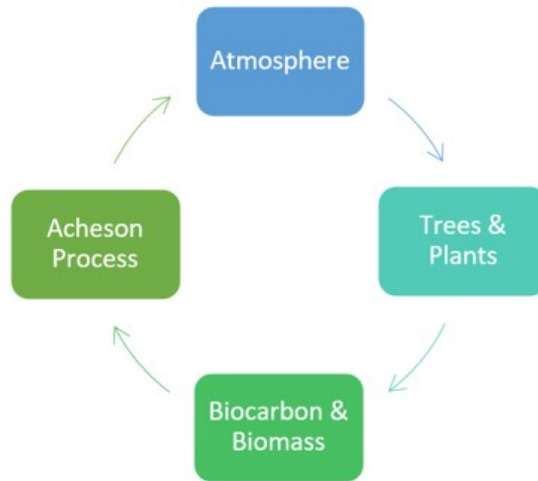
Figure 2.11: The CO_2 cycle of biocarbon

Emissions from silicon carbide plants are often released at all stages of the production process, with largest part of emissions originating from the furnace.

Data is hard to come by, and only a few sources were found. According to a study on the dutch silicon carbide industry, CO and CO_2 emissions are responsible for 28% and 27% of total plant emissions respectively, with H_2 emissions making up another 40% [49]. A report by the U.S. Environmental Protection Agency from 2009 states that total SiC industry emissions in the USA amounted to 100,226 $mtCO_2e$[4], with over 91% of these emissions originating from process-related emissions (furnace, treatment, etc.). Only about 35% of the carbon is retained in the produced SiC, with the rest converting to CO_2 and CH_4 when reacting with air and the compounds present in petroleum coke [50].

However, the overall emissions will naturally vary highly from production site to site. Some SiC production plants utilise fossil fuels to produce the necessary power, whilst others are strategically placed near renewable energy sources such as hydro-electric power-plants [7]. Furthermore, carbon retention and process emissions are also highly dependent on production site, what measures are in place, and what raw materials are used. Whilst the above-given values do not directly represent emissions globally, they may serve as a reference point for the importance of converting to greener raw materials such as biocarbon. Taking the USA as an example, replacing even 30% of the petroleum coke used with renewable biocarbon could reduce

---

[4]million tons of CO_2 equivalents

process-emissions with approximately 27,510 mtCO$_2$e[5] [50]. This further supports the incentive that even gradual change will contribute to reducing emissions by relatively large amounts.

The availability of charcoal and other biocarbon materials is not perfect. In a recent study by WWF Germany, it was found that Europe imports over 750,000 tons of charcoal every year, as only 250,000 tons are made in the EU. The imports come from countries like Ukraine, Nigeria, Cuba and Namibia. These countries often experience political instability which endangers charcoal supply. It is therefore problematic to simply switch over all production to biocarbon, as the social and economic aspects may make availability of these materials scarce and expensive [33].

Finally, an interesting aspect of SiC, according to some reports is that it can be produced from waste products such as risk husks [34]. In countries such as India, which produces a lot of rice husks, this waste is usually burned, generating air pollution and toxic silica ash. However, after Cutler utilised rice husk as a starting material for production of SiC in 1973, a lot of research has been conducted into making this a viable production route [51]. Not only may this reduce climate emissions and air pollution, but it may also provide rice farmers with more economic stability as waste can be turned into valuable product.

2.7   Analytical Methods

This section will go over some of the principles used in the analysis of different samples, such as pycnometry, ICP analysis, and XRD.

2.7.1   Density Analysis

There are many different definitions of density. For this investigation, the two definitions of most interest are bulk density and absolute density. Bulk density is defined as the mass of bulk solids that occupy a unit volume, including the volume of the inter-particle voids [52]. This is calculated using equation 2.9 where ρ is the density of a material, m is the mass, and v is the volume occupied by its particles, including inter-particle voids as mentioned above [52]. Bulk density might change with agitation, as a non-homogeneous particle size distribution could lead to the "Brazil nut effect", where larger particles move to the top of the sample [53]

---

[5]Rough estimate, assuming process emissions originate primarily from carbon sources forming CO_2 and CH_4

$$\rho = m/V \tag{2.9}$$

Absolute density is defined as the density is defined as the mass of a substance per unit volume. This excludes all inter-particle voids in a sample, as well as all pores (closed and open) [52]. To test for absolute density, often a gas displacement pycnometer is used.

An illustration of absolute and bulk density of a sample of particles is shown in figure 2.12 below.
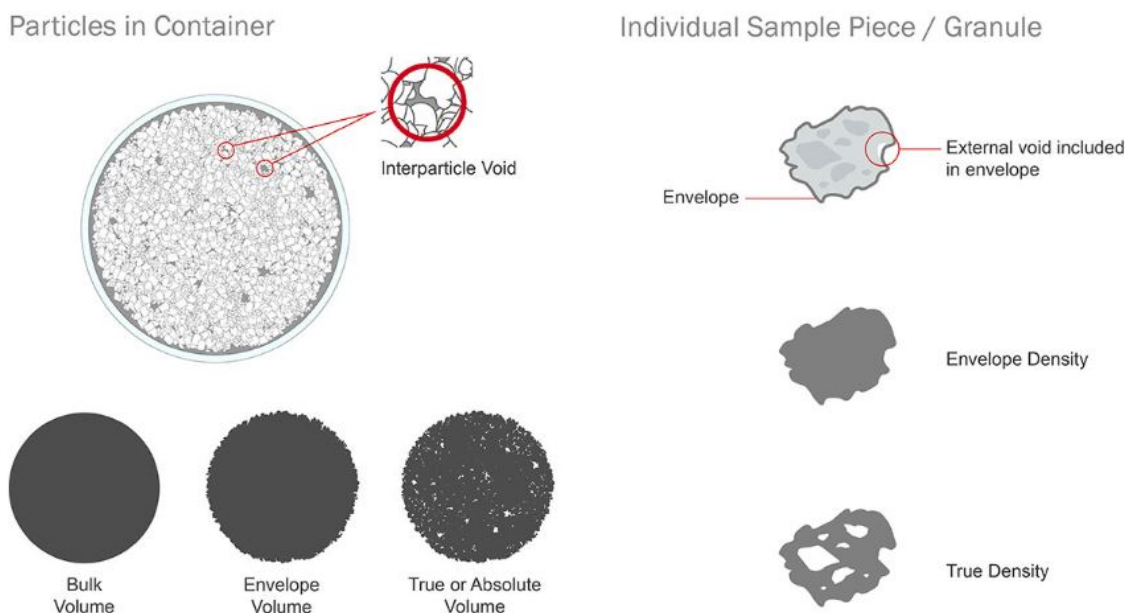
Figure 2.12: Illustrations of bulk, envelope, and absolute density in multi- and individual particle samples [54]

.

The principle behind pycnometry, revolves around filling a sample holder of known volume with a sample of known mass and filling the sample holder with an inert gas (usually helium). The He will infiltrate all the inter-particle voids, as well as open pores [55]. Furthermore, the gas may diffuse into the sample and fill some of the semi-closed porosity [52]. Once reaching a certain pressure, the gas is allowed to expand into a reference chamber with known volume, and equilibrate at a lower pressure. Then Boyle's law in a closed system with constant temperature, based on the ideal gas law (shown in equation 2.10) is used to determine the volume of sample in the system [52].

$$PV = nRT \tag{2.10}$$

However, this method of measurement will not be able to analyse the volume taken up by closed pores, and therefore the absolute density measured will contain a certain amount of closed porosity.

2.7.2 ICP Analysis

Inductively coupled plasma optical emission spectrometry (ICP-OES) is a analytical method that utilises plasma to analyse the elemental concentrations of a sample. The plasma is ionized gas at a very high temperature, which is maintained by the use of induction coils. The sample to be analyzed is introduced to the plasma, breaking all chemical bonds and releasing light due to the extremely high temperature. The light (electromagnetic radiation) emitted will appear primarily in the visible and ultraviolet spectrum and occurs in discrete lines. These lines are separated depending on their wavelength by diffractive optics, and can then be used to identify and quantify the concentration of elements in the sample. This technique is not to be confused with spectroscopy which is the qualitative analysis of samples by spectra [56].

As all atoms and ions emit light simultaneously, this method is an example of a sample-oriented multi-element technique. This means the results of all elements are measured at the same time, meaning analysis time is far shorter than other methods.

Within ICP emission spectrometry there is a linear relationship between intensity of emissions and concentration of an element. This allows for easy determination of elemental concentrations in samples [56].

Most samples to be analysed are originally solids. These must be added to a solution before they can be processed.

FIVEN has developed a standard ICP-OES method for their needs, and has with the help of this created a general specification for impurity contents in crude SiC produced. This is shown in table 2.3. Depending on the application of the product however, these specifications may vary.

Table 2.3: Specifications for Impurity Contents in Crude Supplied by FIVEN in ppm

Al	Ca	Cr	Cu	Fe	Mg	Ni	Ti	V	Zr
369	118	7	2	642	14	201	258	535	50

Typical impurities in SiC are Fe, as well as free-Si and Free-C. Minor metallic impurities that are common also include Ti, Al, Ni and V . Most of these impurities

are reflected in FIVEN's company specifications. Some of these impurities may be chemically removed after production, but depending on the forms of impurities, elements may be harder to extract [57].

2.7.3 XRD Analysis

X-ray diffraction (XRD) occurs when a beam of x-rays enters a material, and the waves are reflected off the uniformly spaced atomic planes, causing an interference pattern in the reflected x-ray waves. Depending on what atomic layer the x-rays hit, they are reflected with varying phase difference compared to x-rays that are reflected off the surface. This phase difference may be used to calculate the crystal structure of a material [58].

For this phenomena to occur, the phase difference causing the interference in the outgoing waves must be a whole number (n) of wavelengths (λ). This is in order to satisfy Braggs law as given in equation 2.11.

$$n\lambda = 2dsin(\theta) \tag{2.11}$$

A diffractometer is an instrument with two axes of independent rotation, and is used to measure intensity of a diffracted x-ray beam as a function of angle. It is typically comprised of a x-ray source, a sample holder and a detector. Running a measurement involves rotating the x-ray source and the detector around the sample, where the detector typically moves twice as much as the x-ray source. Therefore the axis that the detector is attached to is typically referred to as 2θ. The produced graph of intensity and angle is called a diffractogram [59].

The primary identification peaks of SiC polytypes can be found the in range of 0-90°[60]. Furthermore, it must be considered that various forms of carbon[6] and SiO_2 are present in an Acheson furnace. These will also be present in the produced diffractograms.

When investigating samples the most important data is the ratio between α- and β-SiC. Potential polytypes for these categories include 6H, and 3C respectively.

X-ray diffraction of powder samples requires specific particle sizes. Usually these should be between 10-50μm. If Rietveld analysis is to be performed, these sizes should be even smaller, around 1-5μm [61]. It is common to use this form of XRD when analysing SiC samples [60].

---

[6]Primarily graphite, biocarbon, or petroleum coke particles

2.7.4   SEM-EDS

A scanning electron microscope (SEM) is an instrument which uses a focused and energized electron beam to create highly magnified images of samples. The incident electron beam produces two kinds of scattered electrons: secondary electrons (SE) and backscattered electrons (BSE). SE are electrons that are ejected from atoms as the energized electrons take their place. BSE are electrons from the incident electron beam that are diffracted and scattered by interactions with the atoms of the sample. These retain larger proportions of their original energy levels. Finally, the electron beam also causes the release of x-ray photon emissions. There are two types: characteristic x-rays which have specific energies that are different for each element, and continuum x-rays which occur at all photon energies and thereby create a background for the measured spectrum [62].

Energy dispersive x-ray spectrometry (EDS) revolves around utilising these emitted x-rays to measure and quantify elemental contents in samples. This includes all the emissions from the beam-excited interaction volume, which may reach as far as 10μm into the material. A major challenge in this regard is the occurrence of mutual peak interference's, as some elements have similar peak positions in the collected spectrum. Once qualitative analysis has been achieved however, quantitative analysis may be performed. This means that the characteristic intensity of the peaks on the spectrum are measured and used to calculate the overall concentration of the element. Therefore, SEM-EDS is a powerful tool in the analysis of elemental contents and respective quantity in samples, even on μm- and nm-scale [62].

2.8 Earlier Work

The R&D department at FIVEN Lillesand has loosely tested the use of biocarbon in their Acheson pilot furnace previously. Data for furnace measurements was available for a run using 15% biocarbon, as well as another reference run (0% biocarbon). This data is shown below in figure 2.13 and includes resistance, power consumption, and various temperature measurements. It will be plotted alongside the data collected in this investigations under results, section 4.1.
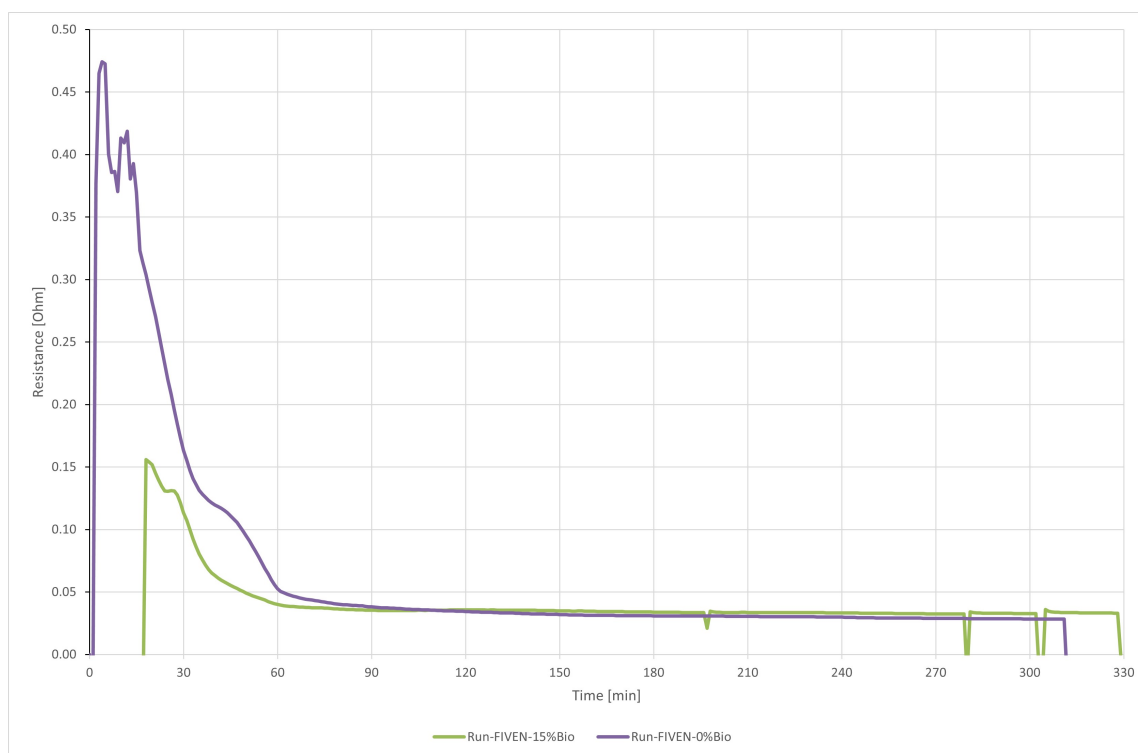
Figure 2.13: Resistance curves for furnace runs performed previously by FIVEN to study the effect of biocarbon on the resistance and yield of the pilot Acheson furnace

The previous experiments performed utilised the same charcoal/biocarbon, petroleum coke, and silica sand as this investigation. Therefore, data from the furnace is directly comparable. However, the crude SiC and firesand were weighed and analysed together, and therefore compositional data is not comparable wit the data collected in this investigation.

28

Chapter 3

Experimental Apparatus, Procedures and Materials

This section concerns the primary methods and materials used throughout this investigation. It includes procedures for the pilot furnace operation, as well as characterisation methods for both the raw materials and final product. Some analyses were outsourced to the R&D department at FIVEN Lillesand (ICP-Slurry analysis).

All experiments were risk-assessed prior to start. The relevant risk-assessment form can be found in appendix E.

3.1   Raw Materials

The raw materials used in the experiments listed below are described here. Primarily the composition of the carbon sources (charcoal/biocarbon and petroleum coke) are described, as seen in table 3.1a and 3.1b.

Content	wt%
Fixed Carbon	>90%
Ash	2-3%
Volatiles	7-8%

(b) Composition of Petroleum Coke Used

Content	wt%
Fixed Carbon	90%
Ash	0.2%
Volatiles	9.8%

Figure 3.1: Compositional data for the biocarbon (a) and petroleum coke (b) used

The silica sand used in the Acheson furnace was reported to have a SiO_2 content between 99-100wt%. Moisture was measured to 4.4% for the silica sand, 15.1% for the petroleum coke, and 2.6% for the biocarbon.

3.2 Sample Preparation

For the sake of clarity, this section gives an overview of the different samples taken from both the raw materials and resulting products. Figure 3.2 shows a typical cross section of an ingot produced in the process. This is meant to give an understanding of where in the ingot the samples are taken from. It should be noted that the area marked as firesand is also referred to as an area of amorphous SiC in the theory section.
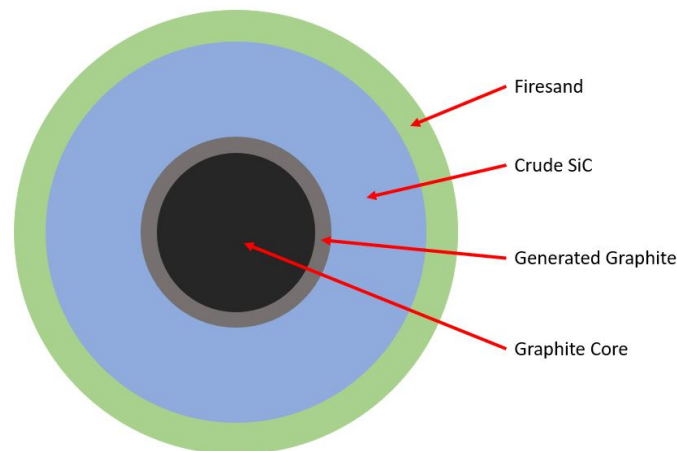

Figure 3.2: Typical cross section of an ingot produced in the Acheson process

Table 3.2 shows an overview of the different samples, sample categories, and meaning. Take note that certain product sample names will be a combination of the furnace run and product sample names. For example, the first sample taken from the firesand section of the ingot produced in the second furnace run would be titled: "Run-Bio-FS-1".

Table 3.1: Overview of Sample Names, Categories and Explanations

Sample Name	Category	Explanation
Bio-#	Raw Material	Collective name for samples of biocarbon. These are numbered differently depending on the analysis.
Pet-#	Raw Material	Collective name for samples of petroleum coke. These are numbered differently depending on the analysis.
Run-Bio	Furnace Run	The primary run of the pilot furnace, in which 30% biocarbon was used
Run-Ref	Furnace Run	The secondary run of the pilot furnace in which no biocarbon was used
Crude-#	Product	Collective name for samples taken from the crude SiC section of the ingot.
FS-#	Product	Collective name for samples taken from the fire-sand section of the ingot.

For the two furnace runs, the charge was mixed according to mixing ratios calculated from the overall reaction for the process, shown in equation 2.1 found in theory section 2.1. Moisture levels of the raw materials were measured prior to the experiments and compensated for in calculation of the final material mass ratio. These mixing ratios are shown below

3.3 Pilot Furnace

The pilot furnace was operated according to the internal routines at FIVEN AS Norway, similar to the procedure described in theory chapter 2.3, simply scaled down. Overall dimensions of the furnace were approximately 1m in length, 0.75m in width, and 0.75 m in height. The total mass of charge that fits in a standard furnace using a mixture of only petroleum coke and sand was estimated to around 400kg. The steps of running the furnace are shown below with illustrations.

1. **Mixing**. The charge was mixed in batches of 25kg. The mixing ratios were calculated from the overall reaction shown in equation 2.1 in theory section 2.1. These ratios can be seen in appendix A. Moisture was measured prior to mixing, and the ratios were adjusted for moisture levels in the raw materials. Finally, to compensate for potential process losses the desired carbon factor (CF) was set at 0.40[1]. These mixing ratios can be found in appendix A. Silica sand, petroleum coke and biocarbon (for run 1) were firstly weighed out in buckets and then mixed together in a cement mixer. An extra batch was mixed and placed in a wheelbarrow.

(a)　　　　　　　　　　　　　　　　(b)

Figure 3.3: Weighing and mixing of raw materials. Materials weighed out in separate buckets (a), and cement mixer with charge (b)

2. **Building**. The furnace was built by first preparing a bed of charge. The electrode material was prepared by mixing graphite with calcinated coke using a paint mixer and filling the steel insert shown in 3.4 (a). Refractory stones used to construct the front wall of the furnace as the charge is built up. More

---

[1]The theoretical CF is 0.33, also derived from the overall reaction

charge was then added until reaching the top of the insert which was promptly removed. Further charge was added until the charge pile reached a height of 20cm above the electrode heads.

Figure 3.4: Building the pilot furnace. Steel insert for electrode (a), and finished furnace (b).

3. **Firing**. The furnace was initiated run according to FIVEN's internal standard procedure. Power was adjusted manually throughout the run to ensure maximum current was not exceeded. At around 10kWh, the CO gas emanating from the furnace was ignited. Throughout the run, resistance, current, and temperature measurements at various different points were monitored. In the event of a gas eruption, the extra charge from step one was used to fill the created hole. At 300kWh the furnace was switched off and left to cool over night.

Figure 3.5: Firing of the furnace. Furnace run 1 (a) and run 2 (b)

33

4. **Cooling**. Due to the size of the pilot oven. Cooling over night was sufficient to reduce core temperature to the point it could be processed using heat resistant gloves. In the event that temperature was still to high the dismantling process would be done in stages, allowing further cooling to occur.

5. **Dismantling and sorting**. The furnace was dismantled stage by stage. First, layers of unreacted charge were removed. Then the cap that had formed above the ingot was removed. The ingot was removed in pieces. The graphite and firesand were brushed off into respective buckets using metal brushes. The crude was then gathered in buckets. Some pieces of crude displaying large crystals and distinct layers were removed for analysis. Samples were also taken from the firesand. The remaining crude was crushed down to a rough powder for further processing and analysis. The rest of the unreacted charge was removed from the furnace.
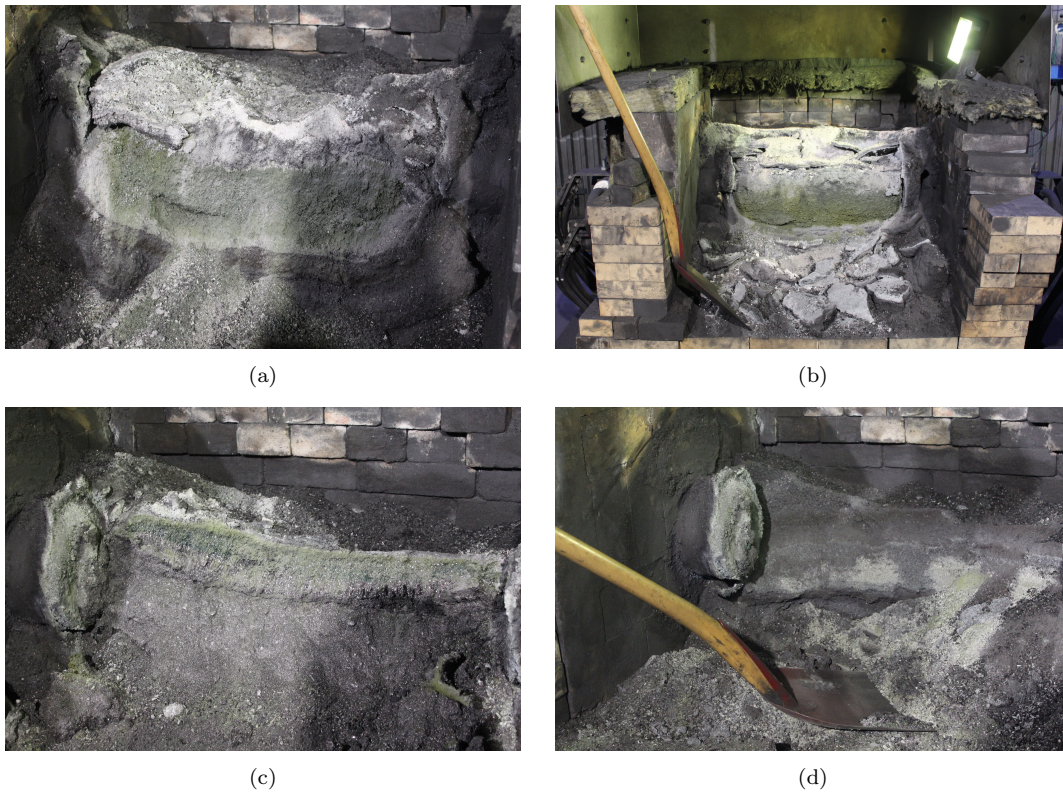

(a)

(b)

(c)

(d)

Figure 3.6: Dismantling of the furnace. Ingot with cap from run 1 (a), ingot with cap from run 2 (b), dismantling ingot from run 1 (c)(d)

The procedure was the same for both furnace runs performed for this project. Mass of the charge was roughly measured for each run.

3.4   ICP-Slurry Analysis

ICP-analysis was done by FIVEN with a specialised ICP-slurry method which build on the principles of ICP-OES. This gave an overview of metallic impurities in the SiC.

3.5   Density Measurements

The absolute, and bulk density of both petroleum coke and biocarbon were measured using pycnometry and rough bulk volume measurements respectively.

3.5.1   Bulk Density

The absolute, and bulk density of both petroleum coke and biocarbon were measured using pycnometry and rough bulk volume measurements respectively.

Bulk density was measured with a simple setup in which volume and mass of sample were measured before and after agitation. This gives an idea of the volume occupied by material during oven construction when using the two different carbon sources. The density was then calculated using equation 3.1 from theory section 2.7.1, shown again below.

$$\rho = m/V \qquad (3.1)$$

The method was designed to be simple and reproducible and was performed on a larger scale in Kristiansand, with the use of larger buckets and sample sizes. At NTNU in Trondheim, the method was performed using smaller volumes of sample.

Firstly, glass beakers were numbered and weighed. Then these were filled with biocarbon to around 2/3 of the total volume. This was done under a fume hood to avoid dust generation. The height of the sample was marked on the beaker, then it was agitated (shaken, tapped, etc.) for 30 seconds. The new height of the sample was also marked on the beaker. Then the beakers were weighed and emptied. After a rough rinse, the beakers were filled with water to the bottom marking and weighed. Then they were filled to the top marking and weighed again. These values were then used to calculate the bulk density of the samples before and after agitation. The

method was repeated five times for biocarbon samples and five times for samples of petroleum coke.

3.5.2 Absolute Density

A Micrometrics Accupyc 1030 pycnometer was utilised to measure absolute density of the samples. Absolute density is a measure of volume particles of a material occupy, excluding the volume occupied by interstitial space, open, and closed pores.

The method was performed using samples that had been pre-dried in a muffle oven at 120°C for a minimum of 12 hours. A 100cc sample cup was filled roughly 2/3 of its total volume with pre-dried sample and placed in the pycnometer. The pycnometer then fills the sample with helium gas, which was later measured in a separate chamber to calculate the amount of gas that was possible to pump into the sample. This would then be combined with the mass of the sample to calculate the absolute density.

3.6 XRD Analysis

In this project, a Rigaku MiniFlex 600 diffractometer with a Cu Kalpha anode was used.

XRD samples were prepared for the crude SiC and firesand for both furnace runs. Firstly, larger samples were reduced to smaller sizes using the "cone and quarter" method in a fume hood. This method of material splitting revolves around mixing the material, creating a rough cone and proceeding to quarter it, removing two of the four parts at random until sample size is as small as desired. This will give a relatively representative sample in terms of particle size distribution.

The reduced samples were crushed in an agate mortar and pestle, before being passed through a 100μ sieve on a piece of paper. From here, the sieved samples were placed in smaller sample containers.

To analyze the samples in the XRD-diffractometer, samples were carefully placed in aluminium sample holders and pressed down with a glass slide. Once pressed, the sample holder was scraped over with the glass slide to ensure even sample height. As a test the sample holder was turned 90°to ensure the sample was packed tight enough not to fall out. The holder was then installed in the machine and the analysis was started. According to the literature, the important peaks for identifying SiC polytypes are below 90°, and therefore maximum angle was set to 90°to shorten analysis time. Potential polytype candidate diffractograms were retrieved from the Crystallography Open Database (COD). Once complete, the data was analyzed in

TOPAS (Total pattern analysis solution; Bruker AXS; Version 5) and Rietveld refinement was done to more accurately estimate the distribution of SiC polytypes and other present phases in the sample.

3.7 SEM-EDS Analysis

For SEM and SEM-EDS analysis at NTNU, a Zeiss Supra 55VP FEG-SEM and a Zess Supra 55 FEG-SEM were used. At FIVEN Lillesand a Zeiss Evo 10 was used. Samples were attached to sample holders using carbon tape, but were not coated.

To allow for good SEM-EDS Analysis the EDS detector was inserted into the SEM stack and the aperture of the electron beam was set $120\mu m$ with high-current mode. This allowed for the best quality results, but larger apertures are also possible to use.

Samples of the crude SiC and firesand from both runs were analysed using point and area analysis to identify major elemental contents. Attempts were also made to perform EDS mapping of smaller areas, ensuring the map had good resolution to be able to distinguish particles clearly. As the main goal of this was not to get exact atom distribution, but rather an indication of particle distribution. To get better results, the ground up samples from ealrier were used that had a maximum particle size of $100\mu m$, but this was still too large as several shadow areas were visible.

3.8 Ash Content Measurement

The ash content of the biocarbon samples was tested by burning samples in air. The internal method supplied by FIVEN specified the use of a muffle oven, but as this was not available for this type of testing at NTNU, a induction furnace (IF75)[2] was used instead. Biocarbon samples with a mass close to 15g were placed in alumina crucibles. The crucible and sample was weighed on a scale with minimum 3 decimals of accuracy and sample mass was noted. The crucible was placed in the IF75 and heated to around 900°C at which point an oxygen lance was inserted with a flow rate of 1.2L/min. The temperature and oxygen flow was held constant until all the biocarbon had reacted and no more glowing particles were left which took approximately 1.5 hours. The crucible was then left to cool and weighed again on the same scale to determine the remaining mass of ash.

---

[2]Inductotherm 75kW/3000Hz VIP PT furnace

Chapter 4

Results

This section discusses different analysis results for samples from the pilot furnace, as well as samples taken of the raw materials feeding into the pilot furnace. To ensure clarity, see section 3.1 for table 3.2 which describes the samples and their names.

4.1   Furnace Data Process Yield

This section discusses observations of note during the firing process of the furnace in run 1 and 2. It also includes a calculated rough yield of both furnace runs. These values are primarily indicative and incorporate large uncertainties due to the human factor in separation of the material layers during the sorting process. During firing of the furnace, the power, resistance, current, and voltage of the furnace were measured, as well as the temperature at several different points in the furnace, smokestack, and filtering unit.

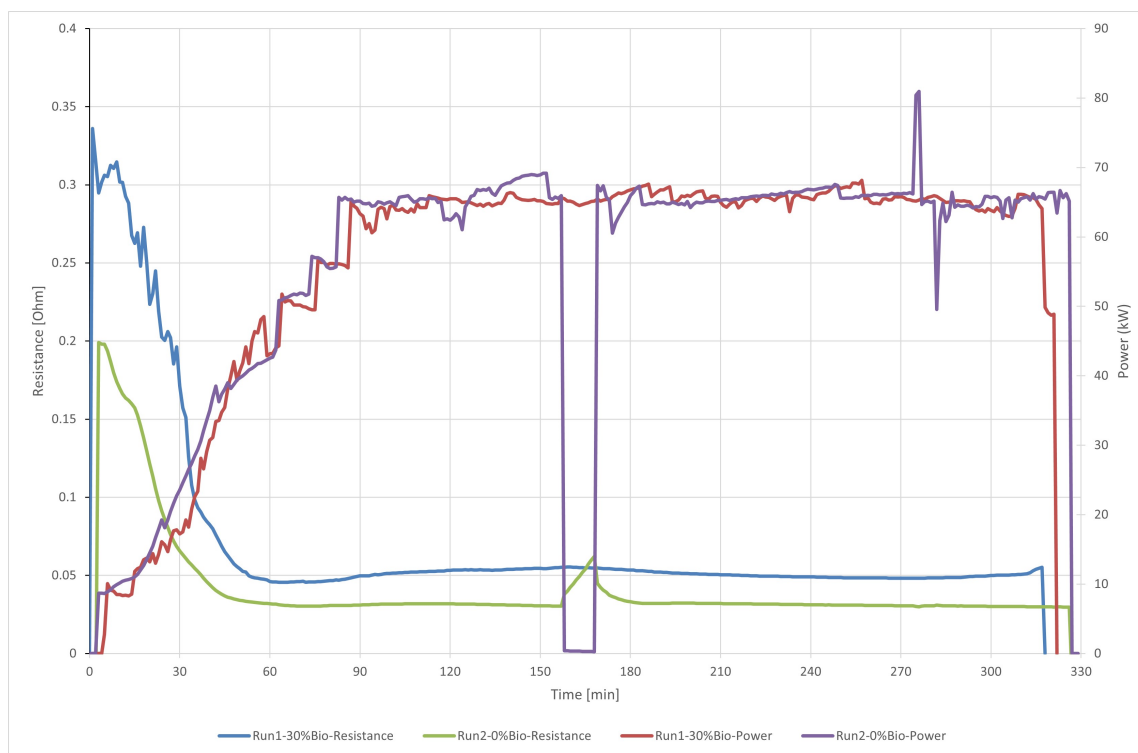Figure 4.1 shows the measured resistance and power for furnace run 1 and 2.

Figure 4.1: Measured resistance and power consumption for furnace run 1 and 2

A special mention should be made for run 2, as a sudden drop in power, and spike in resistance can be seen at 160 minutes into the process. This was due to a fire alarm being activated at the site, which lead to the furnace being powered down for a period of around 10 minutes. This however, did not have any adverse effect on the remaining part of the run, as shown by the relatively similar curves after the shutdown. Another spike in power is visible at around minute 280. This was most likely caused by uneven flow of electricity through the furnace, which required human adjustments, leading to the observable uneven curve.

To compare resistance over time from the furnace runs performed for this investigation as well as the prior data supplied by FIVEN, figure 4.2 shows only the measured resistances of the furnace runs.
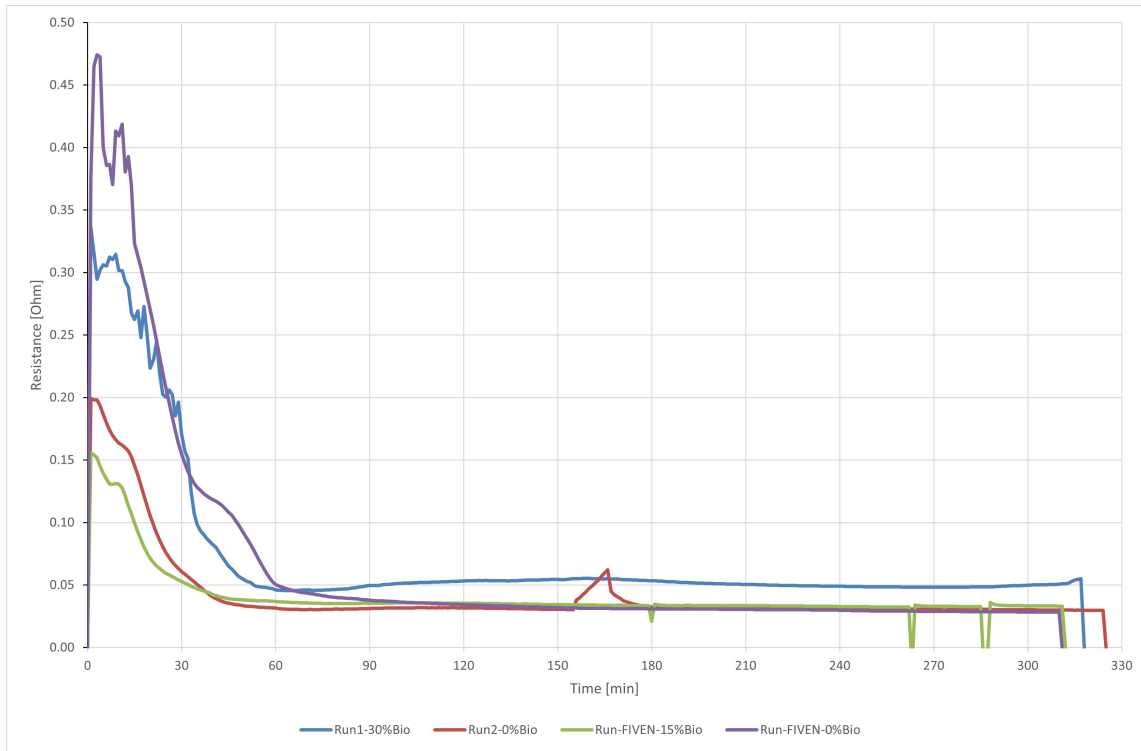
Figure 4.2: Comparison of furnace resistance over time for run 1 (30% biocarbon) and 2 (0% biocarbon as well as data supplied by FIVEN for a furnace with 15% biocarbon and another reference furnace with 0% biocarbon)

It is possible to observe that the reference run ran at a lower resistance all throughout the experiment. The resistance of this run flattens out around 0.030Ω. The biocarbon run starts at a higher resistance, and flattens out higher, at around $0.048\ \Omega$. The data supplied by FIVEN shows that both the run with 15% biocarbon, and the one with 0% biocarbon has resistance curves that similarly flattened out at around 0.030Ω.

Figure 4.3 shows a piece of ingot from furnace run 2 with the different sections marked.
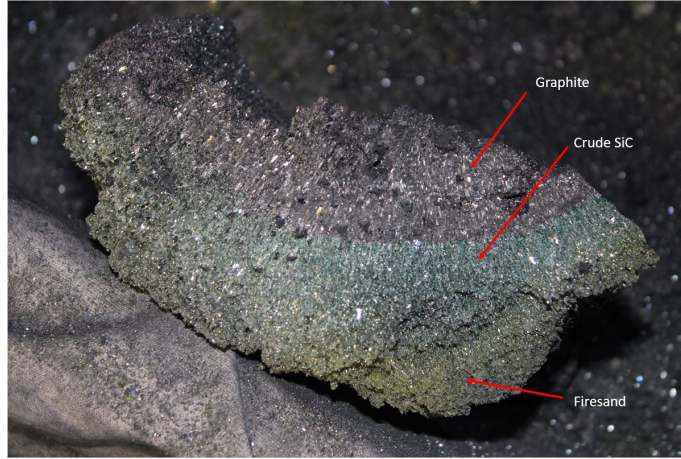
40

Figure 4.3: Piece of ingot from furnace run 2 with graphite, crude sic, and firesand sections marked

After weighing, the total mass of crude and firesand produced in both runs was calculated. Yield was calculated in terms of kWh/kg SiC according to equation 4.1 where P_{total} is the total power consumed in furnace operation, which was set at 300 kWh, and m_{crude} is the mass of crude SiC produced. This is commonly how yield is reported in theory as well [7][49].

$$Yield = \frac{P_{total}}{m_{crude}} \tag{4.1}$$

This is shown in table 4.1 below. The energy needed per kilogram crude SiC is also shown.

Table 4.1: Total Amount of Crude SiC and Firesand Produced in Both Runs

Furnace Run	Mass Crude [kg]	Mass Firesand [kg]	kWh/kg Crude
Run-Bio	6.72	5.00	45.18
Run-Ref	12.24	4.08	24.51

From this data it is possible to see that the furnace run with 30% biocarbon produced approximately 50% less crude SiC than the reference run. However, it produced 25% more firesand than the reference run. During the dismantling and sorting step of the ingot from the biocarbon run, it was apparent that the produced SiC was far more brittle and porous. This caused a larger portion to be removed during crude and firesand separation. Therefore, this may explain the elevated firesand amount.

During the same process for the reference run, the separation between firesand and crude SiC was more pronounced, and the crude SiC was also denser and more cohesive. This allowed for easier separation of the sections of the ingot. The values in table 4.1 therefore incorporate quite large uncertainties, but even when accounting for these, the biocarbon furnace produced less SiC than the reference furnace.

According to theory, normal yield values typically lie between 6-12 kWh/kg SiC [3]. The calculated values are far higher than this. It is important to consider that these values are for a pilot furnace and not full-scale production.

It is also important to note that due to differing bulk densities (as will be described later), less total charge fit into the furnace for run 1 (30% biocarbon). Therefore yield is primarily based on kWh/kg, and not related to mass or volume of furnace charge.

4.2   ICP-Slurry Analysis

Table 4.2 shows the results from the ICP-Slurry analysis performed by FIVEN. The purpose of this analysis is to highlight other metal contents in the given sample. For this, representative samples were selected from both the crude SiC, and firesand regions of the ingot, using a material splitter. To allow for easy comparison the results for crude SiC and firesand respectively, have been placed next to each other in the table.

Table 4.2: ICP-Slurry Results for Metal Impurities in Crude and FS Samples in ppm

Sample	Al	Ca	Cr	Cu	Fe	Mg	Ni	Ti	V	Zr	pH
Run-1 Crude	139	48	1	1	268	2	3	482	221	221	7.4
Run-2 Crude	144	25	1	1	151	1	18	366	293	159	6.4
Run-1 FS	427	1170	5	2	836	27	45	471	338	233	10.1
Run-2 FS	560	384	6	2	817	29	154	360	377	213	7.8
FIVEN Spec	369	118	7	2	642	14	201	258	535	50	

These results have also been shown in the two bar graphs in figure 4.4 on the next page. Not all of the shown impurities have the importance for the final product. FIVEN has an internal standard for impurity contents which is given in table 2.3 found in section 2.7.2, and marked in green in table 4.2 above. All the values that are over specifications are marked in orange. The collected values show that the firesand

samples had a concentration of impurities higher than company specifications for Al, Ca, Fe, Mg, Ti, and Zr. The crude samples had a higher concentration of impurities for both Ti and Zr than the company specifications specify.

Both runs show especially high values for titanium (Ti) and zirconium (Zr), of which the high values of Zr are the most noteworthy. These can be caused by a lack of instrument calibration. According to FIVEN, the impurities that are most important to consider are aluminium, titanium, and vanadium, as these are difficult to chemically remove from the product.
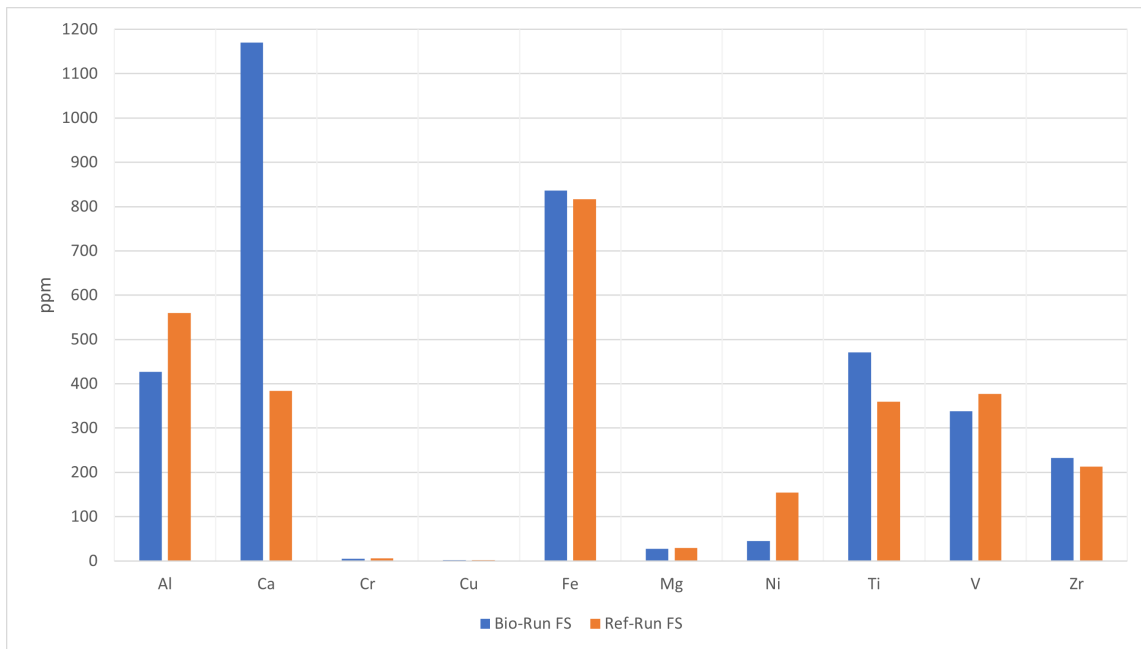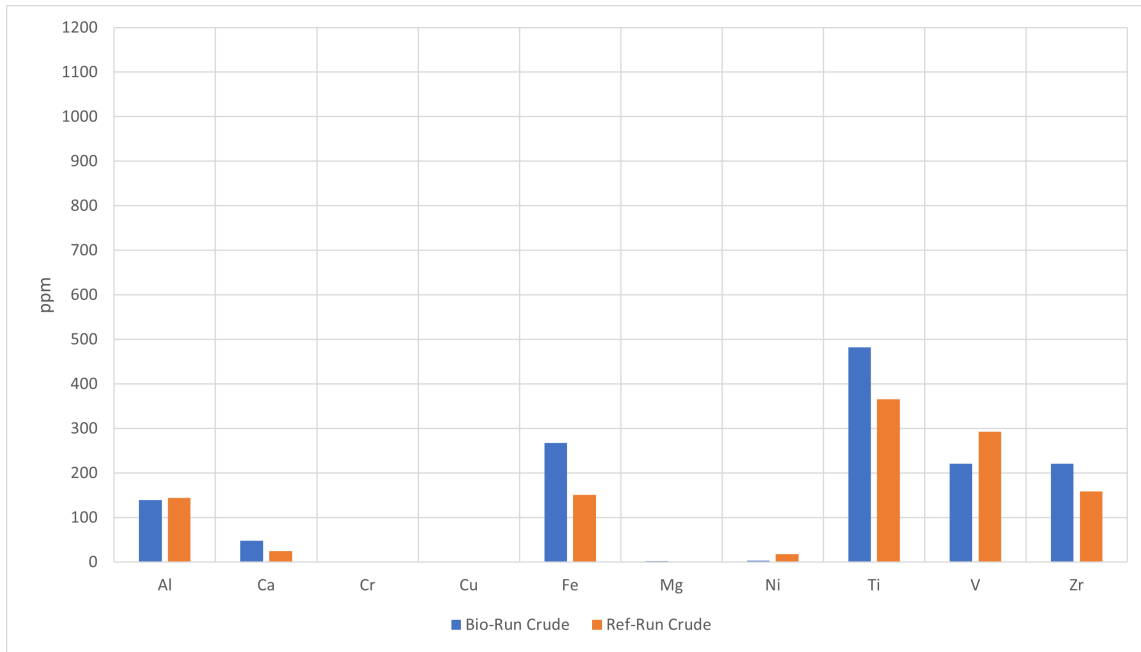
Figure 4.4: Bar graphs showing ICP-Slurry analysis results for samples of crude SiC and firesand (FS) from both the biocarbon and reference runs

4.3   Density Measurements

As mentioned in previous sections, there were two forms of density measurements completed. The results of these methods are shown in this section.

4.3.1   Bulk Density

Bulk density is a rough measurement that is meant to give an indication of the space taken up by material in the industrial process. The data presented in table B.1 shows the different bulk densities recorded for biocarbon and petroleum coke as well as standard deviation of these values. These measurements are results from the experiment done at NTNU Trondheim, and the raw data can be found in appendix B.1. A separate test that was performed on a larger sample of biocarbon[1] at FIVEN in Lillesand is also shown in the table. Due to no repeats of this measurement, no standard deviation was calculated.

Table 4.3: Bulk Density Measurements for Samples of Pet. Coke and Biocarbon

Sample	Density before agitation [g/cm^3]	Density after agitation [g/cm^3]
Bio-Avg	0.13 ± 0.01	0.15 ± 0.01
Bio-FIVEN	0.21	0.24
Pet-Avg	0.53 ± 0.01	0.58 ± 0.01

Whilst the difference is minor, it is possible to observe a bulk density increase in the samples after agitation. This difference is the most pronounced in the petroleum coke samples. Visually, these samples seemed to contain a larger amount of smaller particles which could explain the apparent higher degree of densification. The biocarbon, whilst perhaps having a wider span of particle sizes, also has far larger particles. This could reason for the difference in density change between the two sample types. Further, the values from the test performed by FIVEN are similar, yet show a slightly higher density than the ones shown in table B.1. Whilst this value may contain less uncertainty due to the larger sample volume used, there were no repeats performed, therefore the above values, collected at NTNU, will be considered as the primary data in this case.

---

[1]This sample had a mass of 3.92 kg

4.3.2   Absolute Density

Absolute density was measured using an Accupyc 1340 from Micrometrics. The collected data and calculated standard deviation is shown in table 4.4. The full raw data table is available in appendix B.2.

Table 4.4: Absolute Density Measurements for Samples of Pet. Coke and Biocarbon

Sample	Density [g/cm^3]
Pet-Avg	1.3823 ± 0.0013
Bio-Avg	1.5736 ± 0.0169

The final two runs of the petroleum coke used a different equilibration specification, but this should not have a large impact on results, as the degree of accuracy only changes slightly. From the collected data it is possible to see that biocarbon possesses a higher absolute density at around 0.1913 g/cm^3 more than the petroleum coke. This means that if one had exactly similar volumes of both biocarbon and petroleum coke, one would be able to press more gas into the volume of biocarbon.

4.4   Ash Content Data

Ash content of the biocarbon was tested for two samples. The scale used for measurement of mass was accurate to three decimals. The results are shown in table 4.5.

Table 4.5: Ash Content of Two Samples of Biocarbon

Sample	Mass Biocarbon [g]	Mass Ash [g]	Ash Content [wt%]
1	7.000	0.141	0.020
2	14.000	0.244	0.017

These values are similar to those presented by the supplier of the biocarbon at 2-3wt%.

4.5   XRD Analysis

X-ray diffraction was used to identify the major polytypes of SiC present in both the crude and firesand regions in both runs. Rietveld refinement was done with the help of TOPAS software to more accurately determine phase compositions. The collected diffractograms and phase distributions for samples of crude SiC and firesand from run 1 (30% biocarbon) and run 2 (0% biocarbon) are shown in figure 4.5.
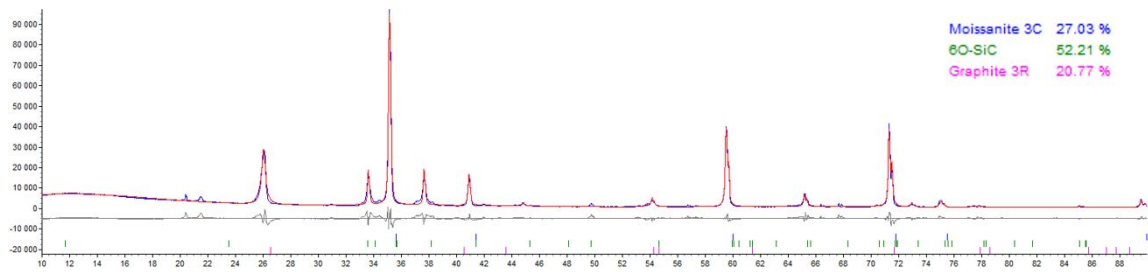
Using the COD database, the best candidates for SiC phases present in the samples were identified to be moissanite 3C (β-SiC), 6O-SiC (α-SiC), and 4H-SiC (α-SiC). Take note that 6O-SiC is described as a transitional precursor to 6H-SiC. Therefore, these two have very similar diffraction patterns, and may both be considered as α-SiC [40].
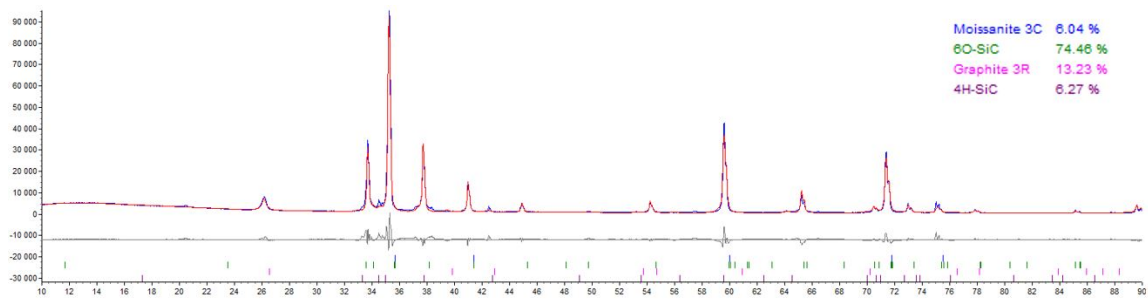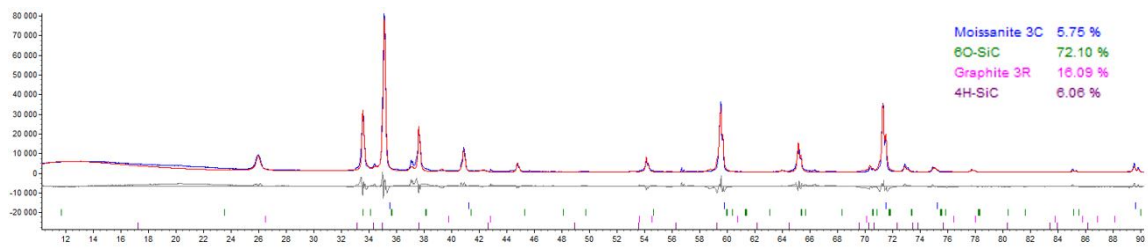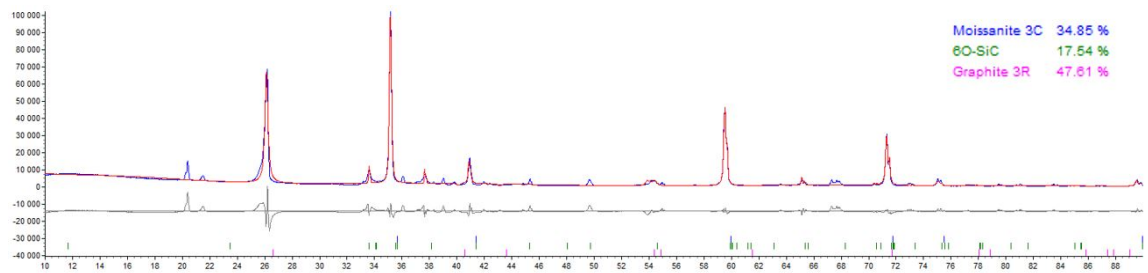
Figure 4.5: X-ray diffractograms of samples of crude SiC from run 1 (a) and run 2 (b), and firesand from run 1 (c) and run 2 (d)

The diffractograms of crude SiC in figure 4.5 show expected distributions of α-

and β-SiC. In the crude area of the ingot more α-SiC is expected due to higher temperature and longer time of reaction. This is shown in the diffractogram of run 1 with 74.46% and run 2 with 72.10%. Furthermore graphite is present in these samples as the crude was separated from the generated graphite mechanically, meaning residues were left. In the diffractograms for firesand, there is a larger concentration of graphite, but due to the position of this area in the furnace, this value reflects the amount of carbon present in form of biocarbon or petroleum coke particles. There are also some unidentified minor peaks which may be attributed to silica as this is another component of the charge which can be present in the firesand. The firesand sample from run 1 still shows a high value of α-SiC, whilst the sample from run 2 shows a far larger concentration of β-SiC.

Higher resolution versions of the XRD diffractograms can be seen in appendix C.

4.6 SEM Imagery and EDS Analysis

This section includes images and visual analysis of the morphological traits of biocarbon and petroleum coke, as well as crude SiC and firesand samples. EDS-point analysis and mapping is also shown to identify particles and compositions.
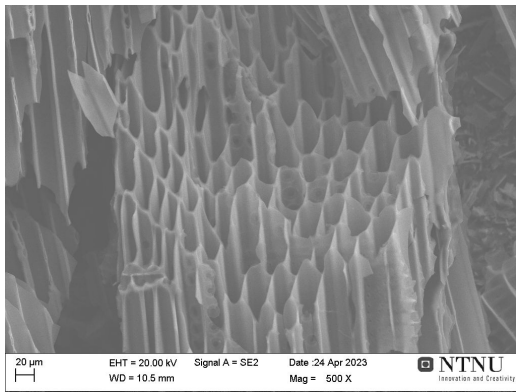
4.6.1 Raw Materials

The two carbon sources (biocarbon and petroleum coke) were analyzed using a SEM microscope. The goal of this was to analyze structure, morphology, and open porosity. The sampels could then be compared to visualise morphological differences.
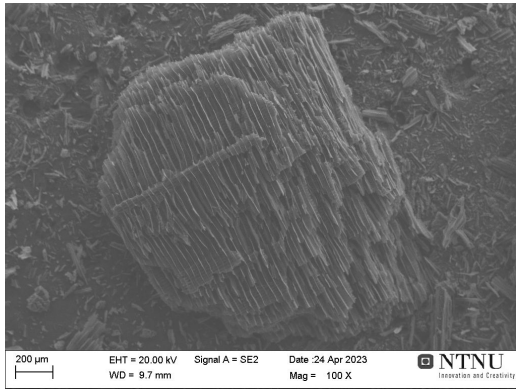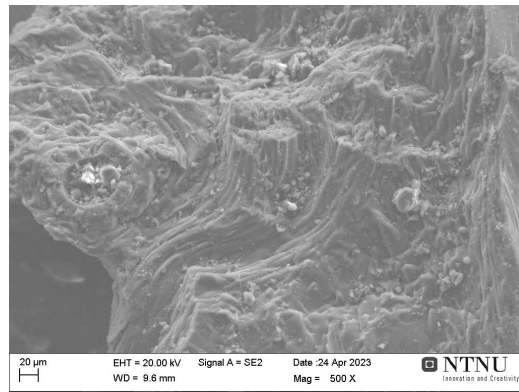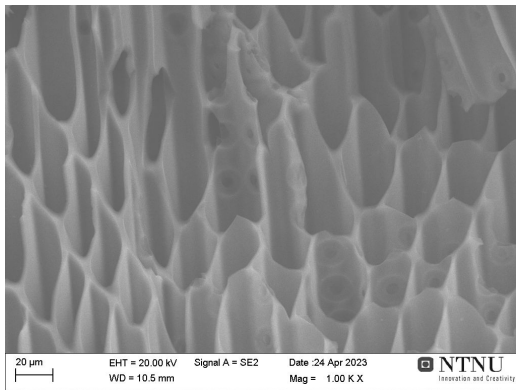
(a) Biocarbon 100x
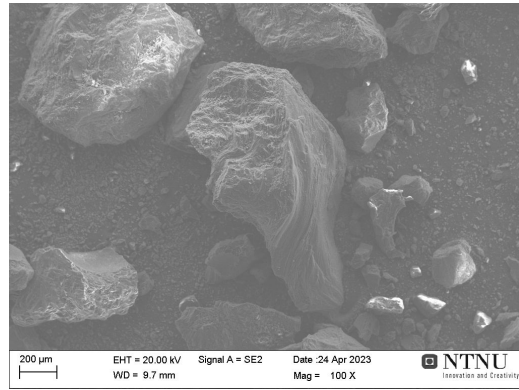
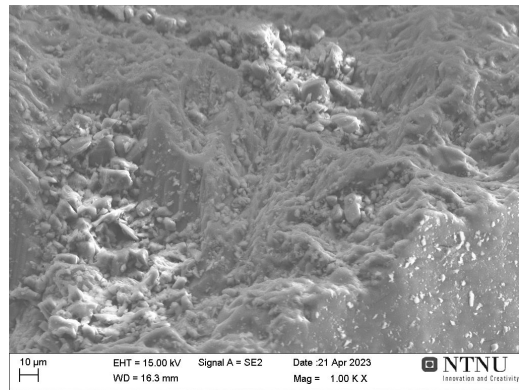(b) Petroleum coke 100x

(c) Biocarbon 500x

(d) Petroleum coke 500x

(e) Biocarbon 1000x

(f) Petroleum coke 1000x

Figure 4.6: Comparison between three different magnifications (100x, 500x, 1000x) of both biocarbon and petroleum coke samples

50

The biocarbon samples clearly show the telltale tube-like pore structure. On image (e) in figure 4.6 it is also possible to see pores between the tube structures. These are around 1-2 μm in size. The petroleum coke on the other hand shows no larger pore structure. However, image (d) does show a larger inclusion in the coke on the left hand side. The petroleum coke displayed a far more amorphous and dense morphology when compared to the biocarbon.

In figure 4.7, a closer comparison between biocarbon and petroleum coke samples is shown.
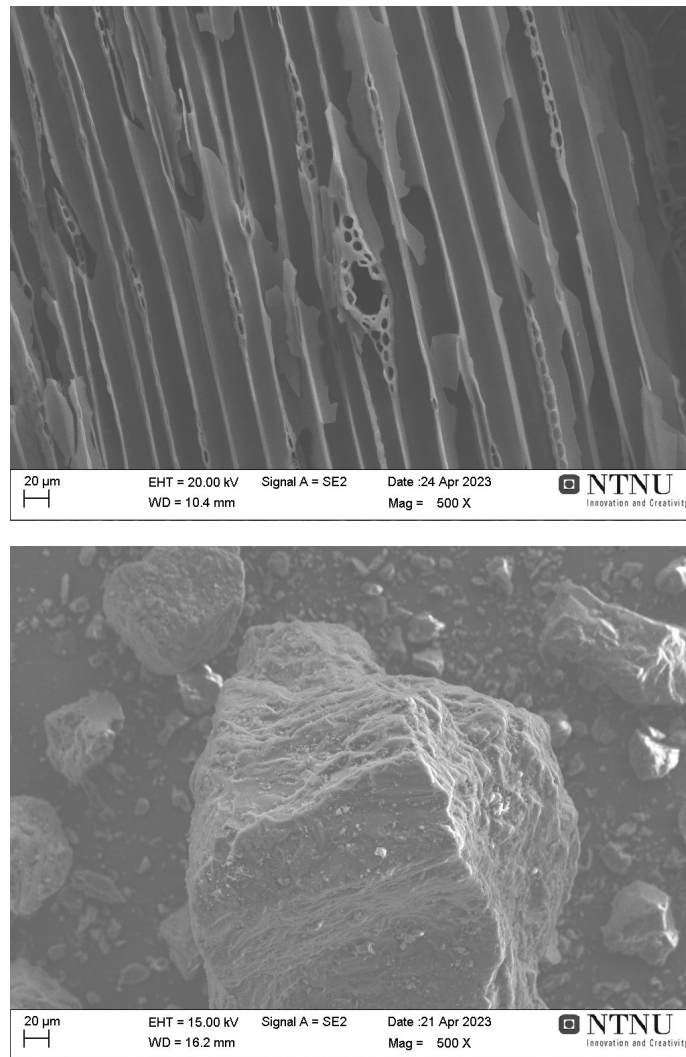

Figure 4.7: Comparison of biocarbon (above) and petroleum coke (below) at 500x magnification

It should be noted that the biocarbon particle is far larger than the petroleum coke. A clear tube-structure is also visible in the biocarbon as well as some smaller pores distributed throughout the material. These can be identified as radial pores, and are common in most biocarbon with wood precursors [21]. The petroleum coke does not display any open porosity on the same scale as the biocarbon. This may be because pores in the petroleum coke are on a nano-meter scale, and therefore not visible at the given magnification. In other samples of the two carbon sources it is also similarly apparent that biocarbon has larger and more abundant open porosity as may be seen in images.

4.6.2 Crude SiC and Firesand

This section compares the crude SiC produced in both furnace runs, as well as the firesand produced in both runs. It was apparent that similar crystal geometries were visible in the analyzed samples, however these macro-structures don't directly mimic the micro-structure, and it is therefore difficult to determine the present polytype based solely on the macroscopic structures.

Collected spectra for all EDS-analyses in this chapter are shown in appendix D.

Crude SiC

Figure 4.8 shows a comparison between SiC from both furnace runs. Take note of the large and defined crystals typical of α-SiC.
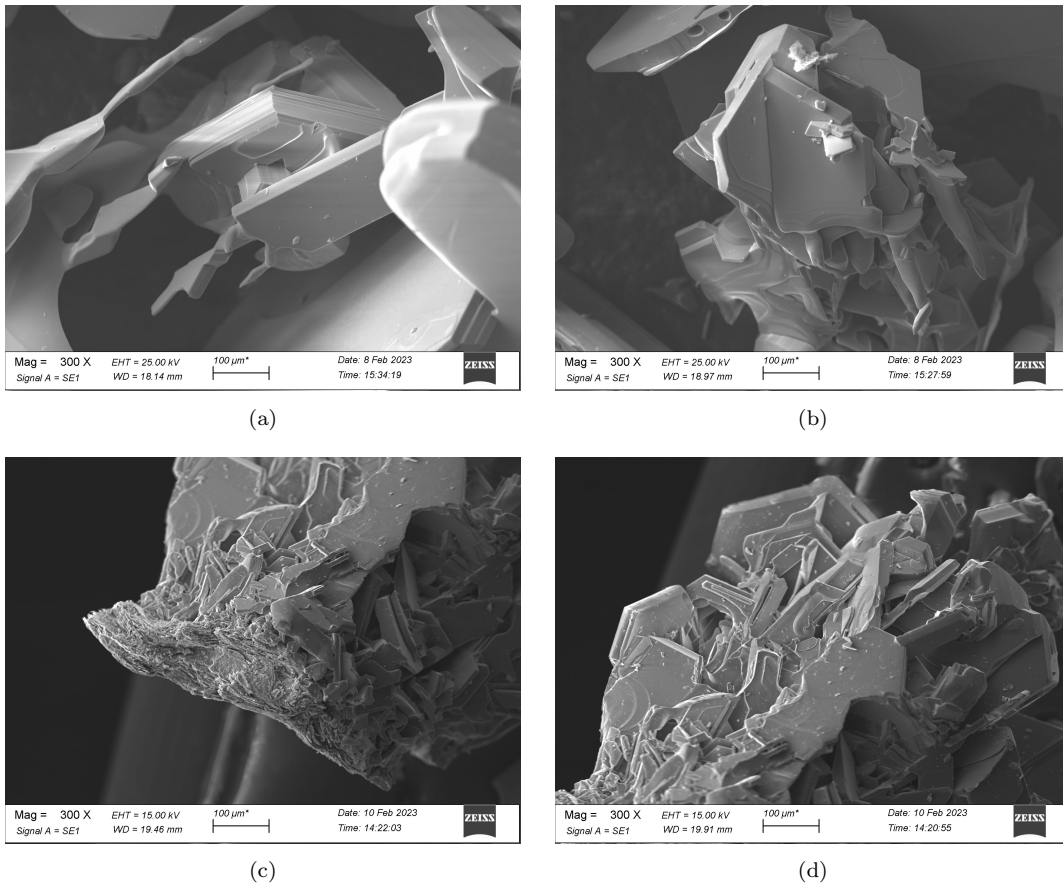
Figure 4.8: Comparison of crude SiC from Run-Bio (a)(b) and Run-Ref (c)(d)

The images of crude shown above demonstrate that crude SiC will maintain its pure crystalline morphology, even when biocarbon is used in the furnace charge. It is also possible to observe that crystal growth occurs in preferred directions. Furthermore, the SiC crystals from the crude area of the ingot have had time to reorganize, and this is visible in the straight edges of the crystals as well as the scale. These crystal samples are several hundred μm in diameter, which is relatively large.
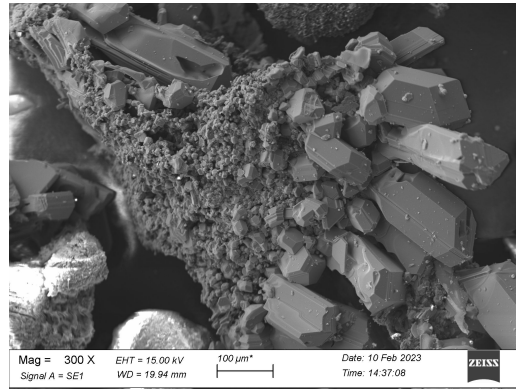
Firesand

SEM-EDS analysis was done on points in samples of firesand to identify different particles and their compositions. This could then be combined with visual analysis, ensuring that left-over carbon particles could be identified in a mass of particles.

In figure 4.9 there is a direct comparison between images of firesand samples
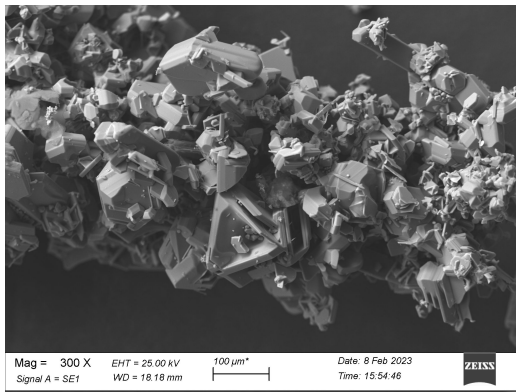
from both the biocarbon and reference run. There are clear crystals growths in both runs, yet the crystal sizes are smaller than those found in SiC. There are also several microscopic crystals that may be in the infant stage of crystal growth.
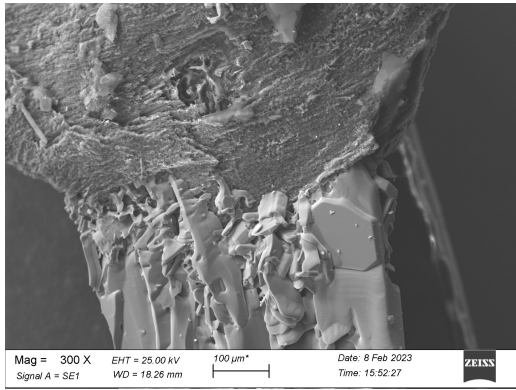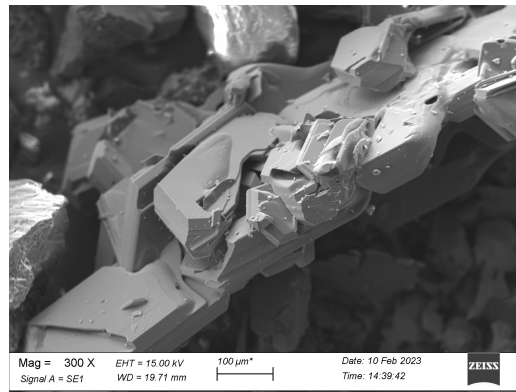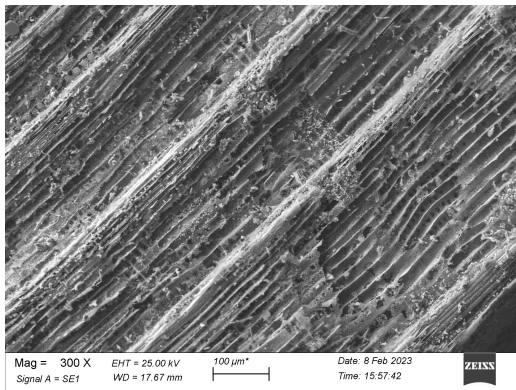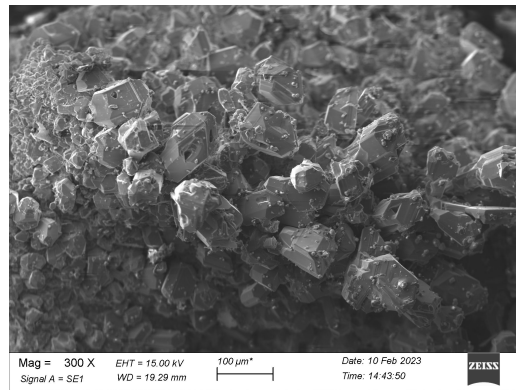
Figure 4.9: Comparison of firesand for the biocarbon run (a)(c)(e) and reference run (b)(d)(f) at 300x magnification

Image (a) from figure 4.9 shows a clear transition between more amorphous material to more crystalline structures. These small areas of image (a) is shown in figure 4.10.An accompanying table with atomic concentrations is also shown.

Figure 4.10: SEM-EDS point analysis of three points in a sample of firesand from Bio-Run

Table 4.6: Atomic composition of points in figure 4.10

Point	Carbon (C)	Oxygen (O)	Silicon (Si)
Area#65 1	61.058	1.806	37.136
Area#65 2	100.000	0	0
Area#65 3	100.000	0	0

This analysis shows that the amorphous sections are fully composed of carbon, whilst the crystals are a mixture of Si and C in approximately 50/50 ratio, meaning

they are SiC. These crystals tend to start small, and seem to grow in a certain direction, forming larger crystalline structures.

Another image and EDS-analysis displaying a clear transition from amorphous carbon particle (right) to crystalline SiC (left) is shown in figure 4.11.
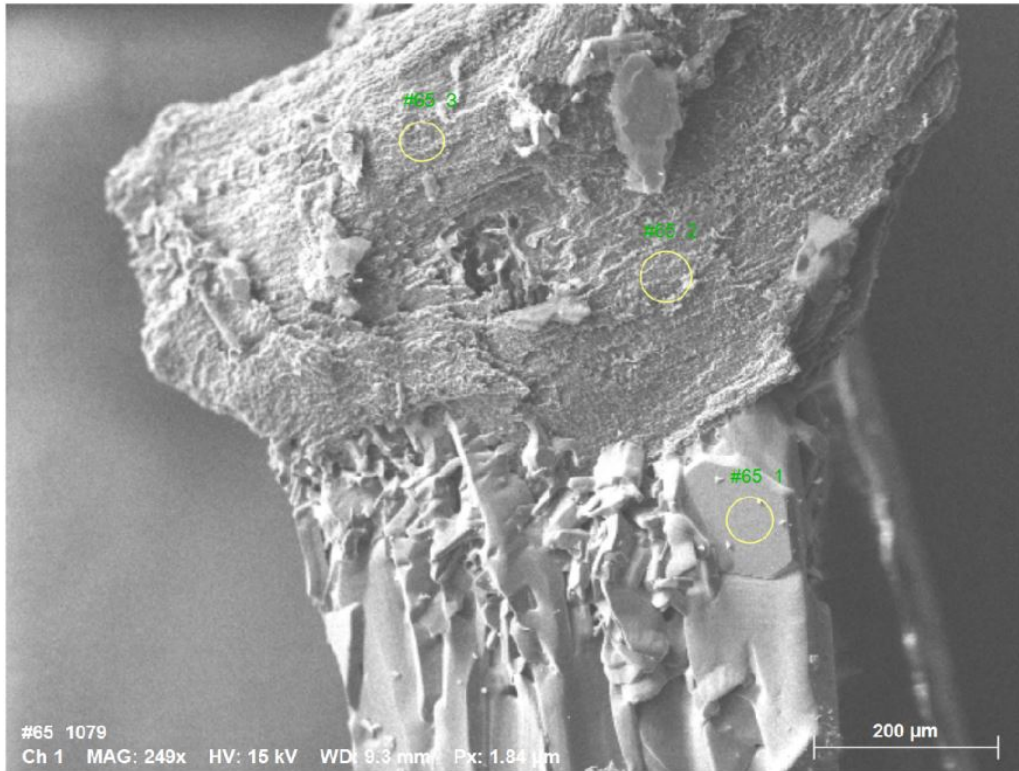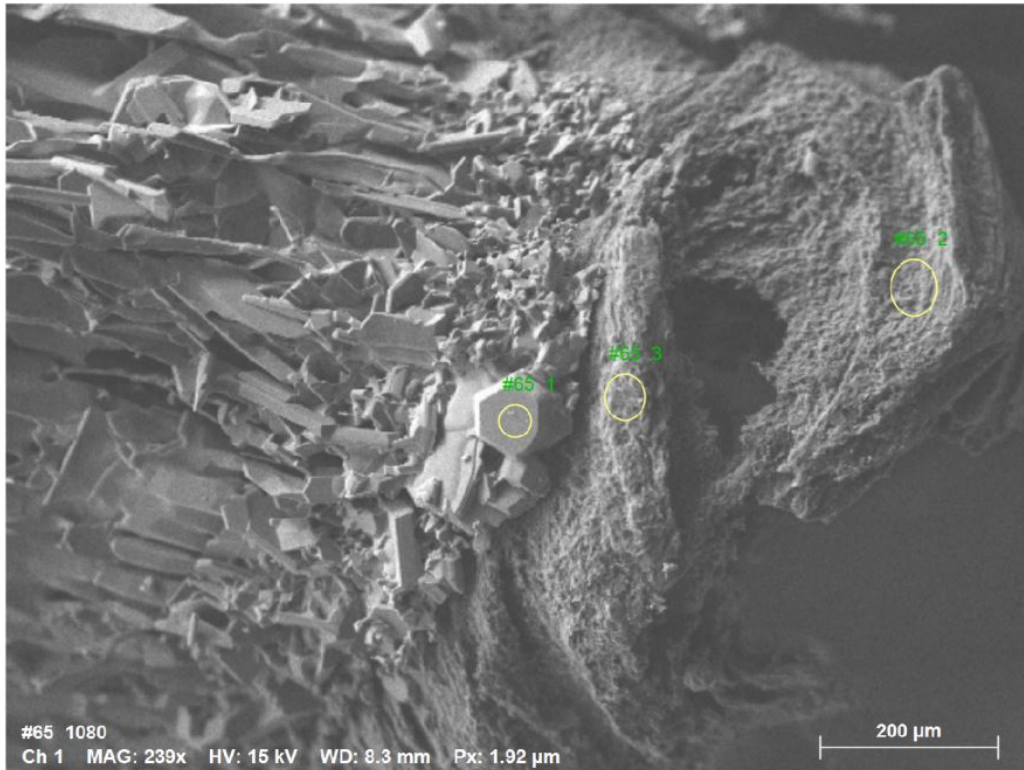

Figure 4.11: SEM-EDS point analysis of three points in a sample of firesand from Bio-Run

Table 4.7: Atomic composition of points in figure 4.11

Point	Carbon (C)	Oxygen (O)	Silicon (Si)
Area#65 1	59.237	0	40.763
Area#65 2	100.000	0	0
Area#65 3	100.000	0	0

In figure 4.11, area 1, the atomic ratio can be approximated to 50% Si and 50% C, which would correspond to pure SiC. This kind of scewed ratio is seen in a lot of

the samples in this project. The other two areas show 100% carbon, meaning they can be identified as parts of a carbon particle.

Both 4.11 and figure 4.10 show examples of SiC crystals growing from carbon grains, with carbon still being present. This can signify that the SiC reaction has not gone to completion in the firesand area. The firesand section of the ingot serves as the transitionary area between the crude SiC formed in the process and the carbon and silica sand mix which makes up the charge. Because of this, it is normal that there are these kinds of particles present in the firesand samples as shown above. A final examples of this phenomenon is shown in figure 4.12 below. Here it is again possible to see clear crystals sprouting from the far more amorphous carbon particles. No EDS analysis was available for this image.
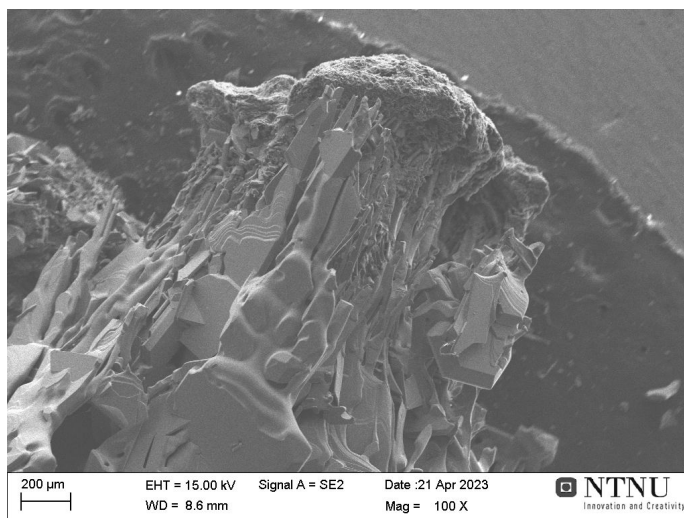
Figure 4.12: Example of the carbon-SiC transition visible in many firesand samples

Several of the firesand samples also displayed interesting structures. One of these is the apparent formation of microscopic SiC crystals on the surface of biocarbon particles. This agrees with the theory, that early in the reaction process, small SiC crystals will form, and with time and temperature, these will reorganise and grow into the large crystals one may find in the crude. Similar findings were also reported by Jayakumari and Tangstad as well as Nordbø, where SiC crystals formed on the surface of biocarbon particles [12][43]. Figure 4.13 shows an example of this formation of microscopic crystals on the surface of a biocarbon sample. Whilst it is difficult to discern the polytype of SiC from the macroscopic crystal structure, this area of the ingot is theorized to have a larger concentration of β-SiC which forms as small crystals. The images could therefore be showing some of these β-SiC crystals.

Figure 4.13: Two examples of microscopic crystals forming on the carbon particles, maintaining the macroscopic geometry of the biocarbon

EDS analysis of a less magnified version of the surface which produced both images in figure 4.13 is shown in figure 4.14.
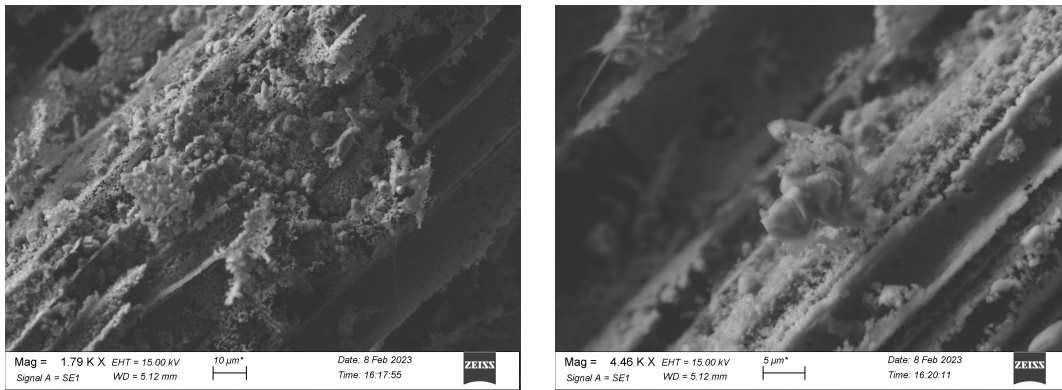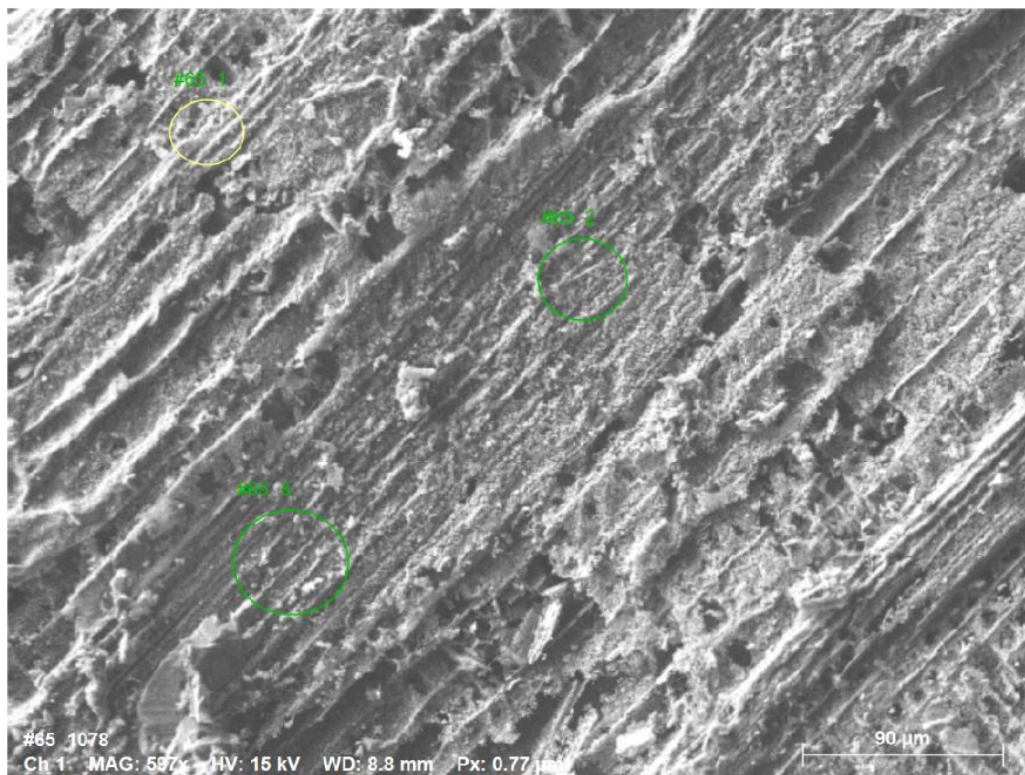

Figure 4.14: SEM-EDS point analysis of three points in a sample of firesand from Bio-Run showing carbon-SiC transition

Table 4.8: Atomic composition of points in figure 4.14

Point	Carbon (C)	Oxygen (O)	Silicon (Si)
Area#65 1	53.330	0.577	46.093
Area#65 2	49.755	1.614	48.631
Area#65 3	50.588	1.970	47.442

This phenomenon was the most pronounced in the samples of firesand from the biocarbon run. The morphological structure of the biocarbon is often more pronounced and is therefore easier to identify. Another example of this is shown in figure 4.15.
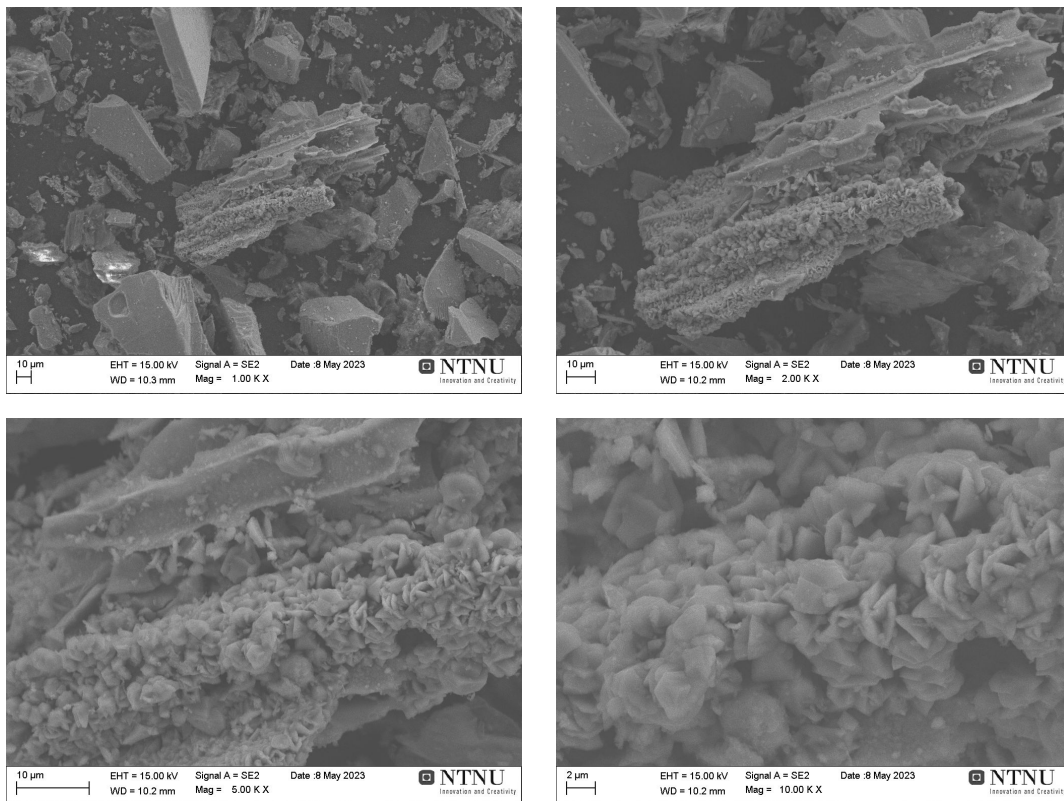

Figure 4.15: A particle of biocarbon covered in microscopic SiC crystals at four different magnifications (1kx, 2kx, 5kx, 10kx)

Whilst the crystals on this particle may have already started growing, the distinct tube-like structures of the biocarbon are still plainly visible.

Another example of micro-crystals forming on a larger SiC crystal is shown in figure 4.16. This crystal was found in a sample from run 2 (0% biocarbon), showing that this kind of crystal formation is present in these samples as well.
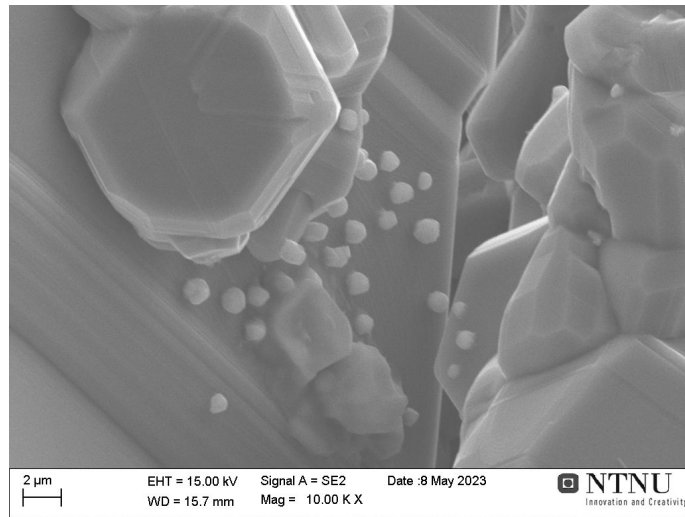
Figure 4.16: Micro-crystals forming on larger SiC crystal in firesand sample from run 2 at 10kx magnification

For bulk analysis of firesand from both runs, random samples were taken. Some point analyses are shown in figure 4.17, 4.18, 4.19, and 4.20.
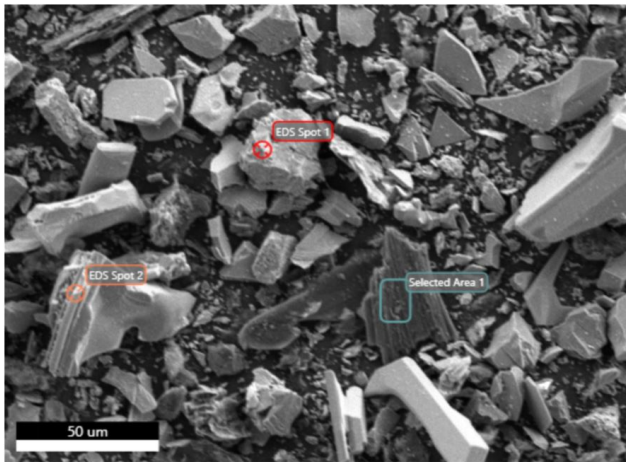
Point	Carbon	Silicon	Oxygen
1	53.9	40.4	5.7
2	31.2	66.0	2.7
Area 1	98.4	1.1	0.5

Figure 4.17: EDS analysis of points in FS1 and atomic composition
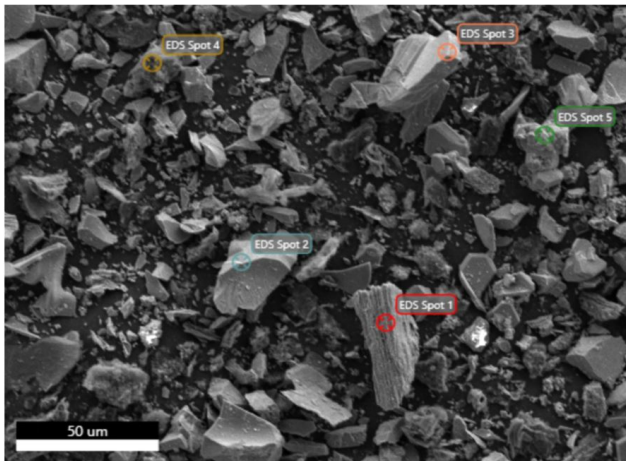
Point	Carbon	Silicon	Oxygen
1	36.4	43.1	20.5
2	65.8	26.5	7.7
3	0	100	0
4	99.1	0.4	0
5	46.3	41.5	12.2

Figure 4.18: EDS analysis of points in FS1 and atomic composition
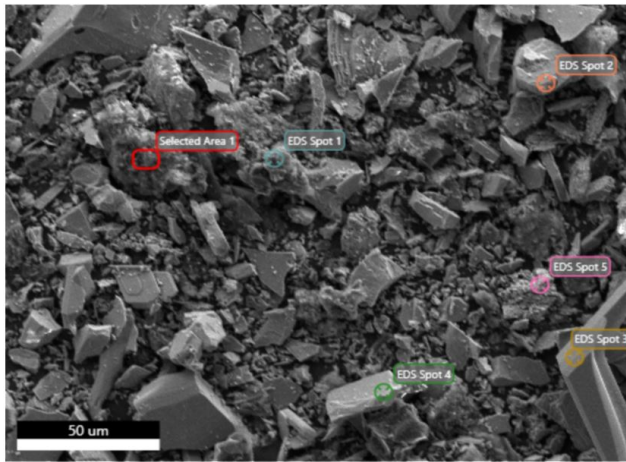
Point	Carbon	Silicon	Oxygen
1	98.8	0.2	0.9
2	0	100.0	0
3	51.0	47.7	1.1
4	61.7	33,8	4.5
5	30.9	63.4	5.7
6	95.9	2.7	1.4

Figure 4.19: EDS analysis of points in FS1 and atomic composition
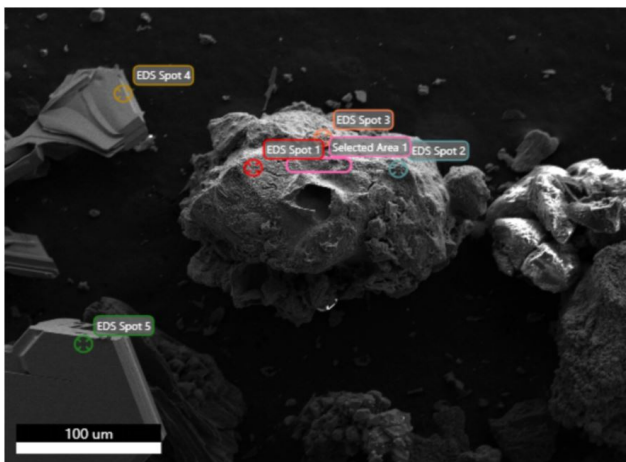
Point	Carbon (C)	Silicon (Si)
1	11.1	94.9
2	22.2	89.1
3	51.2	48.8
4	52.6	47.4
5	26.7	73.3
Area 1	45.6	54.4

Figure 4.20: EDS analysis of points in FS2 and atomic composition.

The point analyses of the firesand show primarily that there is a presence of SiC and carbon particles. Furthermore, small contents of pure Si are present as shown in figure 4.20. Even in the firesand region of the furnace, temperatures will be higher than the melting point, so it could be possible for Si droplets to form and become trapped in this section of the ingot.

SEM-EDS mapping was attempted on some of the above-shown areas of firesand from both the biocarbon and reference run. The samples were crushed to sizes smaller than 100μm to get a relatively even size distribution in the particles. However, there

are still a lot of shadow areas due to larger particles blocking the sensor. This can be seen in figure 4.21 below. This data is not quantitative, and may at most serve as an indication of particle distribution in the firesand of both runs. Whilst more mapping attempts are necessary to draw a stronger conclusion, one may assume that the largest segment of particles is composed of SiC, whilst there are several traces of carbon particles and very few apparent silica particles.

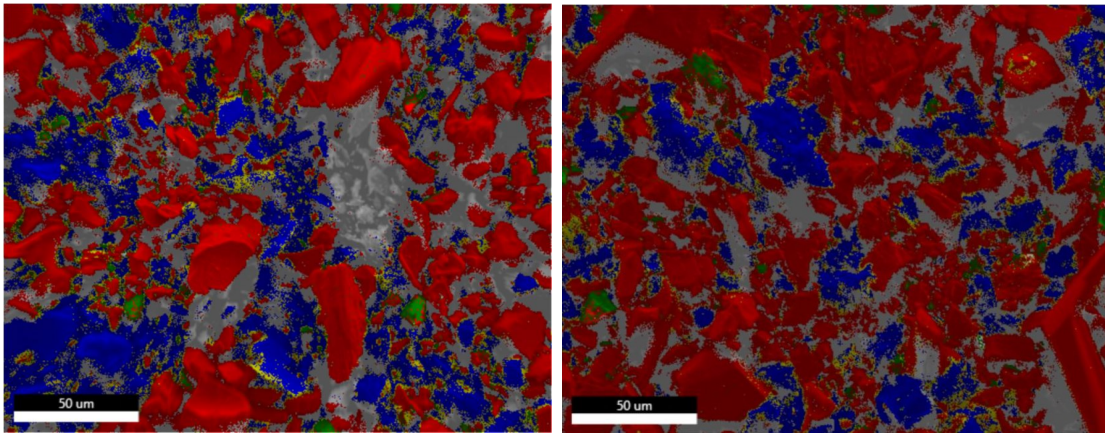Figure 4.21: Mapping of two different areas from sample of firesand from the bio-run. Red shows SiC, blue shows carbon, and green shows SiO_2
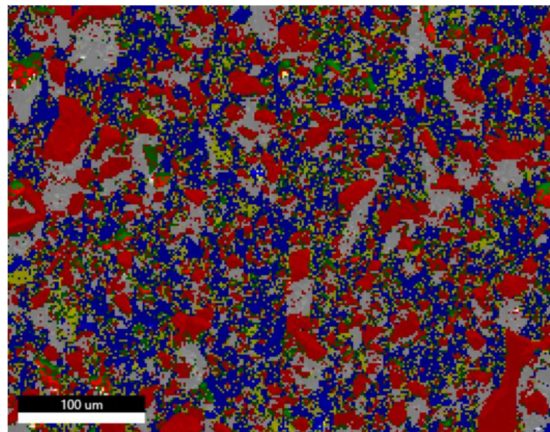
Figure 4.22: Mapping of an area from a sample of firesand from the ref-run. Red shows SiC, blue shows carbon, and green shows SiO_2. Take note of the different scale from figure 4.21

A mapping attempt was also made with a different SEM stack (Zeiss Supra 55VP

FEG-SEM) and detector as shown in figure 4.23. Take note of the different colours for elements.
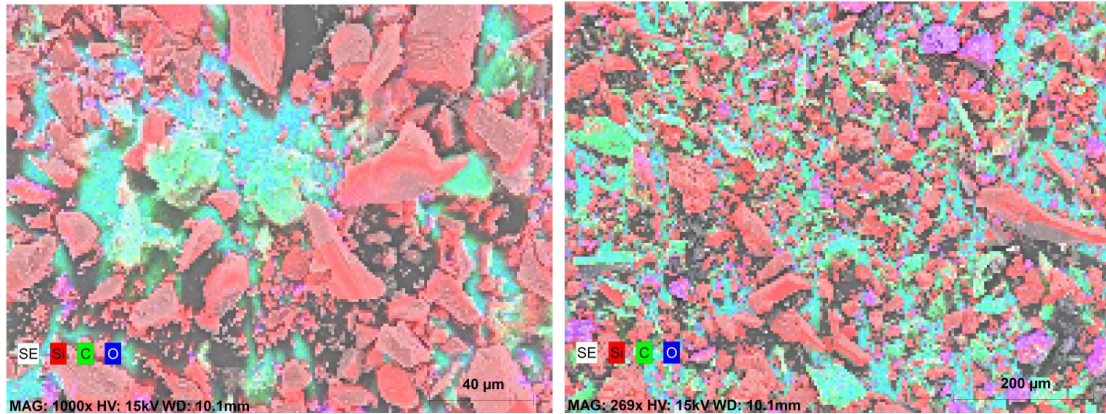
Figure 4.23: Mapping of two firesand samples from run 2 (0% biocarbon)

It is possible to see distinct carbon particles as well as some smaller SiO_2 particles in the images.

The generated spectra are not very reliable due to carbon values having large uncertainty. This leads to strongly scewed C/Si ratios in areas which seem to have SiC crystals present. Carbon tape was used, and this will usually artificially drive the carbon content of the sample up. Still with this new setup, substantial shadow areas were present in the sample which makes general mapping complicated. Another example of mapping is shown for a sample from firesand 1 in figure 4.24.

Figure 4.24: Mapping of a sample of firesand from run 1 (30% biocarbon)

The distribution in this sample shows a higher concentration of SiC particles compared to the other samples.

4.7 Summary

The results for the experimental section are summarized in this section. For better understanding it is recommended to see the relevant sections.

Data collected during furnace runs showed that the biocarbon run operated at an overall resistance around 0.02 Ω higher than that of the reference run. This was not reflected in a previous test run by FIVEN using only 15% biocarbon in the mixture.
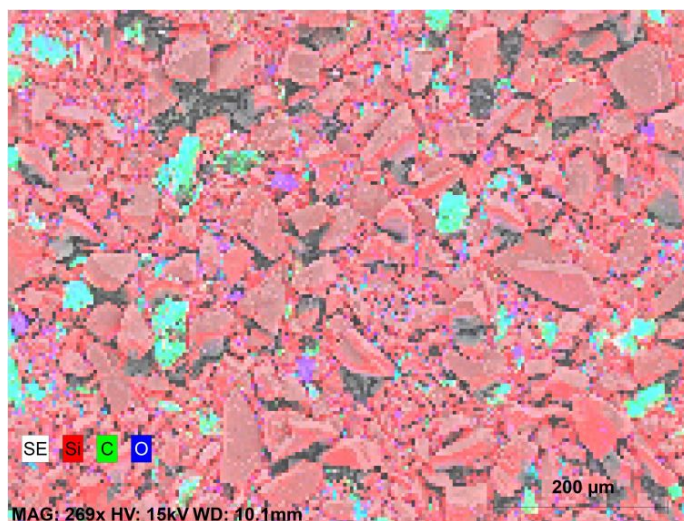
ICP-slurry analysis showed that the biocarbon run had higher impurity levels of Ca, Fe, and Ti, but lower levels of Al, Ni, and V than the reference run. All of these values are below the specifications supplied by FIVEN except Ti content which was between 100-200 ppm higher than the specified value.

Density measurements of the charcoal (biocarbon) and petroleum coke showed that the bulk density of the used biocarbon was lower than that of petroleum coke. The absolute density was measured to be higher for biocarbon, potentially signifying a larger amount of open porosity when compared with petroleum coke.

Ash content of the biocarbon samples was measured, and whilst inaccurate, the measurements fell within the 2-3wt% margin given by the supplier.

XRD analysis showed the large fraction of α-SiC in crude samples from both runs as well as a more even distribution of α- and β-SiC in the firesand samples. The

firesand samples from run 1 had a higher fraction of α-SiC than the samples from run 2, which coincides with the observation that more crude SiC was lost to the firesand in that run.

The SEM and SEM-EDS analysis showed that SiC was formed in both runs, often following the theory of β-SiC particles forming first, and then grow into larger α-SiC crystals given time and temperature. EDS also showed that firesand samples contained several examples of SiC crystals growing out from unreacted carbon particles as well as micro-crystals on the surface of carbon particles.

Chapter 5

Discussion

This chapter discusses the results collected throughout the investigation as well as the analytical methods used. It also considers possible error sources and their potential impact on the collected data.

5.1 Raw Materials

The characterisation of raw materials revolved mainly around density measurements, visual analysis of particle morphology using SEM, and simple determination of ash content. Analysis of surface area through Brunauer-Emmett-Teller (BET) analysis was attempted, but due to dust-generation from the samples, the analysis wouldn't run smoothly, and therefore data was only collected for the charcoal. Therefore, no comparison could be made, and the data was promptly not presented in this thesis. Furthermore this kind of analysis would work better on an even particle distribution. Finding a BET analysis procedure that would allow for the analysis of biocarbon an petroleum coke samples could be interesting to investigate further, as this would allow for direct surface area comparison. Surface area may be directly related to CO_2 reactivity, so being able to measure this would be vital in the biocarbon/petroleum coke comparison [15]. More in-depth analysis of porosity may be crucial to further explain the difference in production yield.

5.1.1 Density Measurements

Throughout the investigation, the absolute and bulk density of the raw materials was measured. When it comes to the industry, bulk density is usually one of the most important factors as it directly determines the amount of material that fits

into a furnace, and thereby how much product is produced [7]. The bulk density of a material is often a value with limited accuracy, depending on how homogeneous the particle distribution is. In this investigation measurements were done on small volumes of sample. This means there is more uncertainty in these measurements. When agitating a mixture of small and large particles, the large particles will usually settle on the top. This is commonly referred to as the "Brazil nut effect" [53]. In smaller sample volumes, this effect leads to larger particles making it difficult to correctly identify the top of the sample after agitation. This further leads to human error, and usually a higher measured volume than what really is present. Therefore several parallel measurements were run to be able to draw an average. Furthermore, the measurement done at FIVEN Lillesand was done on a larger sample size, meaning there would be less uncertainty involved in this measurement.

5.1.2 Ash Content Analysis

Through the investigation, ash content in the biocarbon was investigated, as the supplier did not present good data for this. This was done by burning the samples over approximately 1.5 hours under an oxygen lance and measuring the mass of the remaining ash. During the experiment a scale with low accuracy was used, and this made the results very uncertain. Even so they fell within the ash content range specified by the supplier. This was higher than that of petroleum coke, which could be problematic as it may contribute to formation of a crust of metal oxides on the ingot [7].

Whilst the method itself isn't very complex and doesn't have too many error sources, there is potential to take this step of the investigation further. Measuring the volatile content would be interesting as biocarbon and petroleum have vastly different volatile contents according to the literature. To what extent this is visible in the samples used in this investigation could be beneficial to support any conclusions made. Volatiles could to some extent be responsible for pollution of the produced crude SiC [1].

It would also be interesting to chemically analyse the ash content that was produced from the two different carbon sources. This could explain certain metal impurities that were found through ICP analysis, as these would most likely be present in the ash as metal oxides.

5.2 Analysis of Crude and Firesand

During the analysis of produced crude and firesand there were many sources for errors. This section splits these into categories depending on the type of analysis. It also discusses potential error sources in the preparation of samples, as well as the problems related to taking representative samples.

Preparation of samples from the produced materials was primarily done by hand. The produced ingot of graphite, crude SiC and firesand was separated using handheld steel brushes. This means that the operator was responsible for judging when the firesand and graphite layers were substantially removed from the crude SiC. Furthermore, due to the scale of the furnace and amount of produced material, the crude SiC contains at least minor amounts of both graphite from the electrode and partially reacted materials from the firesand. It was not possible to fully separate everything with the available tools and given conditions.

Since the crude produced in run 1 (30% biocarbon), differed from the crude produced in run 2 (0% biocarbon), primarily in terms of brittleness and cohesion, the uncertainty related to layer separation was larger in the crude produced in run-1. This was due to the separation between crude and firesand being far less defined. During the brush separation of the firesand, substantial amounts of the crude SiC was also removed due to the high brittleness. Therefore, one should consider the yield results for crude and firesand as a whole. Run 1 produced more firesand than run 2, and this may therefore support the argument that a lot of the crude SiC ended up in the firesand. However, even when considering crude and firesand values as a whole, run 1 still produced less than run 2.

Another factor to consider when comparing the two crudes was the colour. Both runs produced crude with layers of black, blue/green and green SiC with a layer of yellow/green firesand. In general, the reference produced a layer of blue/green SiC that was thicker and denser than the biocarbon run. When looking at the theory, the colours observed would suggest a large content of nitrogen in the outer and middle layers, and aluminium in the inner layers. The firesand layer, due to its yellow tint may be composed of N-doped β-SiC, and the middle and inner layers of N-doped α-SiC. This was confirmed by XRD, as the crude SiC and firesand measurements show a larger content of α-SiC, and β-SiC respectively [1]. The content of aluminium in the inner layers was not confirmed to be higher than usual, and the colour may also partially have been caused by graphite pollution. In general, the layers were similar in colour for both runs, but the reference run produced a noticeably thicker layer of crude SiC.

Another challenge that is present when working with larger volumes is finding methods for splitting the samples into sizes that are suited for lab-analyses. When splitting, it's important to retain a representative sample in terms of particle size and distribution. This was originally done using different size material splitters, which simply separate the samples into two even batches. This process was repeated until a desired size was reached. The same splitters were not available at NTNU, and therefore a more rudimentary method of "coning and quartering" was used. This may not have produced the same level of representative samples, and this may have lead to uneven particle distribution. In effect, this may have caused a higher concentration of partially reacted carbon particles in particular in firesand samples, as these were typically larger, and therefore often remained in the sample during splitting due to the above-mentioned Brazil nut effect [53]. This may have caused larger carbon content in the XRD data than what was actually representative for the produced SiC and firesand.

5.2.1 ICP Analysis

The ICP-analysis was performed by lab-technicians at FIVEN Lillesand, and therefore there is no first-hand experience with error sources. However, the results from the analysis showed high values for Zr and Ti content in both the crude and firesand. These were unexpectedly high at four times the specification value for Zr, and twice the specification value of Ti. These specifications were supplied by FIVEN and are based off values from normal production of crude. In this regard FIVEN was contacted as the high values could be due to a calibration issue of the instrument used. Therefore, measurements were repeated after the instrument was calibrated. The results yielded by this repeated measurement showed little change. On one hand this is good, as it shows that the measured values for the other metal impurities most likely is accurate. On the other hand, there were still too high values for both Ti and Zr content.

A new theory was established which blamed this on contamination of the material splitter, used in the splitting of the samples. The same splitter had namely been used to split samples of sand, and not been thourougly cleaned afterwards. According to theory, silica sand often occurs naturally with contents of both rutile (TiO_2) and zircon ($ZrSiO_4$) [35]. Whilst the used silica sand has a very high purity, near 100% SiO_2, it may have contained traces of both rutile and zircon, which would reinforce the theory that this polluted the splitter and therefore ended up in the ICP results.

Through chemical cleaning, leaching, and processing, a lot of the metal impurities can be removed after primary production to meet customer specifications [1]. Some

however, are more difficult to remove than others. The most important impurities are therefore Al, Ti, V, and Zr. These are more difficult than other impurities to remove from the produced crude. This furthers the problematically high values of both Ti and Zr in particular.

One thing that must be considered is that both the crude and firesand from run 1 (30% biocarbon) and run 2 (0% biocarbon) produced similarly high values for Ti and Zr. This further supports the theory of pollution of the material splitter. Therefore, these values are not as emphasized in the conclusion.

When it comes to the other results, it is clear to see that the produced firesand had higher values for several metal impurity concentrations compared to FIVEN's specifications. This is not unnatural, as metal oxides often are driven from the core of the reaction through thermal convection, depositing in lower temperature zones such as the firesand [7][1]. Whilst the firesand does not meet purity requirements for SiC, it may still be utilised as a form of metallurgical grade SiC, where impurity levels are not as important [7].

5.2.2   XRD Analysis

XRD analysis was performed on a powder that had a maximum particle size of 100μm after sieving. Rietveld analysis was performed on the collected data even though this particle size is technically too large for this kind of analysis. Therefore the calculated results for phase distribution may have decreased accuracy. However, the peaks from the scan can still be used to identify dominant crystalline structures. Therefore, the data is usable. If the XRD measurements were to be repeated, a finer particle size should be used (ι5μm).

The results for the crude SiC from both runs had large proportions of α-SiC which was expected. SiC produced in run 1 (30% biocarbon) had a larger porportion, with 74.46 wt% α-SiC compared to 72.10 wt% in the crude produced in run 2 (0% biocarbon). These values are so close together that it is difficult to draw a firm conclusion from them. The proportion of β-SiC in the crude was also near equal. Graphite was present in both samples which was to be expected du to residue from the electrode.

The firesand samples showed larger differences in polytype distribution, as the firesand from run 1 had 52.21 wt% α-SiC and 27.03 wt% β-SiC. Run 2 had 12.54 wt% α-SiC and 34.85 wt% β-SiC. Both samples also had higher contents of graphite according to TOPAS, but this was likely caused by the content of carbon particles in this region of the ingot. Of the two results, run 2 shows the more expected amount of β-SiC, as the lower temperatures around the firesand region would enable stable

growth of this polytype. The fact that firesand from run 1 has such a high content of α-SiC could be due to the more brittle crude the run produced. This would have lead to a lot of crude landing in the firesand during separation, thereby pushing the values of α-SiC up. This would be a challenge the industry would also face, so seeing it in a lab setting is realistic and important. The loss of crude to firesand could be economically bad, and therefore have an impact on future production.

5.2.3   SEM Analysis

Whilst SEM was a good analytical method for inspecting particle morphology, the powder samples were difficult to analyse using SEM-EDS. With point analysis, the only the issue that arose was potential backsides of particles which could not be analysed. However, the mapping function was the most problematic, as the large particles caused a lot of EDS-shadows. This made the quantitative results useless, and whilst it was possible to gain a basic understanding of particle distribution, the EDS-maps served no further purpose than that.

To improve these results in future research, one may attempt to sieve the samples to an even finer particle size, such as 50μm or 10μm. This will permit more access for the sensor and reduce the amount of "shadow areas" present in the map. It could also be possible to cast samples of SiC in thermoplastic and polish these samples down to analyse them both using EDS and Backscattered electrons, but due to several factors, this was not possible to do in this investigation.

5.3   Factors in the Acheson Furnace

The Acheson process is complex, and there are many factors to consider when discussing its SiC yield. Some of the main factors are discussed in this section.

The particle size of the carbon source in the Acheson process may have an effect on the produced SiC for a number of reasons. Firstly, smaller particles will ensure more surface contact with the silica sand, which may allow faster formation of the SiC at the start of the reaction. This will also ensure a better mixture with the silica sand. Smaller particles will also lead to a denser charge, as it will increase the bulk density, not only increasing the amount of raw materials that would fit into an oven, but also potentially ensuring a firmer and less brittle crude layer. This would make the separation process both easier and more precise.

This investigation has analyzed two carbon sources with different levels of bulk and porosity density. Using SEM, porosity was observed to be more apparent in the samples of biocarbon. It has found that the carbon source with more porous

particles yielded less crude SiC. One could argue that porosity is good in most cases as it allows for more available surface area for the SiC reduction reaction to occur. However, with higher porosity comes higher CO_2 reactivity[1], lower bulk density, as well as worse mechanical properties of the carbon source. This could then lead to more brittle crude forming, as well as a generally lower carbon density in the charge, which would generate less crude.

Even if the production of SiC using a mixture of biocarbon and petroleum coke is possible, it is apparent that the yield is not good enough. However, there are many factors that feed into this value, such as charge density, particle size, moisture, particle distribution, porosity and surface area of particles. Therefore, further research into these factors is necessary to implement biocarbon more effectively into the Acheson process.

5.4 Sustainability

Whilst this project did not closely analyse the environmental impact and change in atmospheric emissions as a result of the use of biocarbon, this is an issue which increased to importance of findings. With higher climate awareness, pushing for greener production of SiC is ideal for industry, and biocarbon can contribute to this as it is renewable. As briefly discussed in the theory chapter, replacing even just 30% of the process carbon source with biocarbon could reduce emissions by millions of tons of CO_2 equivalents [50]. Furthermore, the use of biocarbon could contribute to reducing sulphur emissions linked with petroleum coke [16].

In this investigation, the kWh per kg of produced SiC was calculated to be 45.18 kWh/kg for the furnace run with 30% biocarbon, and 24.51 kWh/kg for the reference run with 0% biocarbon. Compared to industrial values, which lie between 6-12 kWh/kg [7][49], these are both very high, but considering they were produced in a pilot furnace on far smaller scale, this difference can be explained. What is more important is the fact that the crude produced from biocarbon required almost twice the amount of power as the reference run. Whilst the emissions from power production in the process are relatively small compared to the process emissions, this can be problematic, especially in countries where the power is produced using non-renewable resources [50]. If one is to compare this with data from the U.S. however, the decrease in overall emissions due to biocarbon will still be larger than the increase in emissions from power production [50]. A similar net reduction was also seen in the Netherlands [49]. Therefore, whilst yielding less SiC, using biocarbon

---

[1]This is due to the Boudouard reaction discussed in the theory chapter, section 2.1

may still be the correct direction for the industry to reduce overall emissions, but this will naturally require further study.

When reviewing the applicability of biocarbon and charcoal in particular, all the factor of sustainability must be considered. On one hand, the potential reduction of climate emissions is important, as well as the development of alternative fuel sources and reducing agents than fossil based ones. Economically this may not be as simple, as biocarbon is not as readily available as fossil materials, and therefore drive up costs. The EU alone imports more than 75% of its charcoal from countries such as Ukraine and Nigeria which have experienced social and political instability [33]. This must be considered when suggesting the use of biocarbon in the industry. Altogether these factors contribute to the idea that partial implementation of biocarbon is preferential over total replacement at least in the short run. This not only will maintain product quality, but may also help in keeping the economic and social costs low, whilst still reducing sizeable amounts of climate emissions as mentioned in the theory section [49]. There must be a balance, as with most industrial processes, to find the ultimate compromise.

5.5   Further Work

During the course of the project, a third run of the pilot furnace was originally planned to test a mixture of 60% charcoal and 40% petroleum coke. However, due to time and availability of the pilot furnace this was not possible to complete. This would be the natural next step in the testing of biocarbon. The rationale behind this is the necessity for more data especially related to yield of firesand and crude SiC to be able to support a better conclusion on the viability of biocarbon in the industry. This would come with the difficulty of a higher amount of dust generation, but would provide valuable data. There is good reason to believe that there is a specific mixing ratio which will give the best results, and to find this ratio would be highly desirable. One could even expand this idea further and attempt a furnace with 100% charcoal. This may not work at all, but that would also be a good result.

There are also several other factors that contribute to the SiC generation in an Acheson furnace, and further investigation into all of these may also be interesting. The factors are listed below, as well as a short rationale for why they may be of importance and how one could investigate them further.

Whilst moisture levels most likely do not heavily impact the amount of SiC yield, this heavily affects energy requirements of the Acheson process, as more energy will be spent evaporating the present water before the temperature can rise and the reaction start.

1. Particle size. A potential investigation into the SiC crude yield at different particle sizes would give insight into the total effect of this variable.

2. Porosity of the carbon source. To investigate this, one may look at a selection of carbon sources with varying grades of porosity and analysing their effect on the crude yield, as well as the overall bulk density of the carbon material.

3. Densification of carbon source. The previous two points have already touched on this subject, but the bulk density of the carbon source is a major factor in the process. It incorporates both porosity and particle size. Currently, there is a lot of research on potential densification processes for biocarbon to increase both bulk density and mechanical strength. This may ensure less carbon is lost to the Boudouard reaction and as fines in the off-gas. Solutions such as pellets, and various forms of mechanical and chemical densification methods have been found. It would be interesting to test some of these alternative in an Acheson furnace. To do this, one could recreate smaller furnaces to allow for cheaper experiments, and then analyze crude yield from the various carbon sources.

4. Density of charge. As stated in the theory, the reaction between SiO gas and C particles is the driving factor for SiC production. It would be interesting to investigate the total charge density and how this effects the yield of SiC. In the early days of Acheson, wood chips and sawdust were used to air out the charge and allow gas transfer [7]. This was in recent years discontinued, but perhaps, the overall bulk density of the charge will alter the outcome.

5. Moisture levels. One could test different drying methods and times and analyze how this effects the overall power consumption of the process.

What remains a major challenge is the quantification of results. In this investigation the purity of the produced SiC is measured using ICP-slurry analysis, however, the yield is simply a rough calculation. If a method could be developed for effective separation of crude SiC, firesand, and graphite, one could more easily measure and compare the variation of different factors within the Acheson furnace.

Chapter 6

Conclusion

In this investigation the effect of the use of biocarbon instead of petroleum coke as a carbon source in the Acheson process for production of silicon carbide was analyzed. To do this, a test furnace was fired with a carbon source mixture of 30% biocarbon, and 70% petroleum coke. A furnace with 0% biocarbon was also fired to function as a reference point for all data collected. The investigation further sought to compare the quality and yield of the produced SiC with that of the reference furnace, as well as internal standards at FIVEN AS Norway. Furthermore, the bulk and absolute density as well as the chemical properties of the raw materials were investigated to support the findings.

The following conclusions have been drawn from the course of the subject work:

1. The direct, partial replacement of petroleum coke with biocarbon in the Acheson process is possible and will yield SiC.

2. Crude SiC produced using a mixture of biocarbon and petroleum coke had a higher content of certain metal impurities (Ca, Fe, Ti, V) compared with the reference furnace. However, these were still below the purity specifications supplied by FIVEN AS Norway.

3. XRD analysis showed that the primary SiC polytype produced in an Acheson furnace with a mixture of biocarbon and petroleum coke is α-SiC, with a minor percentile ($> 8\%$) being β-SiC.

4. The furnace run with 30% biocarbon showcased a higher resistance in the charge when compared with the reference.

5. The crude produced using a mixture of biocarbon and petroleum coke was more brittle than the reference crude. Falling apart more easily upon processing.

6. The overall yield of crude for a pilot furnace with 30% biocarbon is lower compared to a reference furnace of approximately the same charge volume.

7. The biocarbon had a lower measured bulk density than petroleum coke. There were also far larger pores visible in the biocarbon.

Chapter 7

Bibliography

[1] Lindstad LH. Recrystallization of Silicon Carbide. NTNU: Norwegian University of Science and Technology; 2002.

[2] Britannica TEoE. Silicon Carbide; 2022. Available from: `https://www.britannica.com/science/silicon-carbide`.

[3] Kumar PV, Gupta GS. Study of formation of silicon carbide in the Acheson process. Steel Research. 2002;73(2):31-8.

[4] Raj P, Gupta GS, Rudolph V. Silicon carbide formation by carbothermal reduction in the Acheson process: A hot model study. Thermochimica Acta. 2020;687.

[5] Frantsevich IN. Silcon Carbide. Institute of Materials Science, Academy of Sciences of Ukrainian SSR; 1970.

[6] Føreland S, Bakke B, Vermeulen R, Bye E, Eduard W. Determinants of Exposure to Dust and Dust Constituents in the Norwegian Silicon Carbide Industry. The Annals of Occupational Hygiene. 2012 12;57(4):417-31. Available from: `https://doi.org/10.1093/annhyg/mes086`.

[7] Guichelaar PJ. In: Weimer AW, editor. Acheson Process. Dordrecht: Springer Netherlands; 1997. p. 115-29.

[8] About us - Fiven;. Available from: `https://www.fiven.com/company-information/about-us/`.

[9] Knippenberg WF. Growth Phenomena in Silicon Carbide. N.V. Philips' Gloeilampenfabrieken; 1963.

[10] Lupi S. Fundamentals of Electroheat. Springer International Publishing; 2017.

[11] Grujic K, Mathisen H, Simonsen S. Optical Pyrometry in Harsh Environments: Measurement of Extreme Temperatures in a Pilot Scale Acheson Furnace. In: Imaging and Applied Optics 2016. OSA; 2016. Available from: `https://doi.org/10.1364%2Faio.2016.aith3a.4`.

[12] Jayakumari S, Tangstad M. Transformation of -SiC from Charcoal, Coal, and Petroleum Coke to -SiC at Higher Temperatures. Metallurgical and Materials Transactions B. 2020;51:2673–2688.

[13] Inomata Y. 1. In: Inomata Y, Somiya S, editors. Silicon Carbide Ceramics - 1: Fundamental and Solid Reactions. Elsevier Science Publishers LTD; 1991. p. 1-11.

[14] SiC production process - Fiven;. Available from: `https://www.fiven.com/world-of-silicon-carbide/sic-production-process/`.

[15] Wang P, qiang Zhang Y, ming Long H, xin Li J, min Meng Q, cai Yu S. Degradation Behavior of Coke Reacting with H2O and CO2 at High Temperature. ISIJ. 2016;57(4):643-8.

[16] Kaffash H, Surup GR, Tangstad M. Densification of Biocarbon and Its Effect on CO2 Reactivity. Processes. 2021;9(2). Available from: `https://www.mdpi.com/2227-9717/9/2/193`.

[17] Marsh H, Rodríguez-Reinoso F. Activated Carbon. Elsevier Science and Technology Books; 2006.

[18] Edwards L. The History and Future Challenges of Calcined Petroleum Coke Production and Use in Aluminum Smelting. JOM. 2015;67(2):308-21.

[19] Tuset JK, Raanes O. Reactivity of reduction materials for the production of silicon, silicon-rich ferroalloys and silicon carbide. 34th Electric Furnace Conference Proceedings. 1976:101-7.

[20] Bourrat X. Sciences of Carbon Materials. Marsch H, Rodríguez-Reinoso F, editors. Secretariado de Publications; 2000.

[21] Parfen'eva L, Orlova T, Kartenko N, Sharenkova N, Smirnov B, Misiorek H, et al. Thermal conductivity of high-porosity biocarbon precursors of white pine wood. Physics of the Solid State. 2008 12;50:2245-55.

80

[22] Fairchild WT. Electric Furnace Manufacture of Silicon Metal. JOM. 1970;(22):55-8.

[23] Jin Z. Carbon Behaviour during Si Production. Norwegian University of Science and Technology; 2013.

[24] Bartocci P, Wang L, Øyvind Skreiberg, Liberti F, Bidini G, Fantozzi F. In: Biocarbon Production and Use as a Fuel; 2019. p. 295-324.

[25] Niedziółkaa I, Szpryngielb M, Zaklikaa B. Possibilities of using biomass for energy purposes. Agricultural Engineering. 2014;149(1):155-63.

[26] Saletnik B, Saletnik A, Zaguła G, Bajcar M, Puchalski C. The Use of Wood Pellets in the Production of High Quality Biocarbon Materials. Materials. 2022;15(13). Available from: https://www.mdpi.com/1996-1944/15/13/4404.

[27] Chen N, Pilla S. A comprehensive review on transforming lignocellulosic materials into biocarbon and its utilization for composites applications. Composites Part C: Open Access. 2022;7:100225. Available from: https://www.sciencedirect.com/science/article/pii/S2666682021001171.

[28] Ibrahim HAH. In: Introductory Chapter: Pyrolysis; 2020. p. 1-8.

[29] Øyvind Skreiberg, Wang L, Khalil R, editors. BioCarb+: Enabling the biocarbon value chain for energy; 2017.

[30] Jahirul MI, Rasul MG, Chowdhury. Biofuels Production through Biomass Pyrolysis - A Technological Review. Energies. 2012;5(12):4952-5001. Available from: https://www.mdpi.com/1996-1073/5/12/4952.

[31] Meier D, Beld B, Bridgewater T, Elliott D, Oasmaa A, Preto F. State-of-the-Art of Fast Pyrolysis in IEA Bioenergy Member Countries. Renewable and Sustainable Energy Reviews. 2013 March;20:619-41.

[32] Riva1 L, Nielsen HK, Buø TV, Zhuo H, Yang Q, Yang H, et al. LCA Analysis of Biocarbon Pellet Production to Substitute Coke. In: Proceedings of (ICEEE 2019/ICEIV 2019; 2019. p. 46-9.

[33] Zahnen J, Haag V, Lewandrowski T, Hirschberger P. 2020 Analysis of the EU Charcoal Market. 2020 12.

[34] Sharma NK, Williams WS, Zangvil A. Formation and Structure of Silicon Carbide Whiskers from Rice Hulls. Journal of the American Ceramic Society. 1984;67(11):715-20. Available from: `https://ceramics.onlinelibrary.wiley.com/doi/abs/10.1111/j.1151-2916.1984.tb19507.x`.

[35] McLaws IJ. Uses and Specifications of Silica Sand. Research Council of Alberta; 1971.

[36] Silica sands and quartz sands - OEC: The Observatory of Economic Complexity; 2021. Available from: `https://oec.world/en/profile/hs/silica-sands-and-quartz-sands`.

[37] Yolkin KS, Sivtsov AV, Yolkin DK, Karlina AI. The Production of Silicon Carbide and Achievements in the Field of Furnace Gases Collection and Purification. KnE Materials Science. 2020 Dec;6(1):70–77. Available from: `https://knepublishing.com/index.php/KnE-Materials/article/view/8046`.

[38] Production of a high value ceramic material: Silicon carbide - The TyGRe Project;. Available from: `http://www.tygre.eu/cms/project/production`.

[39] Griffin S, Hochberg Y, Inzani K, Kurinsky N, Lin T, Yu T. Silicon carbide detectors for sub-GeV dark matter. Physical Review D. 2021 04;103.

[40] El Mendili Y, Orberger B, Chateigner D, Bardeau JF, Gascoin S, Petit S, et al. Insight into the structural, elastic and electronic properties of a new orthorhombic 6O-SiC polytype. Scientific Reports. 2020 05;10:7562.

[41] Wecht EHP. Feuerfest-Silisiumcarbid. Springer-Verlag; 1977.

[42] Liu Z, Xu J, Scott HP, Williams Q, kwang Mao H, Hemley RJ. Moissanite (SiC) as windows and anvils for high-pressure infrared spectroscopy. Review of Scientific Instruments. 2004 nov;75(11):5026-9. Available from: `https://doi.org/10.1063%2F1.1808123`.

[43] Nordbø EA. Interaction of SiO-gas and Charcoal and the Formation of SiC and Si. Norwegian University of Science and Technology; 2019.

[44] Gerhardt RA. Properties and Aplications of Silicon Carbide. Gerhardt RA, editor. InTech; 2011.

[45] Sintered Silicon Carbide (SiC) Properties and Applications; 2000. Available from: `https://www.azom.com/article.aspx?ArticleID=15`.

[46] Katoh Y, Snead LL. Silicon carbide and its composites for nuclear applications – Historical overview. Journal of Nuclear Materials. 2019;526:151849. Available from: `https://www.sciencedirect.com/science/article/pii/S0022311519312243`.

[47] Jørgensen RB, Kero IT. Real-Time Measurements and Characterization of Airborne Particulate Matter from a Primary Silicon Carbide Production Plant. International Journal of Environmental Research and Public Health. 2017;14(12). Available from: `https://www.mdpi.com/1660-4601/14/12/1611`.

[48] Osterman JW, Greaves IA, Smith TJ, Hammond SK, Robins JM, Thériault G. Work related decrement in pulmonary function in silicon carbide production workers. Occupational and Environmental Medicine. 1989;46(10):708-16. Available from: `https://oem.bmj.com/content/46/10/708`.

[49] Xavier C, Oliveira C. Decarbonisation options for the Dutch silicon carbide industry. PBL Netherlands Environmental Assessment Agency; 2021.

[50] Technical Support Document for the Silicon Carbide Production Sector: Proposed Rule for Mandatory Reporting of Greenhouse Gases. U.S. Environmental Protection Agency, Office of Air and Radiation; 2009.

[51] Singh SK, Mohanty BC, Basu S. Synthesis of SiC from rice husk in a plasma reactor. Bull Mater Sci. 2002;(25):561-3.

[52] Zhao C, Zhou W, Hu QH, Xu H, Zhang C. Porosity measurement of granular rock samples by modified bulk density analyses with particle envelopment. Marine and Petroleum Geology. 2021 nov;133. Available from: `https://doi.org/10.1016%2Fj.marpetgeo.2021.105273`.

[53] Soterroni A, Ramos F. Size Segregation in the Brazil Nut Effect. 2013 10;1558:2385-8.

[54] Density Analysis - Particle Technology Labs; 2023. Available from: `https://particletechlabs.com/analytical-testing/density-analysis/`.

[55] Giesche H. In: Surface Area, Density and Porosity of Powders; 1998. p. 274-86.

[56] Nölte J. ICP Emission Spectrometry: A Practical Guide. 2nd ed. Wiley-VCH; 2021.

[57] Feng D, Qin Z, Ren Q, Sun S, Xia Q, Ru H, et al. Occurrence forms of major impurity elements in silicon carbide. Ceramics International. 2022;48(1):205-11. Available from: `https://www.sciencedirect.com/science/article/pii/S0272884221028777`.

[58] Britannica TEoE. X-ray diffraction; 2023. Available from: `https://www.britannica.com/science/X-ray-diffraction`.

[59] Waseda Y, Shinoda K, Matsubara E. X-Ray Diffraction Crystallography: Introduction, Examples and Solved Problems. Springer-Verlag Berlin Heidelberg; 2011.

[60] Jayakumari S. Formation and Characterization of - and -Silicon Carbide Produced During Silicon/Ferrosilicon Process. Norwegian University of Science and Technology; 2020.

[61] Pecharsky VK, Zavalij PY. Fundamentals of Powder Diffraction and Structural Characterization of Material. 2nd ed. Springer New York, NY; 2008.

[62] Goldstein JI, Newbury DE, Michael JR, Ritchie NWM, Scott JHJ, Joy DC. Scanning Electron Microscopy and X-Ray Microanalysis. 4th ed. Springer Science+Business Media LLC; 2018.

Appendix A

Mixing Ratios for Furnace

These ratios are calculated from the overall reaction for the Acheson process:

$$SiO_2(s) + 3\,C(s) \longrightarrow SiC(s) + 2\,CO(g) \qquad (A.1)$$
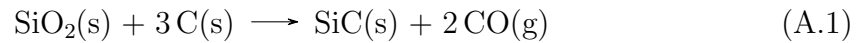
Due to various factors, desired carbon factor has been set at 0.4. Dry base represents mass with no moisture. Real values have been adjusted for measured moisture.

Table A.1: Mixing Ratio for Furnace Run 1 (30% biocarbon)

	Component	Mass [kg]
Dry Base	SiO2	13.24
	Tot C:	8.83
	- Cpet	6.18
	- Cbio	2.65
Real	SiO2	13.88
	Tot C:	11.11
	- Cpet	8.09
	- Cbio	3.02
Total		25.00

Table A.2: Mixing Ratio for Furnace Run 2 (0% biocarbon)

	Component	Mass [kg]
Dry Base	SiO2	13.01
	Tot C:	8.67
	- Cpet	8.67
	- Cbio	0
Real	SiO2	13.64
	Tot C:	11.36
	- Cpet	11.36
	- Cbio	0
Total		25.00

Appendix B

Density Measurements

B.1   Bulk Density Raw Data

Table B.1: Bulk Density Measurements for Samples of Pet. Coke and Biocarbon

Sample	Density before agitation [g/cm^3]	Density after agitation [g/cm^3]
Bio-1	0.14	0.16
Bio-2	0.14	0.15
Bio-3	0.12	0.14
Bio-4	0.12	0.14
Bio-5	0.13	0.15
Average	**0.13**	**0.15**
Pet-1	0.56	0.60
Pet-2	0.52	0.58
Pet-3	0.52	0.56
Pet-4	0.53	0.59
Pet-5	0.54	0.57
Average	**0.53**	**0.58**

B.2 Absolute Density Raw Data

The Accupyc takes five measurements per data point and averages these. Then the software calculates standard deviation as shown the table below. The average of several repeat measurements was taken and the average standard deviation was calculated.

Table B.2: Absolute Density Measurements for Samples of Pet. Coke and Biocarbon

Sample	Density [g/cm^3]	σ	Density Avg. [g/cm^3]	σ Avg.
PET-1	1.3799	0.0009		
PET-1-2	1.3783	0.0006		
PET-2	1.3732	0.0025	1.3823	0.0013
PET-3	1.3869	0.0006		
PET-4	1.3866	0.0005		
PET-5	1.3890	0.0017		
BIO-1	1.5389	0.0121		
BIO-2	1.5348	0.0134		
BIO-3	1.5921	0.0198	1.5736	0.0169
BIO-4	1.6001	0.0222		
BIO-5	1.6021	0.0148		

Appendix C

XRD Diffractograms

This appendix includes larger versions of the XRD diffractograms shown in figure 4.5.
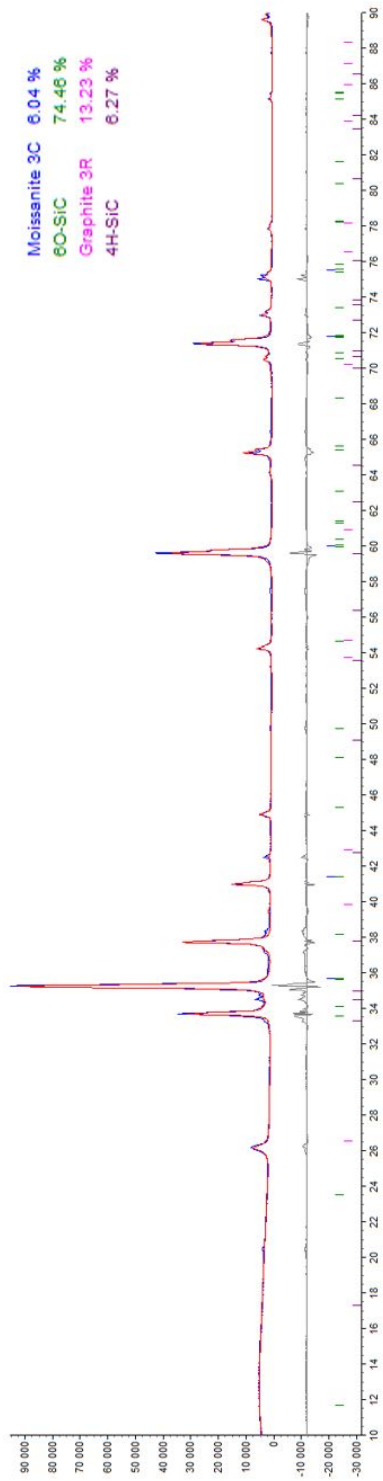
Figure C.1: Run-1 (30% biocarbon) Crude
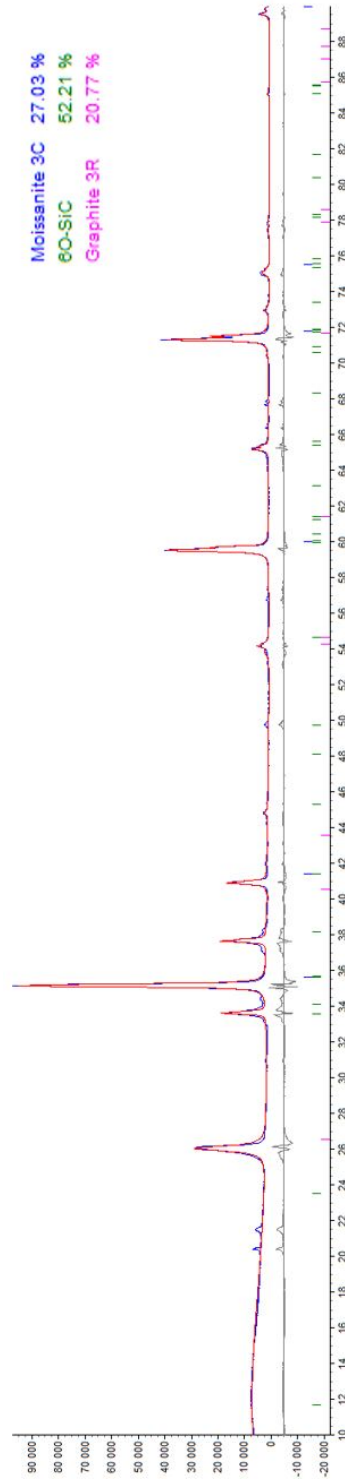
Figure C.2: Run-1 (30% biocarbon) Firesand
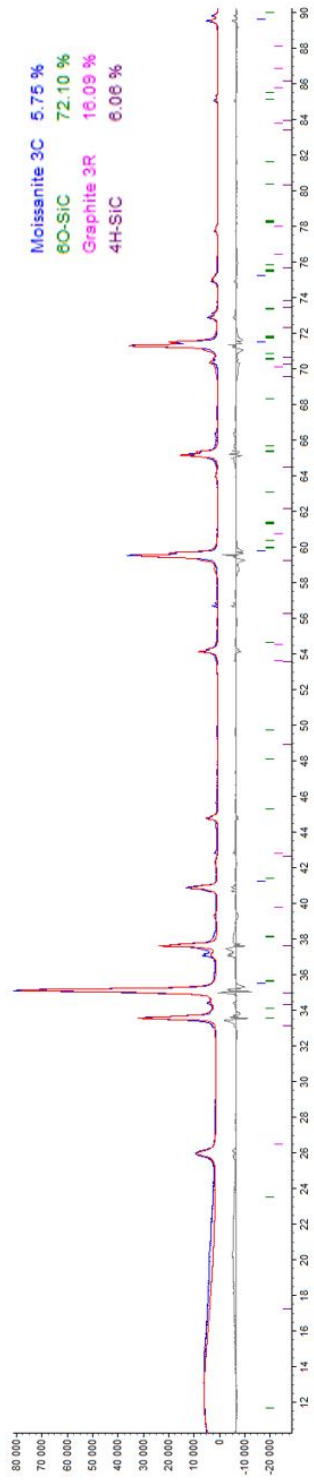
Figure C.3: Run-2 (0% biocarbon) Crude
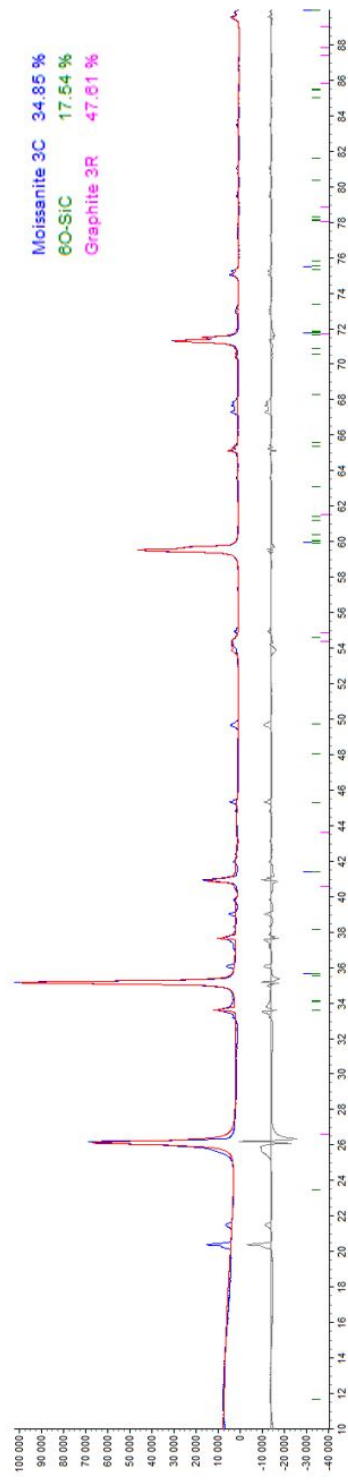
Figure C.4: Run-2 (0% biocarbon) Firesand

Appendix D

SEM-EDS Spectra

This appendix includes spectra for the SEM-EDS analyses shown in the text. Quantification data is not included as this is shown in the text.
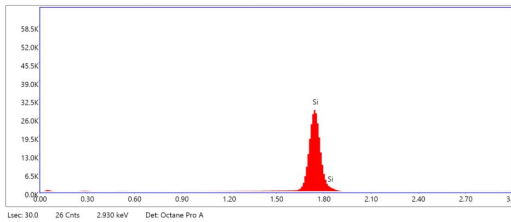
Spectra for figure 4.10
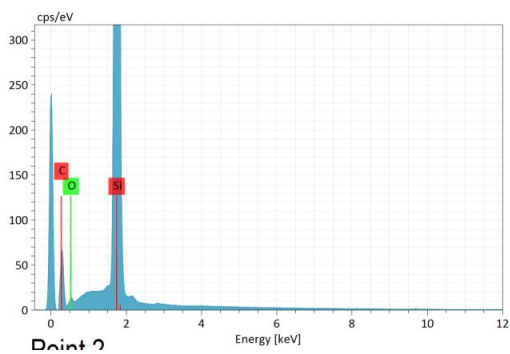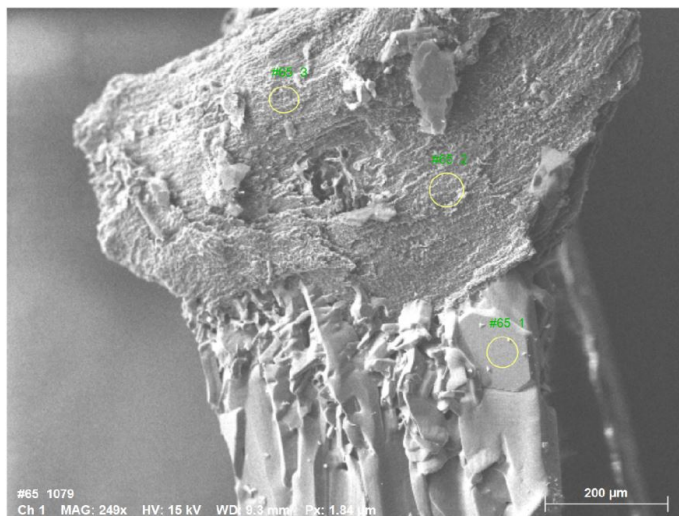
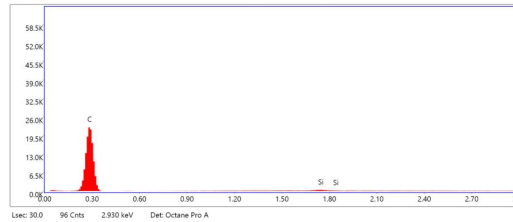(a) Point 1
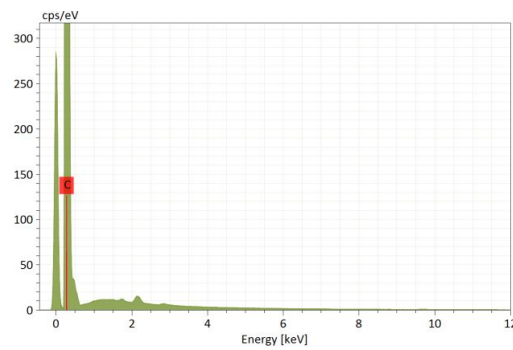
(b) Point 2
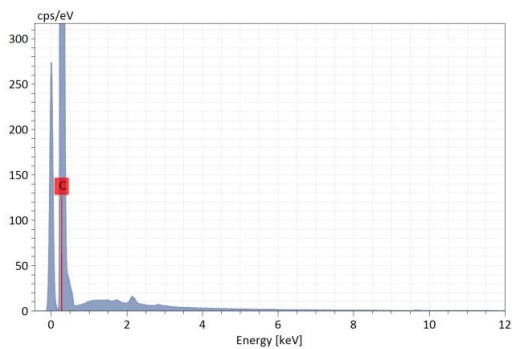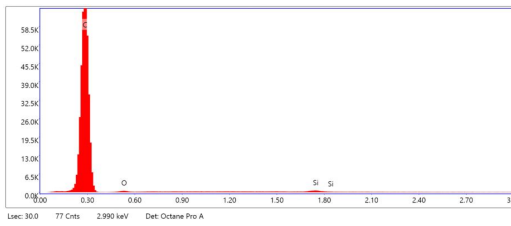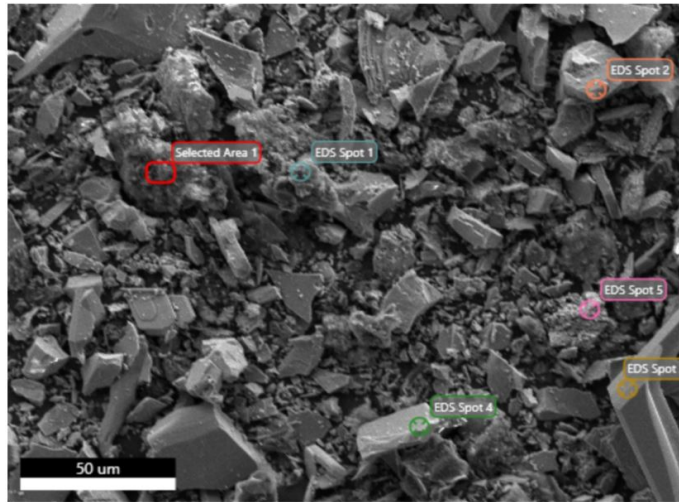

(c) Point 3

Spectra for figure 4.11
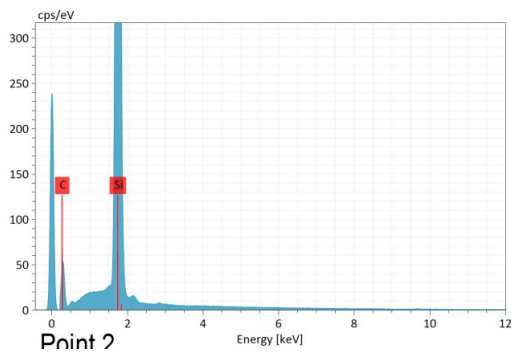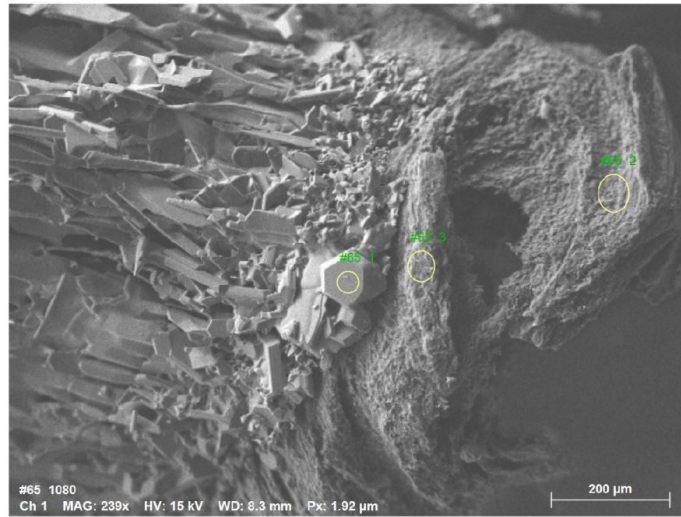
(a) Point 1
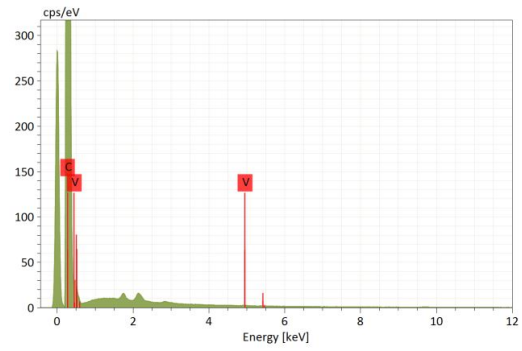
(b) Point 2
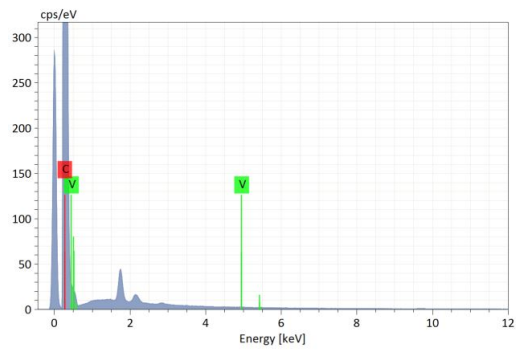
(c) Point 3

Spectra for figure 4.14

Spectra for this sample were not obtained, but the following table was produced by the analysis program:

Atomic concentration [%]

Spectrum	Carbon	Oxygen	Aluminium	Silicon	Calcium
#65 1	53.330		0.341	46.093	0.236
#65 2	49.755	1.614		48.631	
#65 3	50.588	1.970		47.442	
Mean	51.224	1.792	0.341	47.389	0.236
Sigma	1.871	0.252	0.000	1.270	0.000
SigmaMean	1.080	0.145	0.000	0.733	0.000

Spectra for figure 4.17
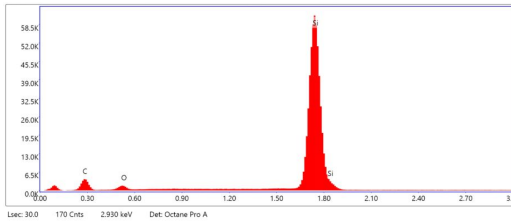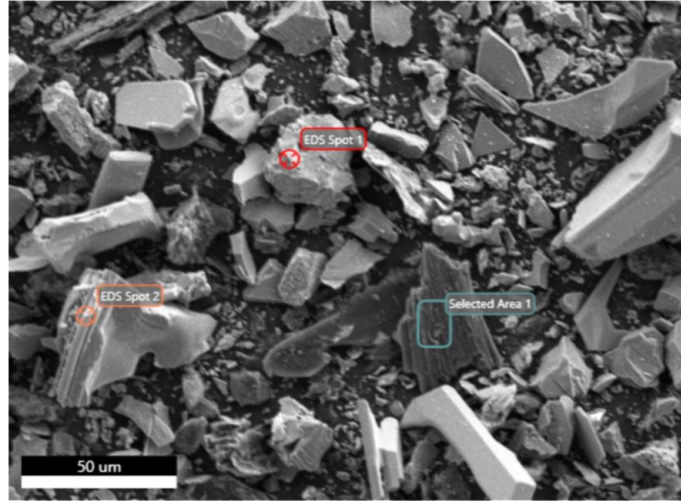
(a) Point 1
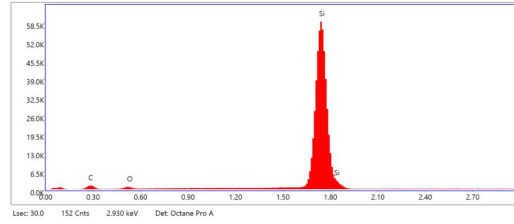
(b) Point 2
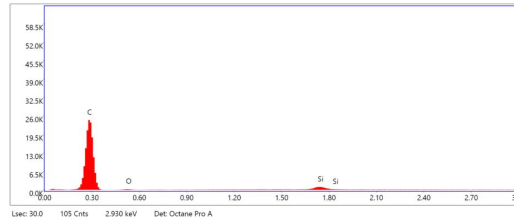
(c) Area 1

Spectra for figure 4.18
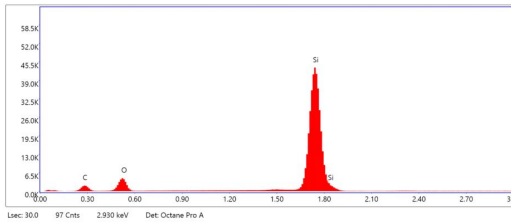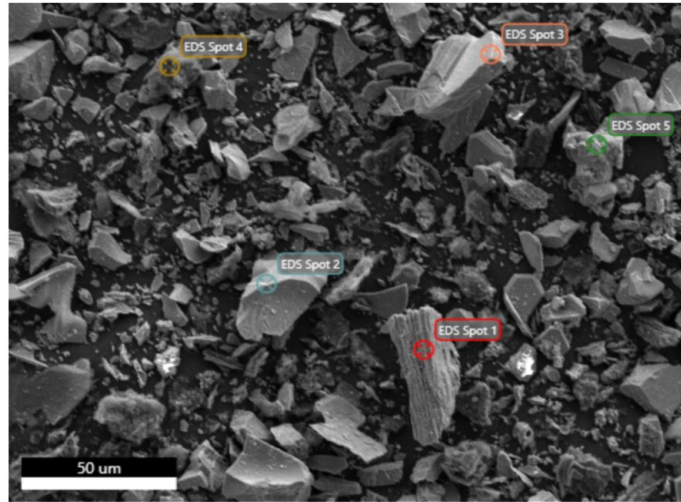
(a) Point 1
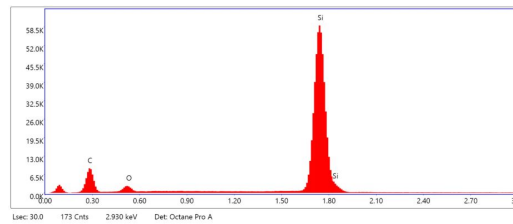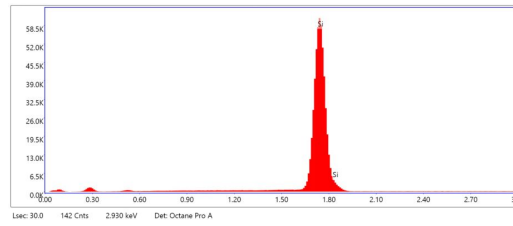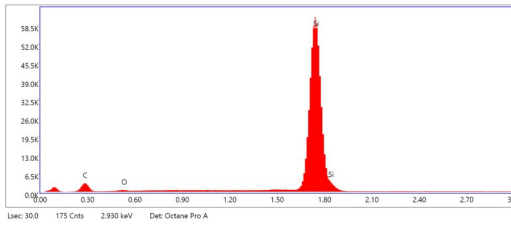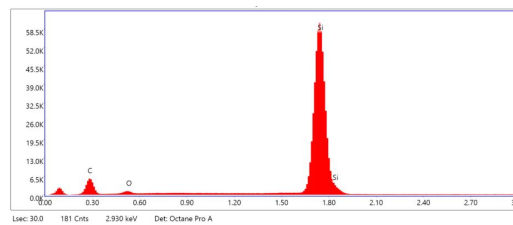

(b) Point 2

(c) Point 3
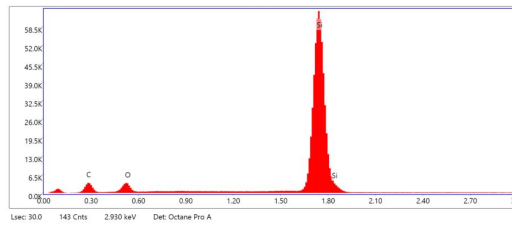
(d) Point 4

(e) Point 5

Spectra for figure 4.19

(a) Point 1

(b) Point 2

(c) Point 3

(d) Point 4

(e) Point 5

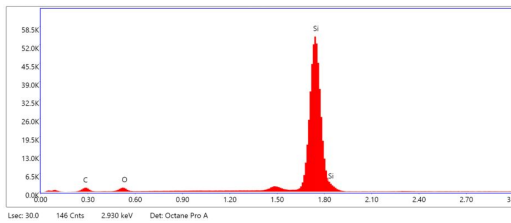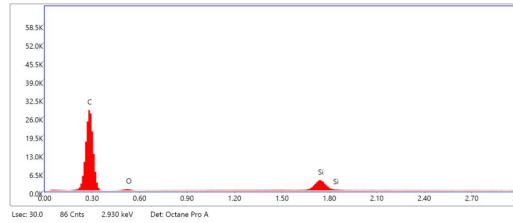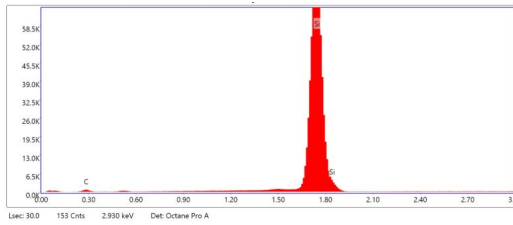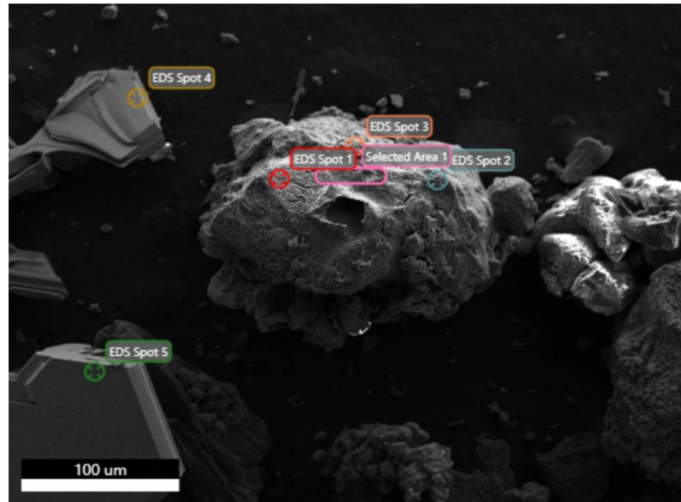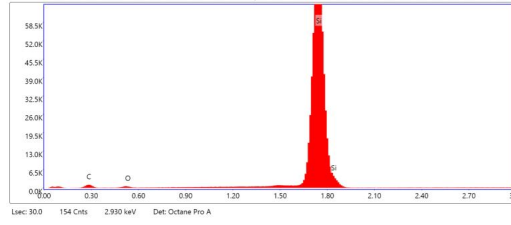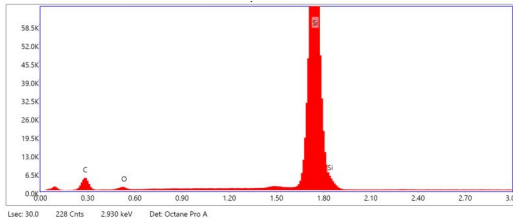(f) Area 1
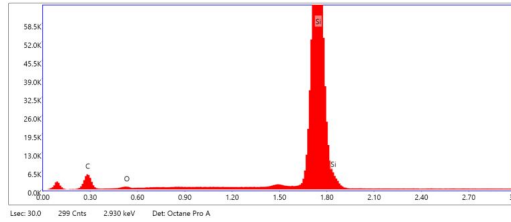
Spectra for figure 4.20
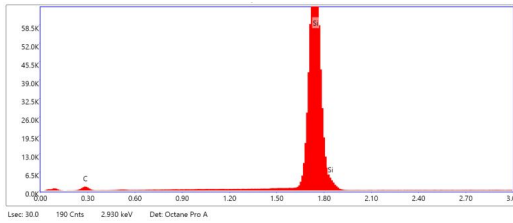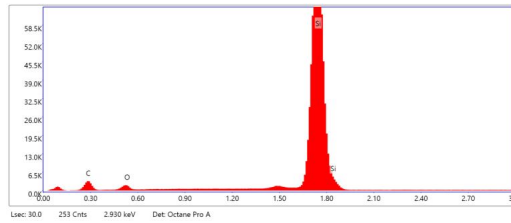

(a) Point 1

(b) Point 2

(c) Point 3

(d) Point 4

(e) Point 5

(f) Area 1

Appendix E

Risk-Assessment

This appendix includes the risk assessment that was done for various stages of the project.

RISK ASSESSMENT

Unit/Institute	Department of Materials Science and Engineering (IMA)		Dato:	02.02.2023
Responsible line manager (name):	Roald Lilletvedt		Revised:	18.05.2023
Responsible for activities being risk assessed (name):	FIVEN Lillesand AS			
Participants in risk assessment (name):	Ole Tesssmer			

Description of the activity, process, area, etc.:

Construction, operation, and dismantling of pilot Acheson furnace at FIVEN Lillesand. Handling and storage of samples of produced SiC as well as charcoal and petroleum coke on campus. Analysis of samples using XRD, SEM, Pycnometer. IMA laboratories at NTNU Gløshaugen and Kalvskinnet. Operation of induction furnace at NTNU Gløshaugen.

Activity/process	Unwanted incident(s)	Existing risk reducing measures	Probability (P) (1-5)	Consequence (C) Evaluate the categories individually. Health				Risk value (P x C)	Risk reducing measures/suggestions Measures reducing the probability of unwanted incident happening should be prioritized.	Residual risk after implementation of measures
				Menneske (1-5)	Øk/materi ell (1-5)	Ytre miljø (1-5)	Omdømm e (1-5)			
Mixing of raw materials	Inhalation of dust and PAH. Skin contact with dust	Mobile fumehood, gas/dust masks, protective clothing, fumehood over furnace.	4	2	1	1	1	8	Use of gloves, full gas/dust mask. Full coverall suit.	3
Constructing furnace	Current in furnace	Current measurement. LOTO procedure for furnace.	1	5	1	1	1	5	LOTO (Lock Out Tag Out)-procedures. Start-up card/consideration.	1
Rotating equipment	Entaglement of hair/fingers	Existing risk reducing measures	1	3	1	1	1	3	Use of correct gloves and protective gear	1
Firing of furnace	Flare up in furnace ("blow")	Fumehood over furnace	3	1	3	2	1	9	Extra charge to cover holes generated by blows. Power shutoff for minimum 10 minutes.	3
Firing of furnace	Risk of fire	Fire extinguishing equipment	1	3	3	3	3	3	Flame-retardant clothing	2

Activity	Hazard	Existing measures						Risk	Measures	
Firing of furnace	Gas poisoning (CO)	Fumehood over furnace. Routine for keeping door open (fresh air)	5	2	1	2	1	10	CO-meter. Reduce movement in furnace room during operation.	3
Firing of furnace	Electricity through body	Measurement of electricity	1	5	1	1	1	5	LOTO-procedures. Reduce movement in furnace room during operation.	1
Firing of furnace	Burning of electrodes	Water cooling system	1	1	4	1	1	4	Fire extinguishing equipment	1
Sorting of products	Burns of the skin, melting of plastic tools	Water cooling system	3	2	1	1	1	6	Use of heat-proof gloves	2
Sorting of products	SiC and PAH penetrate skin	Fumehood over furnace. Mobile fumehood for cement mixer	4	2	1	1	1	8	Use of working gloves with nitrile gloves under	3
Moving on site	Collision with truck or vehicle	Designated walk-zones	1	2	1	1	1	2	Keeping distance and mainainting eye contact with operator	1
SEM	Squeezing injuries, damage of the eye		1	1	1	1	1	1	Gloves. Eye protection.	1
SEM	Damage of internal components.		1	1	4	1	1	4	Positioning of stage to allow easier access. Routines for doublechecking no components are at risk. Use of camera mode when adjusting stage height.	1
Pycnometer	Damage of equipment due to scratching or pollution of sample container	Specialised tongs and other equipment.	1	1	3	1	1	3	Use of cotton gloves to reduce pollution of sample cup. Careful rinsing of sample cup with ethanol after use.	1
Pycnometer	Dust cloud combustion during sample drying	Ventilating heating cabinet	2	1	4	2	1	8	Use of aluminium foil to cover sample holders. This foil is perforated to allow the escape of moisture, but reduce risk of excessive dust formation	2
XRD	Squeezing injuries, damage of the eye		1	1	1	1	1	1	Labcoat. Gloves. Eye protection.	1

XRD	Irradiation	Radiation-safe container	1	2	1	1	1	2	Labcoat. Gloves. Eye protection.	1
Storage of carbon samples	Dust generation and explosion	Routines for sample handling and storage in controlled environments.	1	4	4	3	3	4	Avoid excessive handling. Storing samples in closed container	1
Separation of samples	Dust inhalation		4	2	1	2	1	8	Dust mask. Fume hood. Cleaning routines for surfaces.	3
Handling samples	Dust inhalation. Dust generation and explosion.	Routines for sample handling and storage in controlled environments.	3	2	1	2	1	6	Dust mask when necessary. Avoiding excessive agitation of fine-powdered samples.	3
General lab-safety	Chemical exposure, burns, damage. Damage of equipment.	Rules for use of protective clothing.	1	2	2	1	1	2	Lab coat and eye protection at all times. Closed shoes. Gloves when necessary.	1
Operation of induction furnace	Fire. Burns. Damage of equipment	Protective gear: flame-retardant clothing, eye protection, gloves. Fire extinguishing tools.	2	5	4	1	1	6	Monitoring of water cooling system and furnace temperature. Limiting time in close proximity to furnace	2
Handling of hot crucibles	Burns.	Protective gear: flame-retardant clothing, eye protection, gloves.	3	3	2	1	1	9	Allowing crucibles to cool extensively before handling to reduce risk.	3
Oxygen lancing	Excessive burning.	Flow-rate limit. Fire extinguisher	1	1	2	1	1	2	Closely monitoring oxygen flow rate. Mounting oxygen lance tube outside of high temperature zones.	1